www.medicines4all.vcu.edu

Medicines for All Institute

Summary of Process Development Work on the Synthesis of Frag A of Lenacapavir

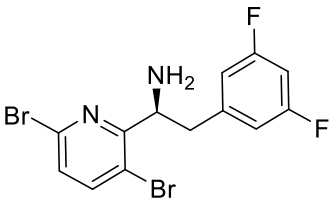

Report Prepared by:

Dr. Limei Jin

Dr. Justina M. Burns

Dr. Anand H. Shinde

Dr. Ramakrishna Sayini

Dr. Piyal Singh

Contact: m4all@vcu.edu

August 2024

Executive Summary

This process development report (PDR) describes the results of synthetic route scouting (SRS) and scale-up optimization (OPT) efforts at the Medicines for All Institute (M4ALL) to discover new, cost-effective synthetic strategies to make a key intermediate and cost-driver in the synthesis of lenacapavir: (*S*)-1-(3,6-dibromopyridin-2-yl)-2-(3,5-difluorophenyl)ethan-1-amine (**Frag A**). Lenacapavir is a first-in-class antiretroviral that targets HIV's capsid protein. It was developed by Gilead Sciences Inc. and approved by the FDA in 2022. Gilead's baseline synthesis of **Frag A** leverages classical chiral synthesis using an expensive enantiopure auxiliary (and other costly raw materials).[1] Herein, we report a chiral resolution-based approach to produce **Frag A** from 3,6-dibromo-2-methylpyridine (LenA 4). [a] This route comprises 7 steps (linear). The key transformations include a two-step aldehyde synthesis, a telescoped three-step racemic amine synthesis, and a dynamic kinetic resolution (DKR) with N-acetyl-D-leucine (NADL). Process development of the LenA 4 enables the production of **Frag A** as a single enantiomer in 25-30% overall isolated yield, demonstrated at scales up to 200 grams. Techno-economic (TE) cost analysis suggests that, compared to the baseline route (Gilead's chiral auxiliary-based approach), LenA 4 offers an overall raw material cost (RMC) reduction of 33-41%.

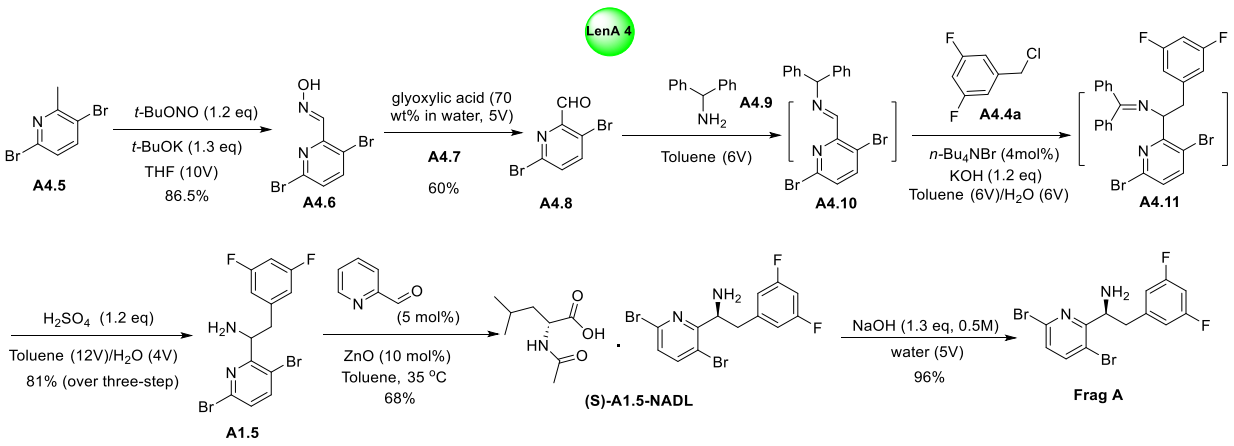

[a] Two additional synthetic approaches to **Frag A** are summarized in the Appendix of this document, LenA 1 and LenC 3. They were not advanced for optimization, in view of the superior performance of LenA 4. Please see the appendices for further details.

www.medicines4all.vcu.edu

Medicines for All – Contributors to the Research and Report

Contributor	Title / Role
Dr. Limei Jin	Sr Scientist (Project Lead)
Dr. Anand H. Shinde	Research Scientist
Dr. Ramakrishna Sayini	Postdoctoral Researcher
Dr. Piyal Singh	Postdoctoral Researcher
Dr. Justina M. Burns	Associate Director of Analytical Chemistry
Dr. Ryan Littich	Head of R&D [b]
Dr. Michel Nuckols	Sr Scientist [b]
Janie Wierzbicki	Project Manager

*With research support provided by WuXi Apptec (China)

[b] PDR review, revisions, additions

Contents

1 Introduction

Human immunodeficiency virus (HIV), the virus that causes AIDS (acquired immunodeficiency syndrome), is one of the world's most serious health and development challenges. Approximately 39 million people are currently living with HIV, and tens of millions of people have died of AIDS-related causes since the beginning of the epidemic.[2] In 2020, there were approximately 20 million people on antiretroviral therapy (ART), a number which was expected to reach 24 million by 2024. Approved HIV treatment regimens currently fall into seven drug classes, based on their distinct mechanism of action. Today, approximately 22 million individuals are on a dolutegravir-based regimen: the "gold-standard" treatment comprises the combination of two nucleoside reverse transcriptase inhibitors (NRTIs), tenofovir disoproxil and lamivudine, and the integrase strand transfer inhibitor dolutegravir.[3]

Lenacapavir (Sunlenca®) is a high-potency HIV treatment in development by Gilead Sciences. The drug is a first-in-class HIV-1 capsid protein inhibitor that displays picomolar activity, extended pharmacokinetics, and little to no cross-resistance with clinically used antiretroviral agents.[4,5] Lenacapavir achieves its revolutionary anti-HIV-1 activity by blocking the viral replication of the HIV-1 virus, which is closely related to many processes of the viral lifecycle: uptake, assembly, and release.[1] Because of this classification, the FDA has designated lenacapavir as a breakthrough drug. The novel therapy earned approval from both the European Commission and the FDA in 2022 as a treatment for multidrug-resistant HIV (MDR HIV) infections.[6–8] In 2023, in the United States, the cost for HIV-indicated injections and tablets (wholesale; not for PrEP) was $42,450 per patient per year.[9–11] To ensure patient access to lenacapavir-for-PrEP globally, significantly lower annual costs must be realized.[8,c]

1.1 Background of **Frag A** in Lenacapavir

Lenacapavir was first reported by Gilead Sciences in a family of patents and publications in 2018-2020.[1,12–14] Structurally speaking, lenacapavir is an extremely complex active pharmaceutical ingredient (API), with three chiral sp^3-hybridized carbon centers and 10 fluorine atoms in four different functional environments. Lenacapavir consists of three advanced intermediates - Fragment A (**Frag A**), Fragment B, and Fragment C - as shown in

[c] For example, "PrEP medications would need to cost <$54 a year per patient for South Africa to afford them."[10]

Figure 1.1.1.

Figure 1.1.1 Retrosynthetic disconnections in lenacapavir

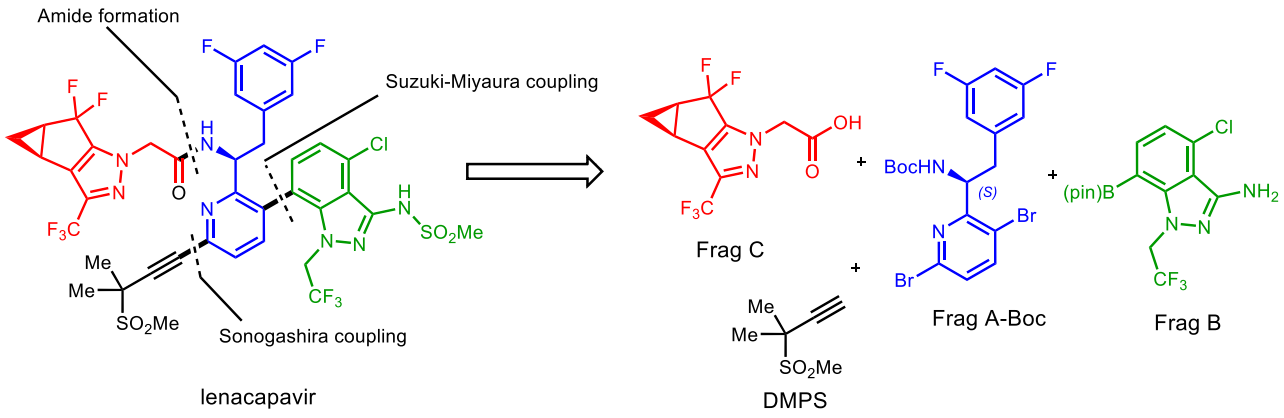

Gilead has published several patents related to the initial synthesis and optimization of this molecule with several approaches to each fragment being demonstrated.[12,13,15,16] These routes utilize expensive starting materials and reagents and rely on costly chiral separation techniques that are not amenable to scaleup. Improvements to **Frag A**'s synthesis will, thus, have a meaningful impact on the overall cost of the molecule.

1.2 Introduction of LenA 4

M4ALL developed a DKR-based approach [d] to decrease raw material costs associated with **Frag A** synthesis (Scheme 1.2.1). M4ALL's development work consisted of four key project milestones: synthesis of aldehyde **A4.8** (Milestone 1), synthesis of the racemic amine **A1.5** (Milestone 2), chiral resolution to **Frag A** (Milestone 3), and the synthesis of 3,5-difluorobenzyl chloride **A4.4a** (Milestone 4).[e] For future work maybe consider use of Na-*t*-amylate as it is cheaper than *t*-BuOK.

[d] It is also known as crystallization-induced diastereomer transformation.[17]

[e] 3,5-Difluorobenzyl chloride is the main cost-driver in LenA 4. We developed a cost-effective two-step process to make this molecule (Milestone 4). The details of the 3,5-difluorobenzyl chloride synthesis are discussed in the Appendix 4.1.

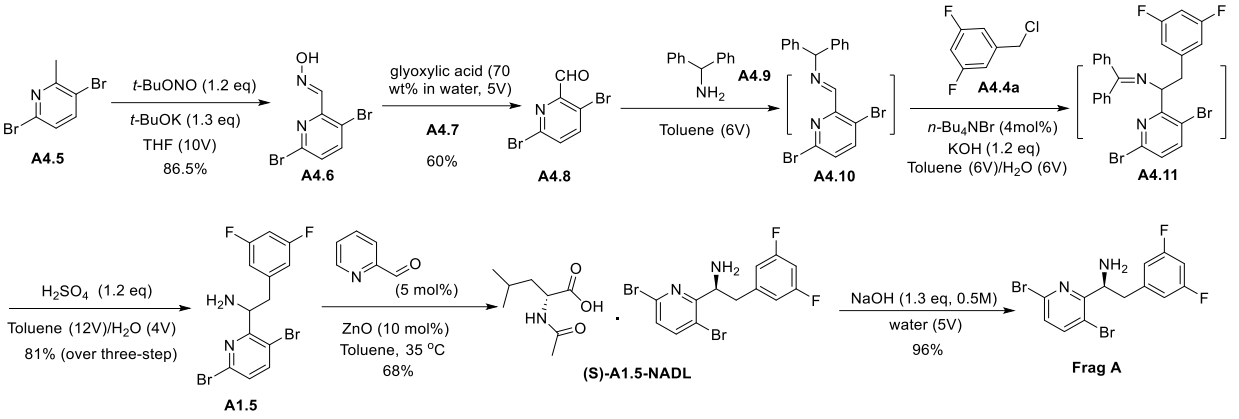

Scheme 1.2.1 M4All approach (LenA 4) for the synthesis of **Frag A**

LenA 4 is a linear-7-step process that utilizes a readily available 3,6-dibromo-2-methylpyridine (**A4.5**) as a starting material. The synthesis commenced with oximation of 3,6-dibromo-2-methylpyridine **A4.5** and tertiary butyl nitrite. The resulting oxime **A4.6** was then hydrolyzed to aldehyde **A4.8** using glyoxylic acid. Aldehyde **A4.8** was converted to a racemic amine **A1.5** through a telescoped three-step process (imination with diphenylmethanamine (**A4.9**), alkylation with 3,5-difluorobenzyl chloride (**A4.4a**), then acidic hydrolysis). Lastly, racemic **A1.5** was resolved using N-acetyl-D-leucine (NADL) *via* dynamic kinetic resolution (DKR) to afford the desired enantiopure **Frag A**.

It should be noted that some chemistry in this report is known in the literature,[13] however, the reported sequence is lacking in sufficient experimental details and thus presenting challenges to reproduce and ultimately scale-up:

- Synthesis of aldehyde (**A4.8**) from 3,6-dibromo-2-methylpyridine (**A4.5**) is reported.[13,18] Its synthesis was demonstrated on a gram scale; the procedure was not appropriate for scale-up, as defined.
- Alkylation of **A4.10** with 3.5-difluorobenzyl bromide (**A4.4**) was reported, however, our results showed low yield and low purity profile.[f] Additionally, the operation suffered from the acute lachrymatory property of the 3.5-difluorobenzyl bromide.

[f] The reaction of **A4.10** with 3,5-difluorobenzyl bromide afforded **A4.11** in 83% yield with 76 wt% by qNMR) while the reaction of **A4.10** with 3,5-difluorobenzyl chloride afforded **A4.11** in up to 94% yield and 87 wt% purity (see section 2.2 for details).

- Resolution of **A1.5** with *R*-mandelic acid and NADL was reported on small scale and lacked sufficient procedural details (i.e., purifications, purity profiles) to judge fitness for scale-up and tech transfer.

All of the abovementioned issues and unknowns presented challenges to our LenA 4 process development. These could only be resolved through independent process research and development. To this end, M4ALL developed DKR-based approach to prepare **Frag A** from readily available 3,6-dibromo-2-methylpyridine. We highlight an efficient 3-step telescoped racemic amine synthesis, alkylation with non-lachrymatory 3,5-difluorobenzyl chloride, and high yielding of DKR to access **Frag A**. Furthermore, we provide detailed process development assessments of the aldehyde synthesis, racemic amine synthesis and chiral resolution. Together, these insights provide informative and valuable data for the large-scale synthesis of **Frag A**.

2 Results & Discussion

2.1 Milestone 1: Synthesis of aldehyde **A4.8**

2.1.1 Optimization of aldehyde **A4.8** synthesis

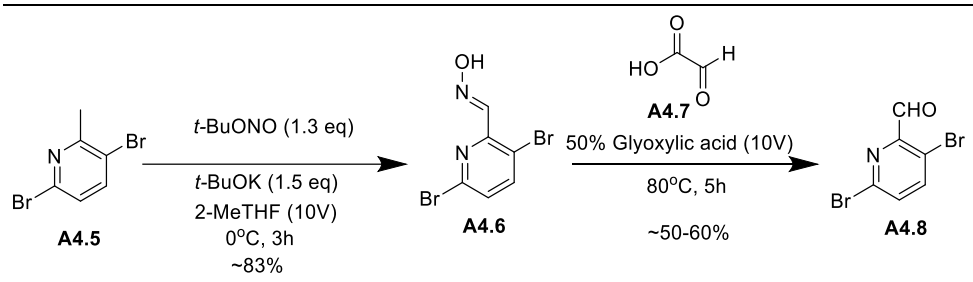

Scheme 2.1.1. Familiarization of aldehyde **A4.8** synthesis

M4ALL's work commenced with familiarization of the synthesis of **A4.8** from commercially available 3,6-dibromo-2-methylpyridine **A4.5** according to the reported method, on a gram-scale.[13,18] As shown in Scheme 2.1.1, oximation of **A4.5** with *t*-BuONO (1.3 eq) in the presence of *t*-BuOK (1.5 eq) gave **A4.6** in approximately 83% conversion (^{1}H NMR). Subsequent hydrolysis with 50 wt% glyoxylic acid (10V) furnished the aldehyde **A4.8** in 50-60% assay yield (qNMR) together with 40-50% starting material **A4.6** remaining. In our hands, as in the reported conditions, both oximation and hydrolysis reactions did not proceed to completion; purification by column chromatography was invoked in the reported preparations. Incomplete conversion and chromatographic purification are impediments to large-scale manufacture. To achieve a scalable process for the synthesis of aldehyde **A4.8**, we aimed to *1)* optimize the equivalents of *t*-BuONO

and *t*-BuOK in oximation of **A4.5** (Section 2.1.1.1) and *2)* identify the best concentration of glyoxylic acid for hydrolysis of **A4.6** to afford **A4.8**; and *3)* to eliminate column purification (thereby minimizing processing costs and enabling scalability).

2.1.1.1 Synthesis of oxime **A4.6**

Using Gilead's disclosed conditions, M4ALL observed ~93% (by HPLC) conversion in the oximation of **A4.5** with *t*-BuONO (1.3 eq) and *t*-BuOK (1.5 eq) (Table 2.1.1, Entry 1). To achieve complete conversion (i.e., improve scale-up suitability), initial efforts focused on screening equivalents of *t*-BuOK.[g] The team hypothesized that increasing the equivalents of the base would facilitate the complete consumption of **A4.5**. Treatment of **A4.5** with *t*-BuONO (1.3 eq) and *t*-BuOK (1.7 eq), however, negated the hypothesis: **A4.6** was obtained in 86 A% (Table 2.1.1, Entry 2). Examining *fewer* equivalents of *t*-BuOK (1.1 eq, Table 2.1.2, Entry 3) showed comparable performance, giving **A4.6** in 84 A%.[h] To complement these experiments in which single-portion charges of *t*-BuOK and *t*-BuONO were enacted, respectively semi-batch additions were investigated.

Table 2.1.3 Optimizations for the synthesis of oxime **A4.6**

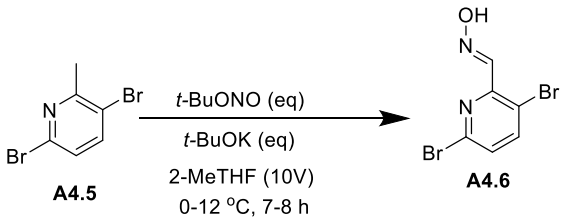

Entry[1]	Conditions	Crude mixture (A%)[2]		
		A4.5	Unknown Impurities	**A4.6**
1	*t*-BuONO (1.3 eq), *t*-BuOK (1.5 eq)	7	4	89
2[3]	*t*-BuONO (1.3 eq), *t*-BuOK (1.7 eq)	6	6	86
3	*t*-BuONO (1.3 eq), *t*-BuOK (1.1 eq)	15	1	84
4	*t*-BuONO (1.2 eq), *t*-BuOK (1.5 eq)	6	6	88

[1]All reactions were carried out on 1.0 g scale at 0-12 °C with 2-MeTHF (10 mL, 10V), followed by the addition of *t*-BuONO and *t*-BuOK, stirred for 7-8 h; [2]The reaction mixture was precipitated by addition of sat. NH_4Cl (5mL, 5V).

[g] KOH and *t*-BuONa were also investigated. Neither afforded oxime **A4.6**.

[h] Employing fewer equivalents of *t*-BuONO also failed to completely consume **A4.5** (Table 2.1.**Error! Main Document Only.**).

The solid was collected for analysis. A% was obtained by HPLC (210 nm) unless otherwise stated; [3]A% was obtained by qNMR.

Incremental addition enabled complete consumption of **A4.5** and robust replicability in **A4.6** oxime formation. On treatment of **A4.5** with 1.1 eq of *t*-BuONO and 1.1 eq of *t*-BuOK (Table 2.1.2), conversion stalled after 3 h. At this juncture (3 h), **A4.6** was present in 85 A% (HPLC, 210 nm). A further 0.1 eq of *t*-BuONO and 0.2 eq *t*-BuOK were then added to the reactor. After an additional 5 h, >96% conversion (A%, HPLC, 210 nm) was observed. **A4.6** was obtained in >89 A% (HPLC, 210 nm) and <3.5A% **A4.5** remained. After the addition of saturated aq. NH_4Cl (5V), precipitated solids were washed by DI water and then dried, affording **A4.6** in 87% isolated yield with 100 A% HPLC (210 nm) purity.

Table 2.1.4 Oximation of **A4.5** under incremental addition approach

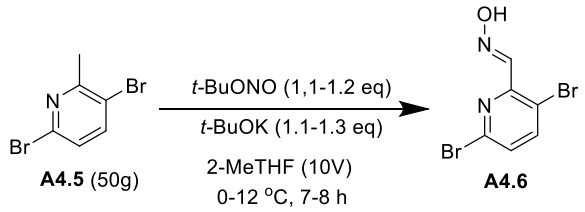

Entry[1]	Time (h)	*t*-BuONO (eq)	*t*-BuOK (eq)	IPC (A%) (HPLC, 210 nm)[2]		
				A4.5	Unknown Impurities	**A4.6**
1	1	1.1	1.1	12	10	78
2	2	1.1	1.1	11	5	84
3[3]	3	1.1	1.1	9	6	85
4	5	1.2	1.3	6	7	87
5[4]	8	1.2	1.3	4	7	89

[1]Reactions were carried out on 50.0 g scale at 0-12 °C with 2-MeTHF (500 mL, 10V), followed by the addition of *t*-BuONO and *t*-BuOK as shown in table, 7-8 h; [2]A% was obtained by HPLC at 210 nm, unknown impurities (< 2 A%/each) were observed at different retention time; [3]At the end of 3h, 0.1 eq of *t*-BuONO and 0.2 eq of *t*-BuOK were added; [4]The reaction mixture was precipitated by addition of sat. NH_4Cl (5V). The solid was collected and dried to afford **A4.6** (48g) in 87% isolated yield with 100 A% HPLC (210 nm) purity.

Thus, optimized conditions of oximation are:

- Incremental addition of *t*-BuONO and *t*-BuOK, using 1.1 eq of *t*-BuONO and *t*-BuOK, 2-MeTHF (10V), at 0 to 12 °C, followed by an additional charge of 0.1 eq of *t*-BuONO and 0.2 eq *t*-BuOK affords **A4.5** in > 96 A% (HPLC, 210 nm).

- Robust repeatability was observed; comparable results were obtained on a 50 g scale.

2.1.1.2 Synthesis of aldehyde **A4.8**

Observing Gilead's baseline conditions, M4ALL found that hydrolysis of oxime **A4.6** with 50% glyoxylic acid (10V) provided aldehyde **A4.8** in 59 A% (LCAP), along with 28 A% (LCAP) residual **A4.6** (Table 2.1.3, Entry 1). Reaction volumes and the concentration of glyoxylic acid were investigated as key variables. The team posited that decreasing the volumes of glyoxylic acid – thereby increasing the concentration of **A4.6** in the reaction medium would favor higher conversion and faster kinetics. Experiments affirmed that decreasing volumes of glyoxylic acid increased the conversion of **A4.6** (Table 2.1.3, Entries 1-3). Notably, 60 A% (LCAP) of **A4.8** was observed using 7.5V of glyoxylic acid (50 wt%) and 68 A% using 5 V of glyoxylic acid (50 wt%).

Table 2.1.5. Screening volumes and concentrations of glyoxylic acid for the synthesis of aldehyde **A4.8**

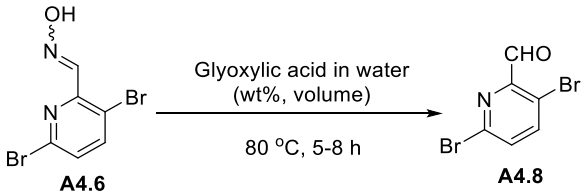

Entry[1]	Concentration of glyoxylic acid[2]	Volumes of glyoxylic acid (eq)	Crude mixture (A%)		
			A4.6[3]	Unknown impurities[4]	**A4.8**[3]
1	50%	10V (20)	28	13	59
2		7.5V (15)	32	8	60
3		5V (10)	24	8	68
4	60%	10V (23)	30	2	68
5	80%	5V (16)	8	4	88
6	70%	5V (14)	2	7	91
7[5]	70%	5V (14)	2	5	93

[1]All these reactions were carried out with **A4.6** (0.2 to 5 g, 1eq), 5-8 h at 80 °C in glyoxylic acid as shown in the table unless otherwise stated; [2]The concentration was wt%, and the aqueous solution of glyoxylic acid was prepared by dissolving glyoxylic acid in water; [3]A% (LCAP) was obtained by HPLC at 210 nm, glyoxylic acid was cut off; [4]Several unknown impurities (< 2 A%/each) were detected by HPLC at different retention time; [5]Reaction was performed with 20 g of **A4.6**, 5h, 80 °C. The precipitated solid was collected and washed by water to remove glyoxylic acid. **A4.8** (13 g) was obtained in 58% isolated yield with 82 wt% HPLC (210 nm) purity.

M4ALL further observed a direct correlation between glyoxylic acid concentration and **A4.6** conversion in the hydrolysis (Table 2.1.3, Entries 4-5). A 68 A% (LCAP) of **A4.8** was observed with the use of 60 wt% glyoxylic acid (10V), and 88 A% (LCAP) with 80 wt% glyoxylic acid

(5V). Ultimately, 5 volumes of 70 wt% glyoxylic acid proved optimal in the aldehyde-forming step, as indicated in Entry 6. Conversion of **A4.6** improved to >98 A% (LCAP). Optimal conditions were then examined on a 20 g-scale; 93 A% (LCAP) of **A4.8** was obtained with a conversion >98 A% (LCAP) (Table 2.1.3, Entry 7). Thus, optimized hydrolysis conditions are 70 wt% of glyoxylic acid (5V), 80 °C, 5 h, resulting in >98 A% (HPLC, 210 nm) of **A4.6**.

2.1.2 Scale-up of aldehyde **A4.8** synthesis

Using the optimized 2-step process for the production of **A4.8**, M4ALL evaluated hundred-gram (100-200 g) scale-up batches in a 2L ChemRxnHub reactor. Commencing with 3,6-dibromo-2-methyl-pyridine **A4.5** (Table 2.1.4), the optimized process generated oxime **A4.6** in 86-87 % overall isolated yield and 93-100 wt% chemical purity (by HPLC). Hydrolysis of **A4.6** produced the aldehyde **A4.8** in 64-68 % isolated yield with 84-94 wt% purity (by GCMS). Further details, particularly regarding isolated intermediate purity, are discussed in the following paragraphs.

As summarized in Table 2.1.4, treating 3,6-dibromo-2-methyl-pyridine **A4.5** with the portion-wise addition of *t*-BuONO and *t*-BuOK provided the desired oxime **A4.6** in good yields. A 100 g-scale batch furnished oxime **A4.6** as a light-yellow solid in 87.4% isolated yield with 100 wt% purity (HPLC) and a 200 g-scale campaign gave oxime **A4.6** in 86.5% isolated yield with 93 wt% purity (HPLC). M4ALL hypothesizes the low wt% in this batch was due to the presence of trace inorganic salts, as the material showed >99 A% (HPLC, 210 nm). The definition of the **A4.5** impurity profile - and associated critical process parameters - is the subject of future work.

Table 2.1.4 Synthesis of oxime **A4.6** on hundred-gram-scale

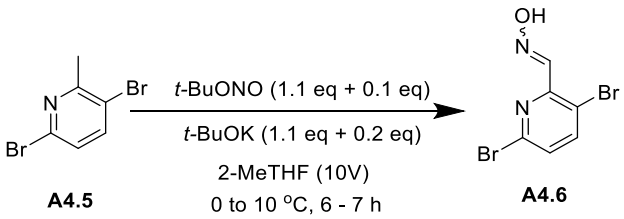

Entry[1]	Input **A4.5** (g)	IPC (A%)[2]			After purification			
		A4.5	**A4.6**	Unknown impurities	**A4.6** (g)	Wt%[3]	A%[4]	Yield (%)[5]
1	100	4	88	8	97.5	100	99	87.4
2	200	4	82	14	207	93[6]	99	86.5

[1]Reaction was performed with **A4.5** (1 eq), *t*-BuONO (1.2 eq) and *t*-BuOK (1.3 eq) with an incremental addition, 2-MeTHF (10V), 0 - 10 °C, 6 - 7 h, see experimental part for details; [2]The reactions were monitored by HPLC A% (LCAP) at 210 nm; [3]Wt% purity was measured by HPLC with a known standard; [4]A% was obtained by HPLC (210 nm); [5]The yield was corrected isolated yield based on wt%; [6]M4ALL hypothesizes the low wt% in this batch is due to the presence of trace inorganic salts, as the material showed >99 A% (HPLC, 210 nm).

Table 2.1.5 summarizes outcomes from the application of optimal conditions for **A4.6** hydrolysis, performed in 50-100 gram-scale batches. With 70 wt% glyoxylic acid (5V) gave >97% conversion and in-process analysis of the crude showed 89-90 A% (HPLC, 210 nm) **A4.8**. After aqueous workup, the isolated assay yield of **A4.8** was 60-64%, and its purity >99 A% (HPLC). Wt% purity was lower, at 84-94%. Low wt% assay was attributable to residual glyoxylic acid,[i] which could ultimately be purged during the racemic amine synthesis. Thus, **A4.8** with 84–94 wt% purity was used for the next step without further purification.

Table 2.1.5 Synthesis of aldehyde **A4.8** on hundred-gram-scale

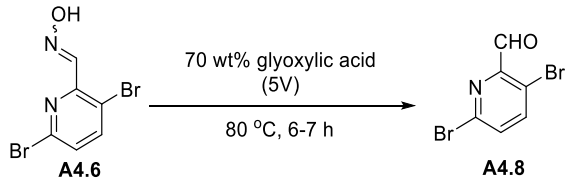

Entry[1]	Input **A4.6** (g)	IPC (A%)[2]			After purification		
		A4.6	**A4.8**	Unknown impurities[3]	**A4.8** (g)	Wt%[4]	Yield (%)[5]
1	50	3	90	7	32	94	64
2	100	2	88	10	60	86[6]	60
3	95	3	93	4	57	84[6]	61

[1]Reaction was performed with 1 eq of oxime **A4.6**, glyoxylic acid (5V, 70 w/w% in water) at 80 °C for 6-7 h; [2]A% was obtained by HPLC at 210 nm; [3]Several unknown impurities were observed (< 2 A%/each); [4]Wt% purity was obtained by GCMS measurement with a known standard; [5]Corrected isolated yield based on wt% purity; [6]Low wt% assay was attributable to residual glyoxylic acid.

[i] Residual glyoxylic acid could be removed by extensive water wash, at the expense of accompanying **A4.8** material loss. **A4.8** loss notwithstanding, the water wash process was also very time consuming. Considering glyoxylic acid is orthogonal to the following chemistry and that it can also be purged during the racemic amine synthesis, **A4.8** was not subjected to further purification.

2.2 Milestone 2: Synthesis of racemic amine **A1.5**

2.2.1 Optimization of racemic amine **A1.5** synthesis

With **A4.8** in hand, our focus shifted to the synthesis of racemic amine **A1.5**. A three-step telescoped protocol for the synthesis of **A1.5**, from aldehyde **A4.8**, is disclosed the public domain (Scheme 2.2.1).[13] Condensation of **A4.8** with diphenylmethanamine (**A4.9**) afforded the imine **A4.10**. The umpolung of imine **A4.10** allowed alkylation with 3,5-difluorobenzyl bromide (**A4.4** in the presence of excess KOH, under phase transfer catalysis, to yield **A4.11**. Hydrolysis of the newly formed imine **A4.11** with aqueous H_2SO_4 gave amine **A1.5**. While the three-step protocol was described on a small scale in the literature,[13] the disclosure lacked sufficient procedural details (e.g., yields, purification methods, purity profiles, and safety assessment) to judge fitness for scale-up.

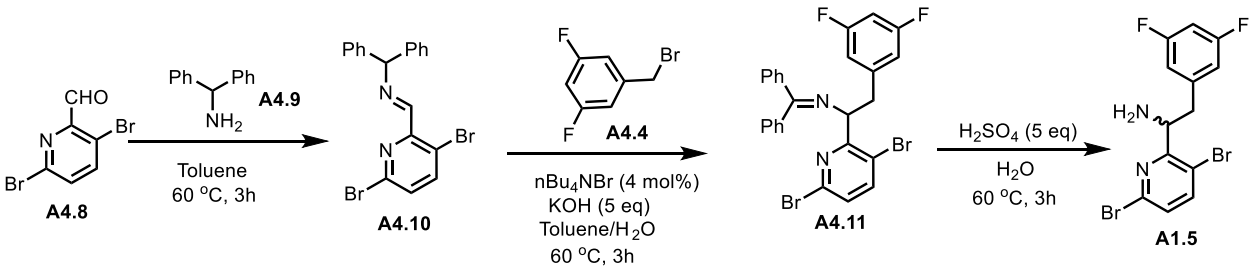

Scheme 2.2.1. Reported telescoped three-step synthesis of racemic amine **A1.5**

To deliver a practical process for the **A1.5** scale-up, key factors and parameters needed to be addressed through practical engagement with the chemistry depicted above. M4ALL would need to:

- Develop analytical standards for intermediates (**A10**, **A4.11**) (for reaction monitoring, in-process assays, development of in-process controls, etc.)
- Determine yields and purity profiles for each step before telescoping the process. The information will also allow us to allocate our efforts to optimization.
- Address the safe use of 3,5-difluorobenzyl bromide (**A4.4**), a potent lachrymator that can present safe-handling concerns at scale.
- Address the use of excess KOH, which may cause issues when scaling up (in the alkylation step).

- Address intensification opportunities in the use of excess H_2SO_4; as currently defined, the process requires large volumes of aqueous base to quench during, thus reducing volume-time-output in the last step.[19]

*2.2.1.1 Step-wise synthesis of racemic amine **A1.5***

To address the abovementioned issues, a stepwise synthesis of the racemic amine **A1.5** was launched. Synthesis of imine **A4.10** commenced with the condensation of **A4.8** (1.0 eq) and diphenylmethanamine (**A4.9**, 1.05 eq). Imination proceeded smoothly in toluene at 60 °C, providing a full conversion after 3h.[j] After removal of solvent, (removing toluene and adding IPA is difficult on scale which was solved by telescoping described below) the crude **A4.10** was obtained as a stable, tacky solid in >90% yield by qNMR; residual amine **A4.9** was the prevailing impurity. Trituration with iPrOH purged amine **A4.9** completely and gave **A4.10** as a white solid in 90% isolated yield with 99 wt% (qNMR) purity (Table 2.2.1). Thus, unknowns related to **A4.10** yield and purity profile were clarified,[k] and analytical reference standards generated.

Table 2.2 Verification of imine **A4.10** synthesis

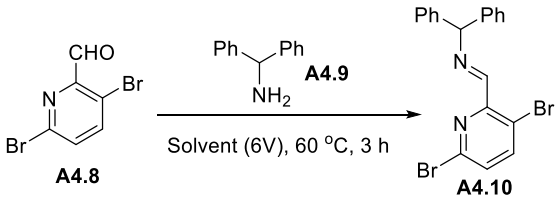

Entry	Input	Solvent	Conversion[1]	Isolated Yield[2]	Wt%[3]
1	5 g	Toluene	100.0 %	90 %	99%

[1] Conversion was measured by ^{1}HNMR; [2]Corrected yield based on qNMR purity; [3]Wt% was obtained by qNMR.

With the purified imine **A4.10** in hand, we evaluated its umpolung alkylation under the reported conditions. The reaction of **A4.10** (1.0 eq) with 3,5-difluorobenzyl bromide (**A4.4**, 1.2 eq) in the presence of KOH (5 eq) and *n*-Bu_4NBr (4 mol%) in toluene (6V) proceeded smoothly. **A4.11** was obtained in 83% yield with moderate purity (76 wt% by qNMR). During this investigation, the authors confronted 3,5-difluorobenzyl bromide's highly potent lachrymatory

[j] The imination was also evaluated in 2-MeTHF. A lower purity profile was observed, so toluene was selected for telescoping process development.
[k] Purification by crystallization will be a time-bound priority during **Frag A** scale-up activities in Year 2. Trituration was pursued here to expedite timelines pursuant Year 1 milestone compliance.

properties.[l] By comparison, its halide congener 3,5-difluorobenzyl chloride[m] (**A4.4a**) is a much less potent lachrymator and easier to handle. Thus, treatment of imine **A4.10** with **A4.4a** under the above conditions provided **A4.11** in up to 95% yield with 76 wt% (qNMR) purity (Table 2.2.2, Entry 1). Further screening of base stoichiometry showed that 1.2 eq of KOH enabled complete conversion, delivering **A4.11** in 94% yield and 87 wt% purity (Table 2.2.2, Entries 2-4).[n] Thus, scale-up concerns associated with materials compatibility (large additions of KOH) and EHS (benzyl bromide as a lachrymator) were mitigated. The unknown yields and purity profiles were also addressed.

Table 2.2.2 KOH equivalent screen in the synthesis of imine **A4.11**

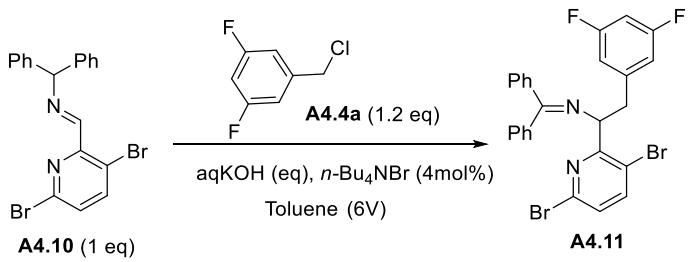

Entry[1]	KOH (eq)	Conversion of **A4.10**[2]	Crude **A4.11**[3]	
			Assay Yield (%)[4]	Wt%[5]
1	5	100%	95	76
2	1.2	100%	94	87
3	2	100%	84	71
4	3	100%	95	75

[1]The reaction was conducted with **A4.10** (1g, 1eq), **A4.4a** (1.2 eq), *n*-Bu_4NBr (4 mol%), KOH (50 wt% in water), toluene (6 mL, 6V) at 60 °C for 3h under the conditions shown in the table unless otherwise stated; [2]Conversion measured by qNMR; [3]The toluene layer was collected and evaporated to dryness for qNMR analysis; [4]Corrected yield based on qNMR purity; [5]Wt% was obtained by qNMR, and major impurity was unreacted **A4.4a**.

[l] Even small quantities have the potential to create challenging EHS conditions. SDS guidance for safe handling should be strictly observed.

[m] A two-step process was developed to synthesize 3,5-difluorobenzyl chloride (Milestone 4). It was discussed in the Appendix 4.1.

[n] Identification of impurities in crude **A4.11** will be a time-bound priority during **Frag A** scale-up activities in Year 2. The crude with 87 wt% purity was pursued here to expedite timelines pursuant Year 1 milestone compliance.

Intensification of the **A4.11**'s hydrolysis to **A1.5** was then investigated. Hydrolysis of **A4.11** with H_2SO_4 (5 eq) – as reported proceeded smoothly. Amine **A1.5** and benzophenone were the major constituents in the crude. After an acid-base workup, benzophenone was purged and the racemic amine **A1.5** was obtained as a white solid in >90% yield and >95 wt% purity (HPLC). The reported protocol invokes a large quantity of aq. KOH (7V, 50 wt%) to quench the reaction mixture, commensurate with the excess H_2SO_4 (5 eq) used in the hydrolysis. Application of 1.2 eq H_2SO_4 delivered complete hydrolysis and enabled materially reduced consumption of aq. KOH (3V, 50 wt%) during the workup,[o] however, the use of 1.2 eq H_2SO_4 generated precipitates that caused issues during the following acid-base workup, as a result, 1.2 -5 eq of H_2SO_4 was used in the hydrolysis.

Thus, optimized conditions for each step, based on the chemistry done on a step-wise basis, are as follows:

- The imine formation from **A4.8** (1.0 eq) and **A4.9** (1.2 eq) afforded **A4.10** in >90% purity (yield) in toluene (6V), 60 °C for 3h. The major impurity was unreacted **A4.9** which won't impact the next alkylation step and also can be purged easily in downstream workup.
- The alkylation of **A4.10** (1.0 eq) with 3,5-difluorobenzyl chloride (**A4.4a,** 1.2 eq) in the presence of KOH (1.2 eq) and *n*-Bu_4NBr (4 mol%) afforded **A4.11** in >95% yield with >87 wt% purity.
- The hydrolysis of **A4.11** (1.0 eq) with H_2SO_4 (1.2 -5eq) afforded racemic amine **A1.5** in > 90% yield with >95 wt% purity after an acid-base workup.

*2.2.1.2 Verification of telescoped synthesis of **A1.5***

The above-optimized conditions were then applied to the telescoping of **A1.5** from **A4.8**. The reported protocol was initially tried on a 1g-scale, followed by 5- and 10-g refinement batches. **A4.8**, treated with **A4.9,** generated **A4.10** in quantitative yield (qNMR; in-solution yield). The resulting **A4.10** solution was submitted to alkylation with **A4.4a** (1.2 eq), KOH (1.2 eq), and catalytic *n*-Bu_4NBr (4 mol%), rendering **A4.11** in 71% yield (qNMR; in-solution). The organic layer (toluene), containing **A4.11**, was retained for the final hydrolysis step. Complete conversion

[o] The hydrolysis of **A4.11** (1.0 eq) with H_2SO_4 (1.2 -5eq) proceeds smoothly, parenthetically, the use of 1.2 eq H_2SO_4 generated precipitates that caused issues during the acid-base workup. Optimization of equivalents of the H_2SO_4 with a reliable purification process will be pursued in Frag A scale-up activities in Year 2.

(hydrolysis) of **A4.11** was observed after 3 h in the presence of H_2SO_4 (5 eq). The aqueous layer was collected and the pH was adjusted to > 12 with KOH (50 wt%, 7V). The precipitated solid, crude **A1.5**, obtained in an overall 67% assay yield (qNMR) with a purity of 76 wt% (qNMR) (Table 2.2.3, Entry 1). With a 5g-scale, **A1.5** was obtained in 78% overall yield (by qNMR) with a purity of 81 wt% (qNMR) (Table 2.2.3, Entry 2). Finally, the process was verified with a 10 g-scale of **A4.8** with further purification. After imination, alkylation, and hydrolysis, the obtained solid (crude **A1.5**) was washed with toluene (2V × 3) and heptanes (2V × 3) to give **A1.5** in 75% overall isolated yield (three-step) with 96 wt% purity (by qNMR) (Table 2.2.3, Entry 3).

Table 2.2.3 Telescoped synthesis of **A1.5** from **A4.8**

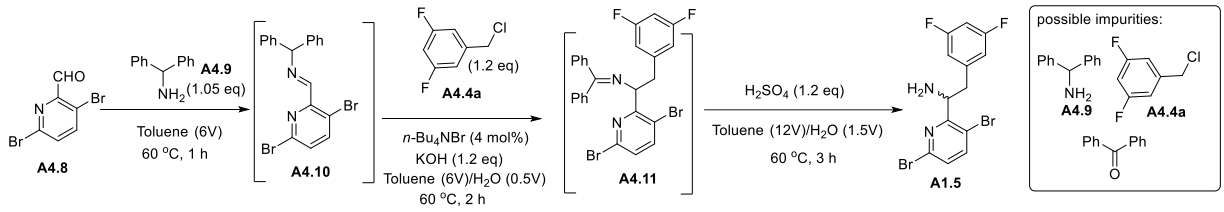

Entry[1]	Input **A4.8**	Assay yield (%)[2]		*Step-C*: Output (**A1.5**)[3]		
		Step-A **A4.10**	*Step-B* **A4.11**	Three-step yield[4]	Mass (g)	Wt%[5]
1	1g	100	71	67%	1.3	76%[6]
2	5g	100	87	78%	6.3	81%[6]
3[7]	10g	100	-[8]	75%	11.6	96%

[1]Reaction conditions: *Step-A*: **A4.8** (1 eq), A4.9 (1.05 eq), toluene (6V) at 60 °C for 3 h; *Step-B*: *n*-Bu_4NBr (4 mol%), KOH (50 wt% in water, 1.2 eq), 60 °C, 3 h; *Step-C*: H_2SO_4 (5 eq, 15 wt%), 60 °C, 3h; [2]Assay yield was obtained by qNMR; [3]After the reaction, the water layer was basified with KOH (50 wt%) to afford crude **A1.5** without further purification, unless otherwise stated, then an acid-base treatment, see experimental section for details; [4]Corrected isolated yield based on wt%; [5]Wt% purity was obtained by qNMR; [6]Low wt% of the crude was probably due to the impurities as shown in the scheme, the major impurity was byproduct benzophenone, all these impurities can be removed as shown in entry 3. [7]Crude **A1.5** was purified by toluene/heptane treatment, see experimental section (80 g scale) for details; [8]Known from Entries 1 and 2, this reaction was monitored by [1]HNMR/TLC (thin layer chromatography), and the formation of **A4.11** was not quantitated in this batch to save operating time.

2.2.2 Scale-up of racemic amine **A1.5** synthesis

The telescoped synthesis of racemic amine **A1.5** was verified on a 53 g and 80 g scale. Both batches showed similar yields and purity profiles. **A1.5** was obtained in 80-81% overall yield (three-step) with 95-97 wt% purity (HPLC). The results are summarized in Table 2.2..

Table 2.2.4 Scaling up the telescoped synthesis of **A1.5**

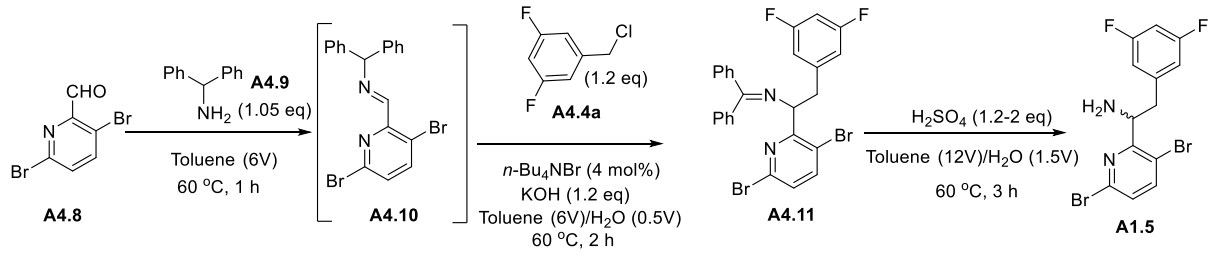

Entry[1]	Input **A4.8** (wt%)[4]	Output **A1.5** (g)	A%[5]	Wt%[6]	Yield (%)[7]
1[2]	53 g (87%)	57	99	95	80
2[3]	80 g (87%)	86	99	97	81

[1]See experimental section for details; [2]H_2SO_4 (2 eq) was used in hydrolysis; [3]H_2SO_4 (1.2 eq) was used in hydrolysis; [4]**A4.8** was made from Milestone 1; [5]A% was obtained by HPLC (210 nm); [6]Wt% was obtained by HPLC (210 nm), lower wt% might be due to solvent residues; [7]Corrected yield based on wt% purity.

2.3 Milestone 3: Resolution approach to **Frag A**

2.3.1 Optimization of **Frag A** synthesis

With the racemic amine **A1.5** in hand, our efforts were focused on dynamic kinetic resolution (DKR) to access **Frag A**.[p] DKR is also known as crystallization-induced stereoisomer transformation, which was emerged as an important tool in practical asymmetric synthesis.[17,20] More importantly, the DKR of a racemate allows for a theoretical yield of 100% rather than a theoretical yield of 50% in a classical resolution approach.

The DKR approach for resolution of **A1.5** was discovered by Gilead Sciences, Inc.,[12] however, the reported resolution was on a small scale and the lack of procedural details (i.e. purification, purity profiles) made it difficult to judge fitness for scale-up. Gram-scale reactions were conducted to familiarize ourselves with the DKR of **A1.5**. To our delight, using N-acetyl-D-leucine (NADL) as a resolving agent, the resolution of **A1.5** in the presence of 5 mol% pyridine-2-carboxaldehyde and 10 mol% ZnO afforded **(*S*)-A1.5-NADL** in 61% yield with excellent diastereoselectivity (99.6 %de) (Table 2.3.1, Entry 1). Replacement with inexpensive (*R*)-(-)-mandelic acid as the resolving agent, the resolution afforded **(*S*)-A1.5-Mandelate** in a much lower isolated yield (28%) but excellent enantioselectivity (100 %de) (Table 2.3.1, Entry 2). Thus, the

[p] Resolution of **A1.5** under traditional conditions with (*R*)-(-)-mandelic acid, L-(+)-tartaric acid, N-acetyl-D-leucine (NADL) and (1R)-(-)-10-camphorsulfonic acid was also investigated. It was found that (*R*)-(-)-mandelic acid was the best resolving agent, affording the enantiomer in 31% isolated yield with 100%de.

reaction with NADL was repeated in a 10g-scale of **A1.5 (**Table 2.3.1, Entry 3). After resolution, **(*S*)-A1.5-NADL** salt was obtained in 63% corrected overall yield with 100%de. Notably, wt% of the obtained salt was 80% and careful ^{1}HNMR scrutiny of the salt found the presence of approximately 20 wt% of free NADL. To remove NADL, the salt was treated with aq. NaOH (1.3 eq, 1M). This treatment rejected NADL completely and free amine **(*S*)-A1.5** (**Frag A**) was obtained in 95% yield with 99% qNMR purity and 100%ee (Scheme 2.3.1). The X-ray structure of **(*S*)-A1.5** obtained by single crystal X-ray crystallography confirmed the (*S*)-absolute configuration of the enantiopure amine.[q]

Table 2.3.1 Chiral acids screen for DKR of **A1.5**

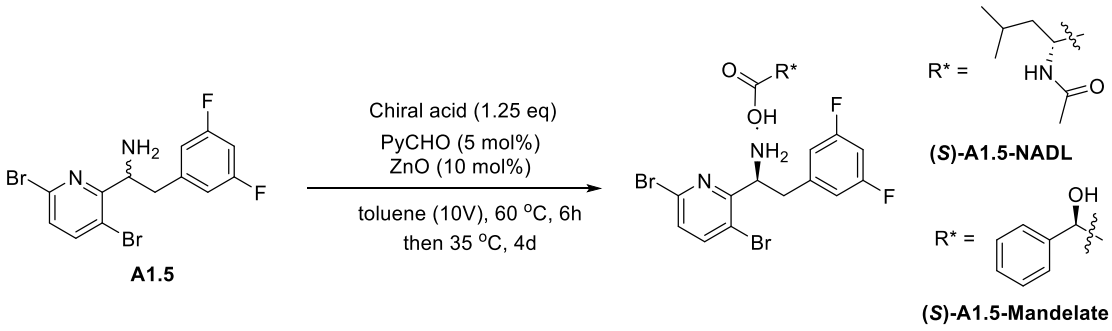

Entry	Scale	Chiral acid	Product (output)	de (%)[3]	Yield (%)[4]	Wt%	$[\alpha]_D^{20}$[5]
1[1]	1 g	N-Acetyl-D-Leucine	**(*S*)-A1.5-NADL** (1.2 g)	99.6	61	73[6]	+66.1
2[2]	1 g	(*R*)-Mandelic acid	**(*S*)-A1.5-Mandelate** (0.4 g)	100	28	60[6]	+31.2
3	10 g	N-Acetyl-D-Leucine	**(*S*)-A1.5-NADL** (11.5 g)	100	63	79[7]	+64.4

[1]Dynamic Kinetic Resolution of **A1.5** with N-Acetyl-D-Leucine (1.25 eq), 2-PyCHO (5 mol%), ZnO (10 mol%), toluene (10V), 60 °C, 6h, then 35 °C, 4 days; [2]Dynamic kinetic resolution of **A1.5** with R-(-)-Mandelic acid (1.25 eq), 2-PyCHO (5 mol%), ZnO (10 mol%), toluene (10V), 60 °C, 6h, then 35 °C, 4 days; [3]The diastereomeric excess (de) was measured by SFC (210 nm); [4]Corrected isolated yield based on wt% purity; [5]Specific rotation was recorded in MeOH (10mg/mL) at 20 °C under 589 nm; [6]Wt% was obtained by qNMR; [7]Wt% was obtained by HPLC (210 nm).

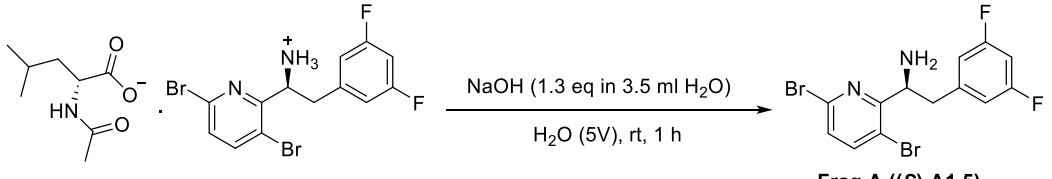

(*S*)-A1.5-NADL
1 g scale (80 wt% purity, 100%de)

Frag A ((*S*)-A1.5)
530 mg, 95% (99 wt% purity, 100%ee)

[q] Notably, enantiomers resolved from NADL and (*R*)-(-)-mandelic acid showed 100%de and (+)-sign of optical rotation number as the free amine (*S*)-**A1.5**, it is assumed that the same (*S*)-absolute configuration was obtained.

Scheme 2.3.1. Synthesis of enantiopure free amine **Frag A**

Thus, the optimized DKR conditions are:

- Resolution of **A1.5** with N-acetyl-D-leucine (1.25 eq), 2-PyCHO (5 mol%), ZnO (10 mol%), toluene (10V), 35 °C, 4 days, gave **(*S*)-A1.5-NADL** in 80 wt%, 99 A%, 100%de.
- The complex was treated with aq. NaOH (1.3 eq, 1M), 25 °C, 1h, and **(*S*)-A1.5** was obtained in 95% isolated yield with 99 wt% (qNMR), 100%ee
- This two-step protocol showed robust repeatability and afforded 65-70% overall isolated yields on 1-10 g scales.

2.3.2 Scale-up of **Frag A** synthesis

The above optimized DKR conditions for the synthesis of **Frag A** were demonstrated on two 25g-scale batches (Table 2.3.2).[r] Both batches showed similar isolated yield and purity profiles, affording **(*S*)-A1.5-NADL** in 66-68% isolated assay yield with 76-80 wt% purity (HPLC) and 100%de. As expected, the main impurity in **(*S*)-A1.5-NADL** was the remaining resolving agent NADL. To demonstrate the scalability of the de-NADL reaction, 10g of **(*S*)-A1.5-NADL** was treated with aq NaOH using the above-developed condition. After completion of the reaction, a simple aqueous workup delivered **Frag A** as a white solid in 96% assay yield with 97 wt% purity and 100%ee. As a result, the overall isolated yield of **Frag A** from **A1.5** was expected to be 63-65% under the current conditions.

Table 2.3.2 Demonstration of DKR approach to **Frag A** on decagram-scale

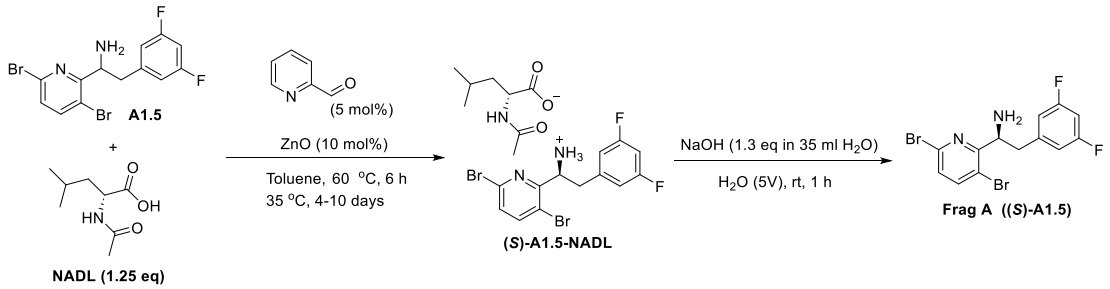

Entry[1]		Output after DKR[2]	Output after de-NADL[3]

[r] Due to the timeline of the project, we just verified the DKR conditions on 25g-scale reactions for now. Several elements related to the scale-up of this approach, such as reduction of reaction time, demonstration of 100g-scale, etc. will be addressed when we work on the API project during the next year.

	Input **A1.5**	**(S)-A1.5-NADL**	Wt%[4]	de (%)	Yield[5]	**Frag A**	Wt%[4]	Ee (%)[6]	Yield[5]	$[\alpha]_D^{20}$[7]
1	25 g	31 g	80%	100	68%	5.5 g	97	100	96%	+92.2
2	25 g	32 g	76%	100	66%	-	-	-	-	-

[1]See experimental section for details; [2]After the reaction, the precipitates were collected and washed by cold toluene (10V × 2); [3]The de-NADL was carried out with (***S*)-A1.5-NADL** (10 g, 1eq), aq NaOH (1.3 eq, 1M), H_2O (5V), 20 °C, 1h, after completion of the reaction, the precipitates were collected and dried for analysis; [4]Wt% was obtained by HPLC (210 nm); [5]Corrected yield based on wt% purity; [6]Ee was measured by SFC; [7]Specific rotation was recorded in MeOH (10mg/mL) at 20 °C under 589 nm.

3 Experimental sections

3.1 Analytical report for lenacapavir **Frag A**

Based on the 7-step process plus an additional 2 steps for **A4.4a** starting material synthesis developed by M4All for lenacapavir **Frag A** (Scheme 3.1.1), the M4All analytical team developed achiral LC-UV and chiral SFC-UV detection methods for it, its intermediates and starting materials.

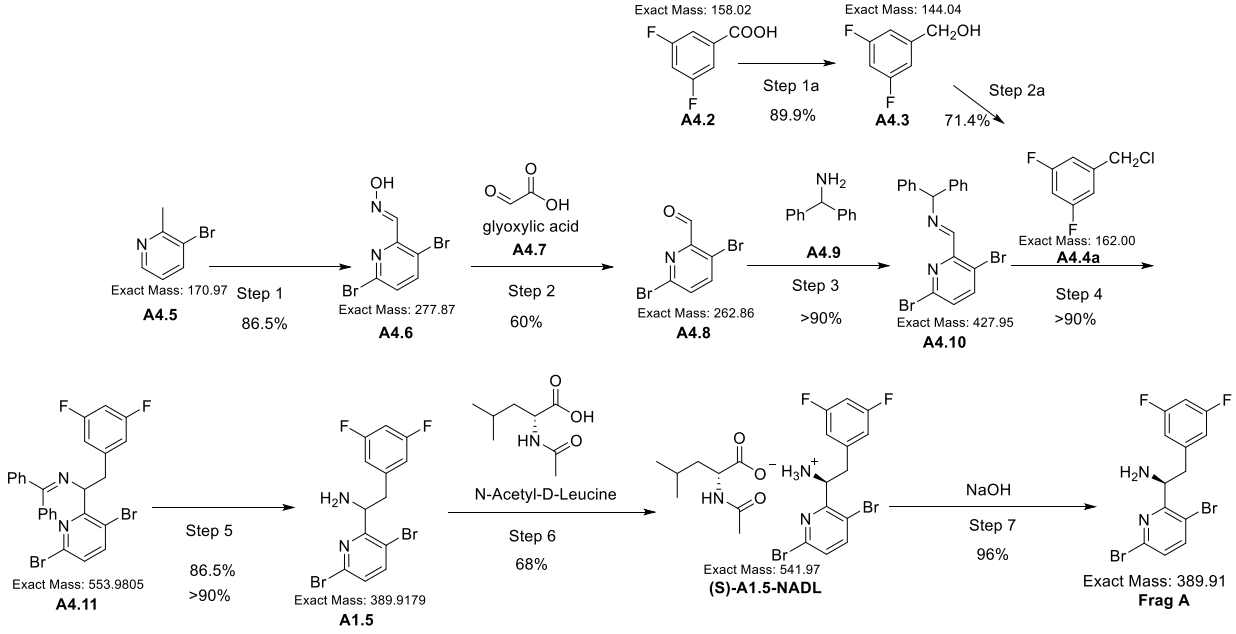

Scheme 3.1.1. Synthesis of lenacapavir **Frag A**.

3.1.1 Pharmacopoeia methods

Monographs from the United States Pharmacopoeia and the European Pharmacopeia are not available for lenacapavir **Frag A**.

3.1.2 Method development

3.1.2.1 3.1.2.1 Chromatographic conditions

Initially, method development work was performed using a GC-MS. GC-MS was chosen due to the nature of some of the initial route scouting work. As the project progressed, a LC-UV method was adopted which utilized an Agilent ZORBAX RR Eclipse Plus C18, 4.6 x 100 mm, 3.5 µm with gradient elution (0.1% phosphoric acid in water: acetonitrile) in order to allow for easier in process testing. It was later discovered this method was problematic for intermediates **A4.8** and **A4.10** as the acidic nature of the mobile phase caused degradation of these molecules.

The on-column degradation of **A4.8** and **A4.10** was solved by increasing the mobile phase buffer pH. This necessitated a change in column to comfortably accommodate a more basic mobile phase without shortening the column lifetime. The final method adopted an Agilent ZORBAX Extend-C18, 4.6 x 250 mm, 5 µm with gradient elution using 25 mM potassium phosphate buffer, pH 8.5 and methanol as mobile phases. Methanol was chosen for mobile phase B as potassium phosphate solubility in acetonitrile is low. Initial conditions were set to 60:40 (phosphate: methanol) and held for 0.5 min. At this time the mobile phase B was increased to 90% over 9.5 min and held for 15 min. Column temperature was set to 30 °C and a flow rate of 1 mL/min was used. Injection volume was 1 µL and chromatograms were collected at 210 nm and 225 nm (Figure 3.1.1). Details for LenA-1 can be found in Section 4.4.

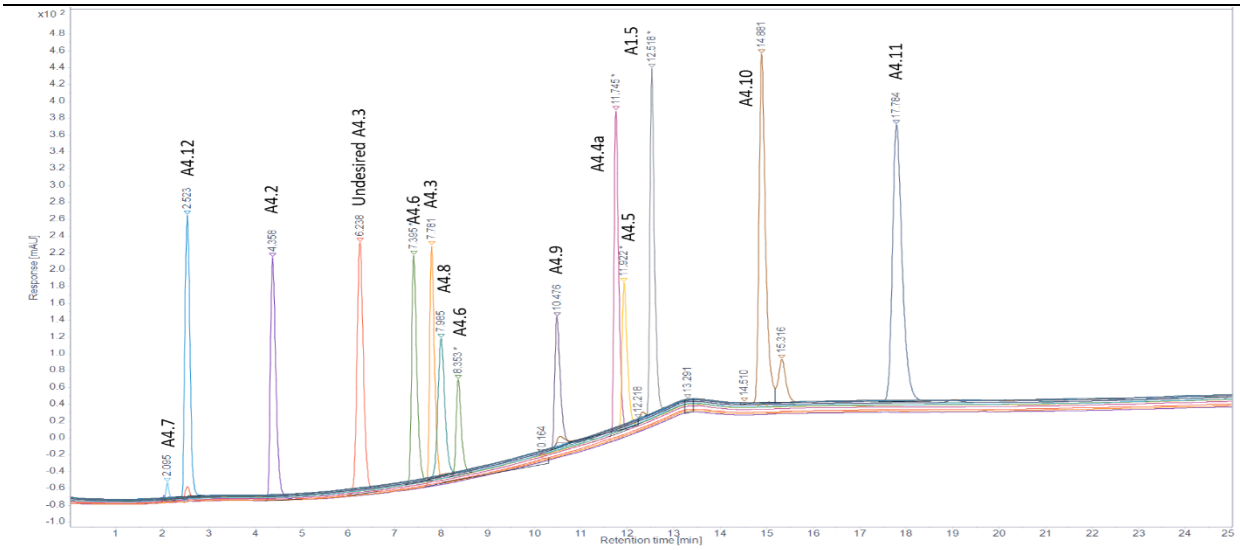

Figure 3.1.1. Chromatogram for all starting materials, intermediates and product in the synthesis of **Frag A**.

Chiral separation was needed for **A1.5** (Figure 3.1.2). This was achieved using an SFC-DAD with a Chiral Technologies CHIRALPAK IA SFC, 4.6 x 250 mm, 3 µm column. Flow rate was set to 2 mL/min with an injection volume of 5 µL. Column temperature was 25 °C. Isomers were separated isocratically with 90:10 CO_2: methanol over 10 min. Details for LenA-2 can be found in Section 4.4.

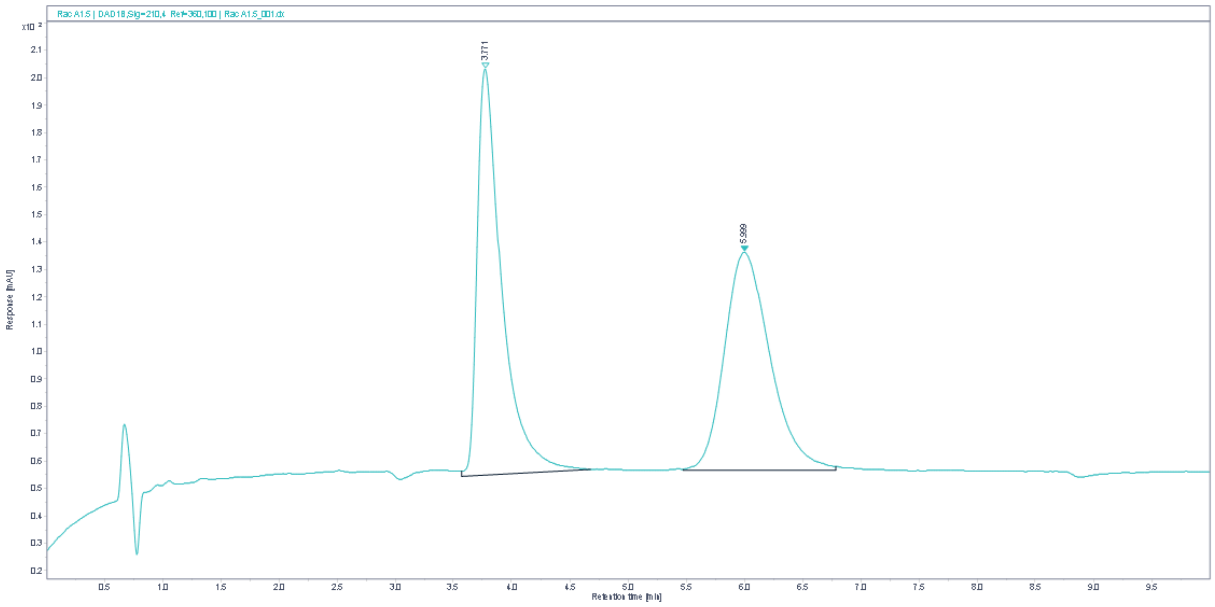

Figure 3.1.2. Chiral separation of **A1.5** after resolution (**Frag A**).

3.1.2.2 Wavelength selection and relative response factors

Ideal detection wavelengths were determined isosbestically on a stepwise basis. Starting material steps for **A4.4a** (Figure 3.1.3) and **Frag A** steps 1 and 2 (**A4.5** through **A4.8**) have the most similar responses using 210 nm (Figure 3.1.4, Figure 3.1.5). The remaining steps to **Frag A** (**A4.8** through **A4.12** and **A1.5**) have the most similar responses when 225 nm is used (Figure 3.1.6, Figure 3.1.7, Figure 3.1.8). Relative response factors (Table 3.1.1) for each step were determined stepwise using both mass concentration and molar concentrations (Eqn 3.1.2.1).

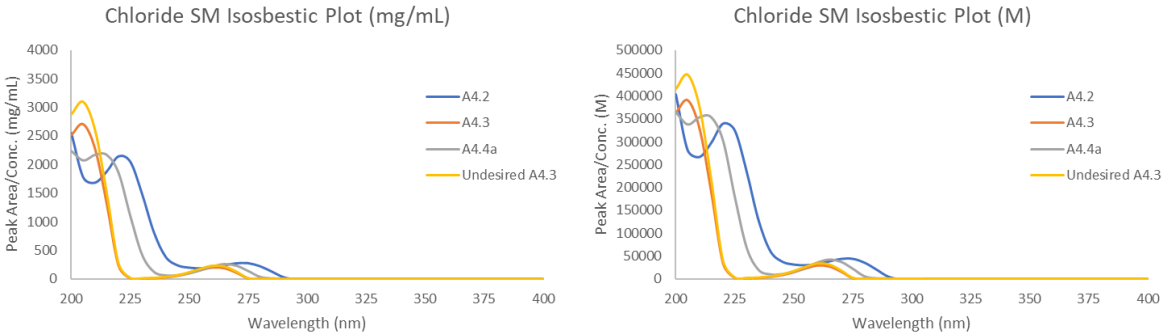

Figure 3.1.3. Isosbestic plots for synthesis of the chloride starting material **A4.4a**.

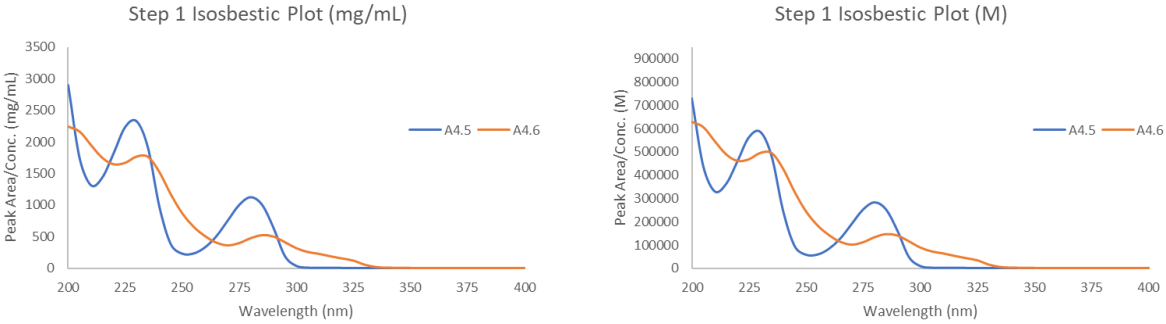

Figure 3.1.4. Isosbestic plots for synthesis of the **A4.6**.

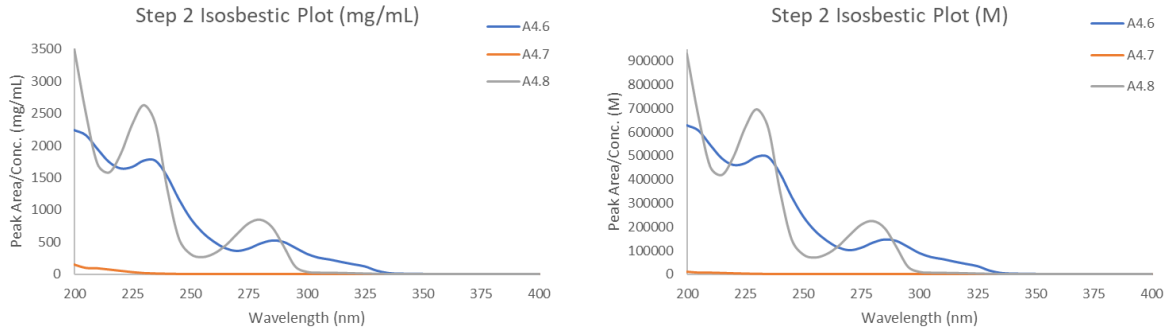

Figure 3.1.5. Isosbestic plots for synthesis of the **A4.8**.

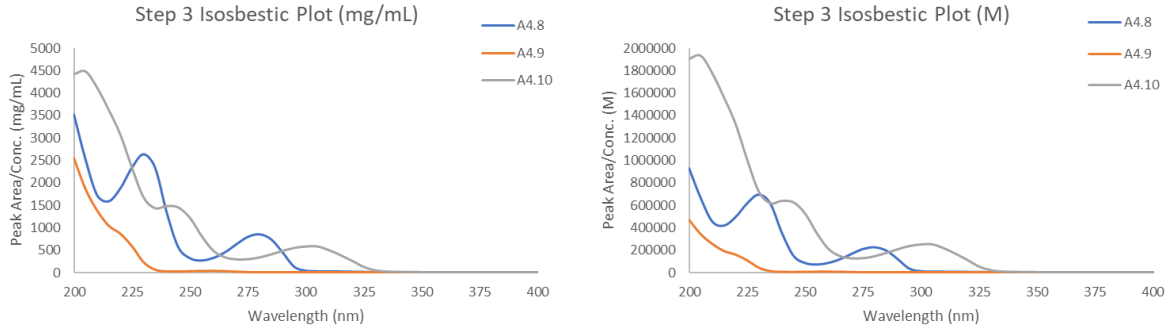

Figure 3.1.6. Isosbestic plots for synthesis of the **A4.10**.

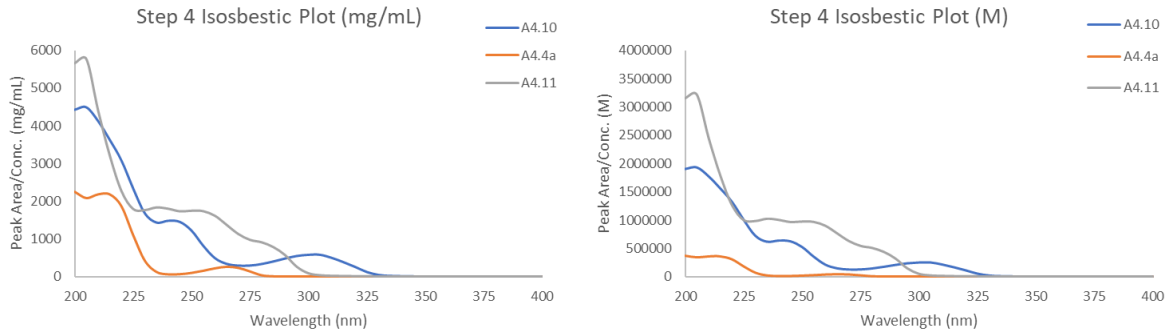

Figure 3.1.7. Isosbestic plots for synthesis of the **A4.11**.

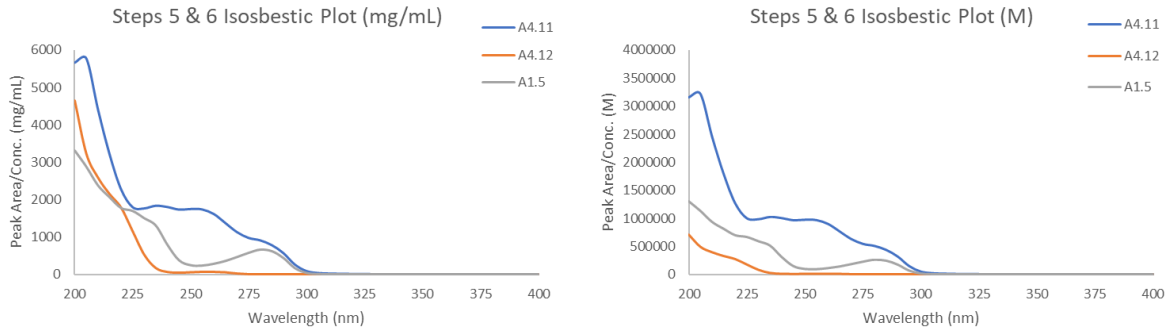

Figure 3.1.8. Isosbestic plots for synthesis of the racemic and enantiopure **A1.5**.

$$Relative\ RF = \frac{\left(Analyte\ 2\ Peak\ Area / Analyte\ 2\ Conc.\right)}{\left(Analyte\ 1\ Peak\ Area / Analyte\ 1\ Conc.\right)} \qquad (3.1.2.1)$$

Table 3.1.1. Retention Times and Relative Response Factors for Starting Materials, Synthetic Impurities and **Frag A** at 210 and 225 nm

Synthesis of A4.4a, Step 1						
Compound	**Time (min)**	**RRT***	**RRF at 210 nm**		**RRF at 225 nm**	
			(mg/mL)	**(M)**	**(mg/mL)**	**(M)**
A4.2	4.4	0.56	0.93	1.0	123	135
Undesired A4.3	6.3	0.81	1.1	1.1	1.1	1.1

A4.3	7.8	1.0	1.0	1.0	1.0	1.0
Synthesis of A4.4a, Step 2						
Compound	**Time (min)**	**RRT**	**RRF at 210 nm**		**RRF at 225 nm**	
			(mg/mL)	**(M)**	**(mg/mL)**	**(M)**
Undesired A4.3	6.3	0.54	1.1	1.1	0.02	0.01
A4.3	7.8	0.67	0.83	0.73	0.01	0.01
A4.4a	11.7	1.0	1.0	1.0	1.0	1.0
Synthesis of Frag A, Step 1						
Compound	**Time (min)**	**RRT**	**RRF at 210 nm**		**RRF at 225 nm**	
			(mg/mL)	**(M)**	**(mg/mL)**	**(M)**
A4.6	7.4 8.4	-	-	-	-	-
A4.5	11.9	-	-	-	-	-
Synthesis of Frag A, Step 2						
Compound	**Time (min)**	**RRT**	**RRF at 210 nm**		**RRF at 225 nm**	
			(mg/mL)	**(M)**	**(mg/mL)**	**(M)**
A4.7	2.1	0.26	0.05	0.01	0.01	0.004
A4.6	7.4 8.4	0.93 1.05	-	-	-	-
A4.8	8.0	1.0	1.0	1.0	1.0	1.0
Synthesis of Frag A, Step 3						
Compound	**Time (min)**	**RRT**	**RRF at 210 nm**		**RRF at 225 nm**	
			(mg/mL)	**(M)**	**(mg/mL)**	**(M)**
A4.8	8.0	0.54	0.42	0.26	1.0	0.61
A4.9	10.5	0.71	0.33	0.14	0.25	0.11
A4.10	14.9	1.0	1.0	1.0	1.0	1.0

Synthesis of Frag A, Step 4						
Compound	**Time (min)**	**RRT**	**RRF at 210 nm**		**RRF at 225 nm**	
			(mg/mL)	**(M)**	**(mg/mL)**	**(M)**
A4.4a	11.7	0.66	0.49	0.14	0.61	0.18
A4.10	14.9	0.84	0.93	0.72	1.3	1.0
A4.11	17.8	1.0	1.0	1.0	1.0	1.0
Synthesis of Frag A, Step 5						
Compound	**Time (min)**	**RRT**	**RRF at 210 nm**		**RRF at 225 nm**	
			(mg/mL)	**(M)**	**(mg/mL)**	**(M)**
A1.5	12.5	1.0	1.0	1.0	1.0	1.0
A4.11	17.8	1.4	1.8	1.6	1.1	1.5
Synthesis of Frag A, Step 6						
Compound	**Time (min)**	**RRT**	**RRF at 210 nm**		**RRF at 225 nm**	
			(mg/mL)	**(M)**	**(mg/mL)**	**(M)**
A4.12	2.5	0.20	1.1	0.42	0.68	0.26
A1.5 (**Frag A**)	12.5	1.0	1.0	1.0	1.0	1.0

*RRT = relative retention time

3.1.2.3 UV spectra

UV spectra of each compound can be found in Section 4.4.

3.1.2.4 Linearity

A1.5, which corresponds to **Frag A**, was tested over the range of 0.07 mg/mL to 1.1 mg/mL. A 1/x weighted, 7-level curve over this range was linear with an $R^2 > 0.99$ (Figure 3.1.9).

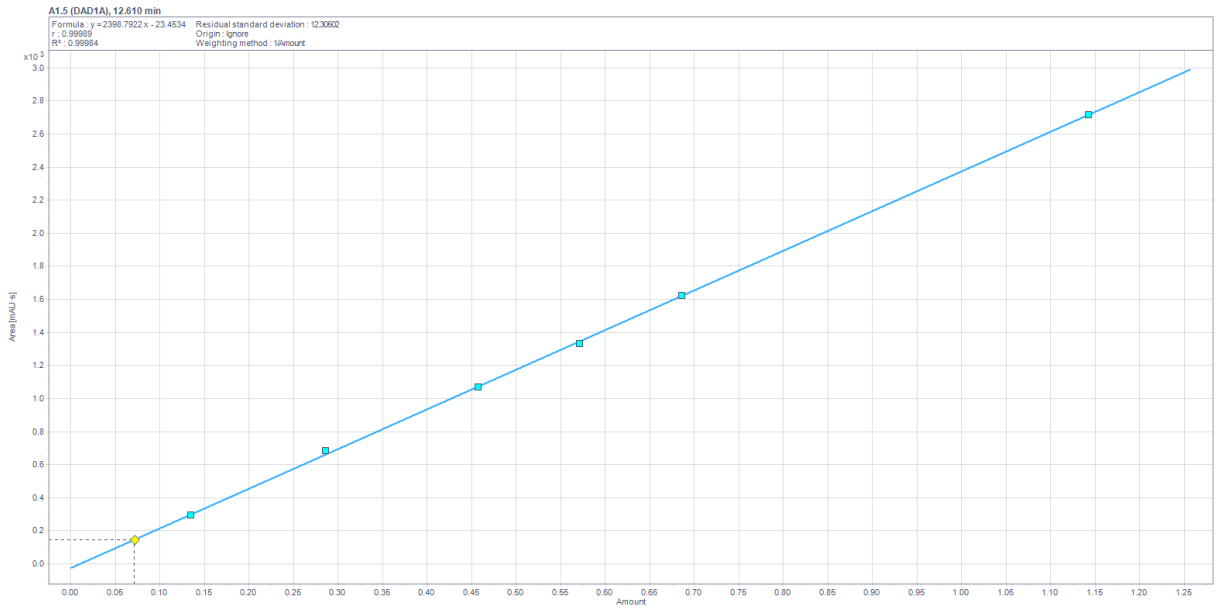

Figure 3.1.9. 7-Level calibration curve for **A1.5**.

3.1.2.5 Limit of detection (LOD) and limit of quantitation (LOQ)

Limits were not determined for the starting materials, intermediates, impurities or product.

3.1.3 Impurities

3.1.3.1 Starting material impurities

Impurities were not specified nor determined for lenacapavir **Frag A** (salt of **A1.5**) starting materials.

3.1.3.2 Synthesis impurities

Impurities were not isolated and characterized for lenacapavir **Frag A** (salt of **A1.5**) or for the intermediates en route to **A1.5**.

3.1.4 Forced degradation studies

Forced degradation studies were not performed for lenacapavir **Frag A** (salt of **A1.5**) nor its starting materials, intermediates and impurities.

3.1.5 Methods

Analytical methods used to support the synthesis of lenacapavir **Frag A** (salt of **A1.5**) are appended to this report (Section 4.4).

3.1.5.1 Key starting materials

A4.2, **A4.3**, **A4.4a**, **A4.5**, **A4.7**, **A4.9**, and **A4.12** are analyzed via LC-UV using the method "LenA-1".

3.1.5.2 Reagent and solvents

Toluene, dichloromethane (DCM) and heptane were analyzed using the GC-MSD method "GC Solvents".

3.1.5.3 Intermediates

The **A4.6**, **A4.8**, **A4.10** and **A4.11** are synthetic intermediates in this process. These intermediates as well as crude and isolated **A1.5** are analyzed via LC-UV using "LenA-1".

3.1.5.4 In-process controls (IPC)

Requirements for IPCs were not set on this process. However, when IPCs were collected, they were analyzed via LC-UV using the "LenA-1" method.

3.1.5.5 Final product analysis

Isolated **Frag A** (enantiopure **A1.5**) was assayed using the "LenA-1" method on LC-UV. This material was also subjected to chiral SFC-UV analysis (LenA-2), KF titration of water content and residual solvent analysis by GC-MS for toluene, dichloromethane (DCM) and heptane ("GC Solvents").

3.1.5.6 Method appropriateness

During development of the "LenA-1" certain performance characteristics were evaluated to select analytical conditions. These results are described above and include linearity and limits of detection. This method was not tested for specificity. Method validation was not performed.

3.2 Detailed experimental procedure

3.2.1 General method

Reagents and solvents were obtained from commercial suppliers and used as received unless otherwise indicated. Where applicable, reactions were conducted in oven-dried (120 °C) glassware, which was assembled while hot, and cooled to ambient temperature under an inert atmosphere. Reactors were pre-rinsed with reaction solvent and subjected to evacuation/back-fill cycles (3×) as necessary. Reactions were monitored by TLC (precoated silica gel 60 F254 plates, EMD Chemicals), Agilent GCMS or crude ^{1}H NMR. HRMS was recorded using Perkin Elmer Axion 2 ToF MS, ionization mode: positive with scan range: 100 - 1000 m/z, flight tube voltage: 8 kV, spray voltage: 3.5 kV, solvent: methanol. TLC was visualized with UV light. The proton (^{1}H NMR), carbon (^{13}C NMR) and 2-DNMR spectra of the compounds were recorded on Bruker Avance III HD Ascend 600 MHz spectrometer. The NMR solvents used were DMSO-d_6, $CDCl_3$ and CD_3OD. The chemical shifts were reported in parts per million (ppm). Coupling constants J

are reported in hertz (Hz). The abbreviations used to designate signal multiplicity were: s, singlet; d, doublet; t, triplet; q, quartet, p, pentet; dd, doublet of doublets; ddd, doublet of doublet of doublets; dt, double of triplets; ddt, doublet of doublet of triplets; m, multiplet; br, broad.

3.2.2 Experimental section

Synthesis of oxime **A4.6**

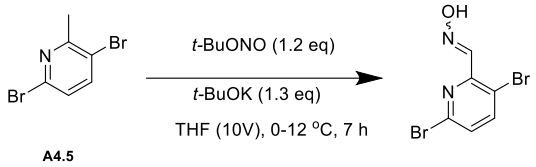

A 5L jacketed reactor equipped with an overhead stirrer and thermocouple for internal temperature monitoring was charged with 2-MeTHF (2L, 10V) and 2,5-dibromomethylpyridine **A4.5** (200 g, 797 mmol). The mixture was stirred for 10 min at 210 rpm, then cooled to 0-5 °C. *t*-BuONO (116 mL, 876.8 mmol, 1.1 eq) was added slowly over 20 min, then followed by the addition of *t*-BuOK (98.38 g, 876.8 mmol, 1.1 eq) in 2-MeTHF (878 mL) over 30 min, maintaining the internal temperature below 10 °C. After addition, the reaction mixture was stirred at 0-5 °C. During the course, the reaction was monitored by HPLC every 1 h. About 2 h later, HPLC showed 16 A% **A4.5** remaining. Additional *t*-BuONO (5.3 mL, 39.85 mmol, 0.1 eq) and *t*-BuOK (6.70 g, 59.78 mmol, 0.15 eq) in 2-MeTHF (59.8 mL) were added at 0-5 °C then the mixture was stirred for another 5 h. The A% of **A4.5** was < 1%. The mixture was diluted with 2-MeTHF (200 mL), then 10% sat. NH_4Cl (5V) was added slowly over 30 min (temperature was slightly increased +2 °C). The mixture was concentrated until 2-MeTHF (400 mL, 2V) remained. The obtained heterogeneous mixture was diluted with DI water (1 L, 5V). The precipitate was filtered and washed with DI water (600 mL, 3V). The solid was dried at 45 °C under 25 mmHg to afford 207 g of light-yellowish oxime **A4.6** in 86.5% of yield (93.1 wt% purity by HPLC, KF: 0.26 wt%).

^{1}HNMR (600 MHz, DMSO-d_6): δ 11.70 (d, *J* = 3.5 Hz, 1H), 8.15 – 7.97 (m, 1H), 7.67 (s,1H), 7.64 – 7.55 (m, 1H).

^{13}C NMR (151 MHz, DMSO): δ 151.74, 143.22, 143.03, 139.15, 129.35, 119.44.

Melting Point: 191 °C

IR (ATR, DCM) ν_{max} = 3309, 1587, 1388, 1140, 892.

HRMS *m/z*: $[M+H]^+$ calcd for $C_6H_4Br_2N_2O \cdot H^+$, 278.8763; found: 278.8743.

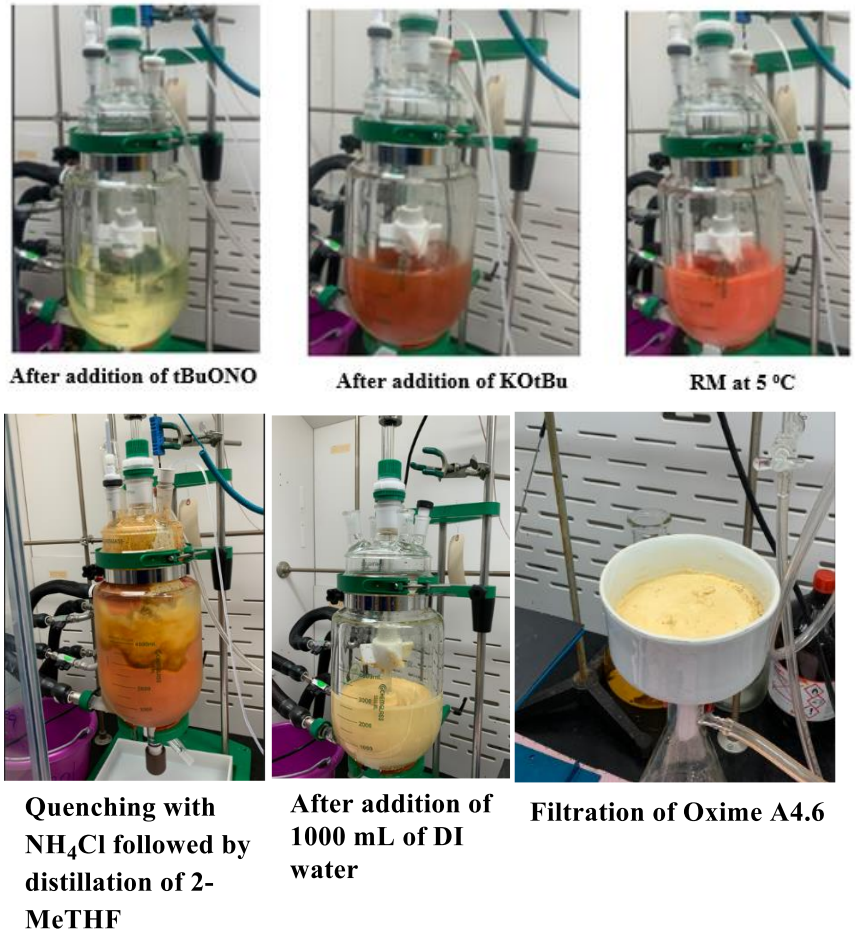

Figure 3.2.1. Pictures of scale-up synthesis of oxime **A4.6**

Synthesis of 3,6-dibromopicolinaldehyde **A4.8**

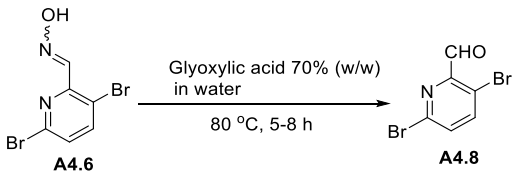

To a 2 L jacketed glass reactor equipped with an overhead stirrer and thermocouple was charged with 70% (w/w) glyoxylic acid (467 g) in water (200 mL) and stirred for 5 min at 370 rpm. The solution was warmed to 80-85 °C, and oxime **A4.6** (100 g, 332.60 mmol) was added in one portion *via* an addition funnel. The reaction mixture was stirred at 80-85 °C for 7-8 h. After completion of the reaction (monitored by HPLC), the mixture was cooled to 0-5° C and stirred for 30 min. The suspension was drained and the reactor was washed with cold water (300 mL, 3V). Suspensions

were combined and filtered. The filter cake was washed with cold water (100 mL, 1V) (pH of the filtrate was found to be 2-3). The wet solid (85g) was taken back into the reactor and suspended in water (250 mL, 2.5V) and stirred for 30 min at 20 °C. The precipitate was collected by filtration and washed cold water (250 mL, 2.5V) (filtrate showed pH 3-4). The washing process was repeated until the pH of the filtrate was 5-6. The resulting solid was dried at 55 °C under vacuum to afford 60 g of **A4.8** (86 wt% by GCMS, KF: 0.2%, corrected assay yield: 60%).

^{1}H NMR (600 MHz, DMSO-d$_6$): δ 9.95 (s, 1H), 8.21 (d, *J* = 8.4 Hz, 1H), 7.86 – 7.82 (m, 1H).

^{13}C NMR (151 MHz, DMSO): δ 189.45, 148.70, 145.74, 140.22, 133.24, 120.34.

Melting Point:125 °C.

IR (ATR, DCM) ν_{max} = 2877, 1694, 1543, 1412, 1382.

HRMS *m/z*: $[M+H]^+$ calcd for $C_6H_3Br_2NO{\cdot}H^+$, 263.8654; found: 263.8637.

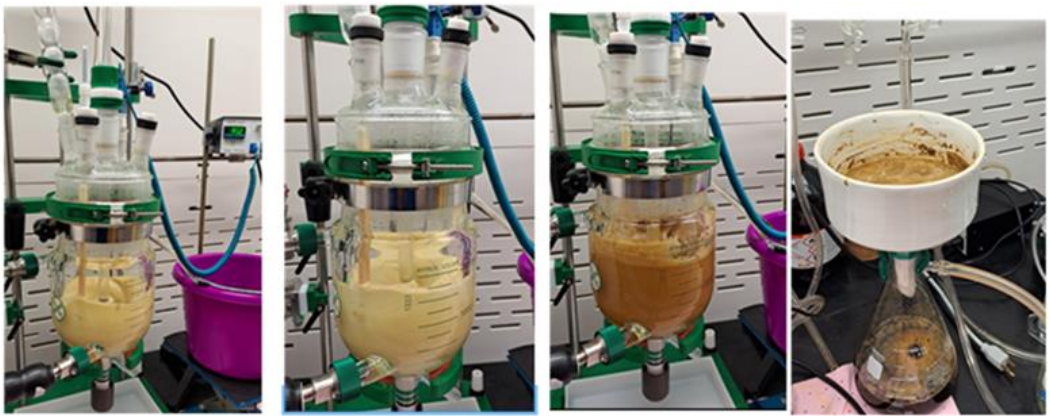

Figure 3.2.2. Pictures of scale-up synthesis of aldehyde **A4.8**

Synthesis of 3,5-difluorobenzyl alcohol **A4.3**

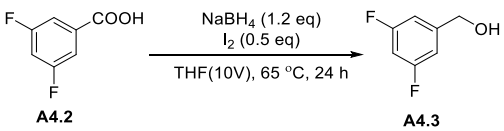

A 2 L round bottle flask equipped with an overhead stirrer was charged $NaBH_4$ (28.7 g, 759.0 mmol) in THF (400 mL, 4V), followed by the addition of 3,5-difluorobenzoic acid **A4.2** (100 g, 632.5 mmol) in THF (300 mL, 3V) at 0 ºC. To the mixture, iodine (80.2 g, 316.2 mmol) in THF (300 mL, 3V) was added slowly. After addition, the mixture was heated at 65 °C and stirred for 24 h. After completion of the reaction, the mixture was cooled to 0-5 °C. Ice-cold water (1 L, 10V)

was added and the mixture was extracted with ethyl acetate (1 L (10V) × 2). The combined organic layer was washed with 10% *aq.* NaCl solution (1L, 10V). The organic layer was evaporated under reduced pressure to obtain the desired alcohol **A4.3** as colorless liquid (104.12 g, corrected assay yield: 89.9 %, purity: 93.7 A% by HPLC).

^{1}H NMR (600 MHz, $CDCl_3$): δ 7.25 (dq, *J* = 8.3, 6.6 Hz, 1H), 6.88 (t, *J* = 7.8 Hz, 2H), 4.76 (d, *J* = 5.4 Hz, 2H), 2.21 (s, 1H).

^{13}C NMR (151 MHz, $CDCl_3$): δ 163.11 (dd, *J* = 249.1 Hz, 12.6 Hz), 144.80 (t, *J* = 8.6 Hz), 109.10 (dd, *J* = 20.2, 5.1 Hz), 102.69 (t, *J* = 25.6 Hz), 63.91.

^{19}F NMR (564 MHz, $CDCl_3$): δ -108.5.

IR (ATR, DCM) ν_{max}: 3400, 1627, 1595, 1554, 1459, 1414, 1187.

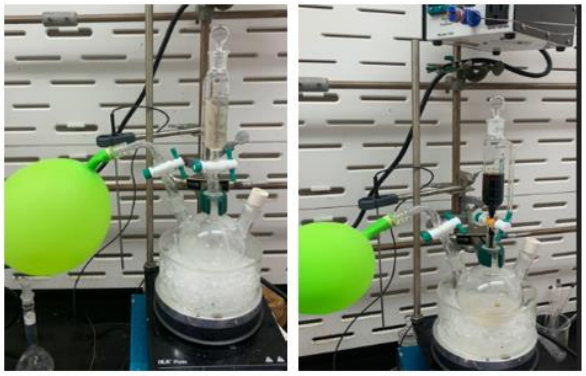

Addition of 3,5-difluorobenzoic acid **A4.2**

Addition of I_2 to the reaction mixture

Figure 3.2.3. Reaction set up for synthesis of 3,5-difluorobenzyl alcohol **A4.2**

Synthesis of 3,5-difluorobenzyl chloride **A4.4a**

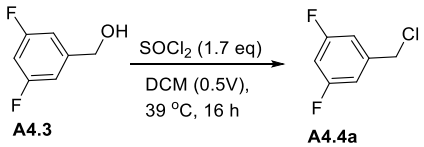

3,5-Difluorobenzyl alcohol **A4.3** (40.9 g, 284.14 mmol) and DMF (0.944 g, 1.0 mL, 4 mol%) dissolved in CH_2Cl_2 (20 mL). To the mixture thionyl chloride (58.95 g, 35.7 mL, 1.7 eq) was added slowly at 0 °C (internal temperature was maintained between 2-5 ° C during the time of addition). After addition, the mixture was refluxed at 39 °C for 16 h. After the completion of the reaction (confirmed by TLC monitoring and HPLC analysis), the reaction mixture was subject to

distillation. The distillate at 89.3 °C under 22-88 mmHg was collected (38.4 g, containing trace amount of $SOCl_2$). The collected fraction was washed with aq. saturated solution of $NaHCO_3$ (50 mL) and ice-cold water (100 mL). The organic layer was concentrated under reduced pressure to obtain the product as a pale-yellow liquid (See Figure 3.2.4) (33 g, isolated yield: 71.4%, purity: 100 wt% by HPLC).

^{1}H NMR (600 MHz, $CDCl_3$): δ 6.93 (dd, *J* = 7.8 Hz, J = 1.8 Hz, 2H), 6.77 (tt, *J* = 8.9 Hz, J = 2.2 Hz, 1H), 4.53 (s, 2H).

^{13}C NMR (151 MHz, $CDCl_3$): δ 162.97 (dd, *J* = 249.5, 12.7 Hz), 140.92 (t, *J* = 9.3 Hz), 111.38 (dd, *J* = 20.4, 5.4 Hz), 103.81 (t, *J* = 25.2 Hz), 44.64 (t, *J* = 2.1 Hz).

^{19}F NMR (564 MHz, $CDCl_3$): δ -109.8.

IR (ATR, DCM) ν_{max}: 1627, 1600, 1461, 1442, 1326, 1269, 1120.

MS-EI (*m/z*): 162 and 127

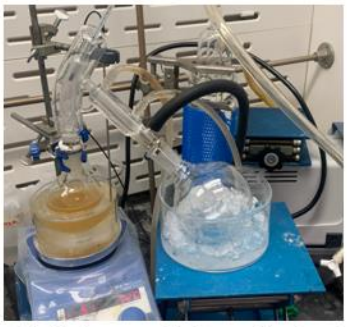

Distillation setup for the purification of 3,5-Difluorobenzyl chloride **A4.4a**

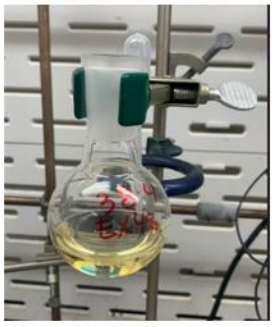

Isolated 3,5-Difluorobenzyl chloride **A4.4a**

Figure 3.2.4. Purification of 3,5-difluorobenzyl chloride **A4.4a**

Synthesis of racemic amine **A1.5**

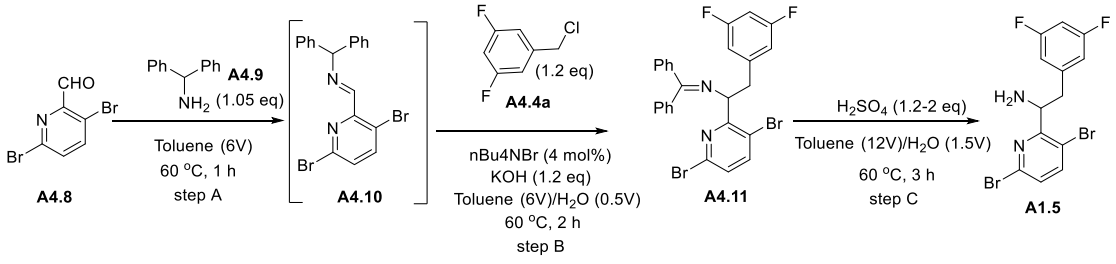

Step A: To a 2 L RB reactor was charged 3,6-dibromopicolinaldehyde **A4.10** (80.0 g, 87 wt%, 1 eq, 262.7 mmol), toluene (480.0 mL, 6V, Sigma, anhydrous) and diphenylmethanamine **A4.9** (50.55 g, 1.05 eq, 275.90 mmol). The reaction mixture was heated to 60 °C and stirred for 1 h. HPLC showed completion of the reaction.

Step B: To the above reaction mixture tetrabutylammonium bromide (3.39 g, 0.04 eq, 10.51 mmol), 3,5-difluorobenzyl chloride **A4.4a** (51.25 g, 1.2 eq, 317 mmol) and 25% aqueous KOH (20.81 g, 85 wt%, 1.2 eq, 315.3 mmol in 46 mL water) was added. The reaction mixture was stirred for 3 h at 60 °C. After 3 h (^{1}HNMR showed completion of the reaction), 160 mL of toluene (2V) and 160 mL of water (2V) were added and stirred for 10 min. The toluene layer was collected and washed with water two times (240 mL (3V) and 160 mL (2V)). The combined water layer was extracted with toluene two times (160 mL (2V) × 2). The combined toluene layers were charged to the reactor for the next step (Step C).

Step C: The above toluene solution was heated to 60 °C. Sulfuric acid (31.53 g, 98% wt, 1.2 eq, 315.3 mmol) was dissolved in 127 mL water and this resulting solution was added to the warm toluene solution. The reaction mixture was stirred at 60 °C for 2 h. After 2 h, the reaction mixture was cooled to 20 °C. The toluene layer was separated, and washed with water 3 times (160 mL, 240 mL, and 160 mL, 7V in total). The combined water layers were washed with heptane 2 times (240 mL, 160 mL, 5V in total). During the heptane wash, pale-yellowish solids were precipitated. The heptane layer was discarded and both solids and water layer were collected for further purification. The solid (~30 g) was dissolved in methanol (105 mL, 3.5V) at 60 °C, stirred for 10 min, and cold water (300 mL, 10V) was added slowly at 20 °C to obtain the 1st crop of **A1.5** as a beige solid (30 g). The aqueous layer was further washed with toluene 3 times (160 mL, 240 mL, and 160 mL, 7V in total). The colorless aqueous layer was basified with 35 mL (50% KOH) solution. The precipitate was filtered and dried to afford the 2nd crop **A1.5** as a beige solid (56.5 g). After combined two crops of solids, 86.5 g of **A1.5** was obtained, 81% assay corrected yield; wt%: 97% by HPLC; A%: 99% by HPLC.

^{1}H NMR (600 MHz, $CDCl_3$): δ 7.64 (d, *J* = 8.2 Hz, 1H), 7.33 – 7.17 (m, 1H), 6.74 (d, *J* = 6.9 Hz, 2H), 6.67 (t, *J* = 8.9 Hz, 1H), 4.67 – 4.41 (m, 1H), 3.06 (dd, *J* = 13.5, 5.1 Hz, 1H), 2.84 – 2.67 (m, 1H); 1.80 (bs, 2H)

^{13}C NMR (151 MHz, $CDCl_3$): δ 163.0 (dd, *J* = 248.0, 13.0 Hz), 162.7, 142.7, 142.5 (t, *J* = 8.9 Hz), 140.6, 128.2, 119.1, 112.3 (dd, *J* = 19.7, 4.7 Hz), 102.2 (t, *J* = 25.4 Hz), 56.1, 43.7.
^{19}F NMR (565 MHz, $CDCl_3$): δ -110.3.

Melting point: 92 °C.

IR (ATR, DCM) ν_{max} = 3360, 3030, 3060, 1590, 1490, 1120, 1000, 830.

HRMS *m/z*: [M+H]+ calcd for $C_{13}H_{10}Br_2F_2N_2 \cdot H^+$, 390.9252; found: 390.9253.

Figure 3.2.5. Pictures of scale-up of synthesis of *racemic* amine **A1.5**

Synthesis of **(S)-A1.5-NADL** *via* DKR reaction

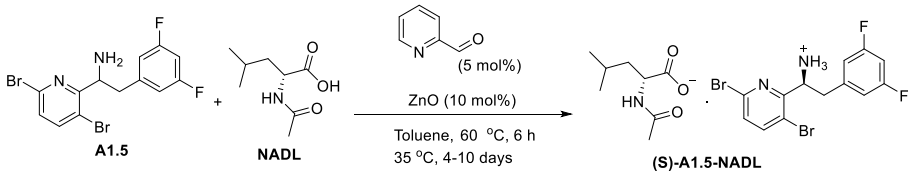

A 1 L three-necked round bottom flask was equipped with an overhead stirrer and a N_2 bubbler. **A1.5** (25 g, 63.76 mmol, 1 eq), N-acetyl-D-leucine (13.80 g, 79.71 mmol, 1.25 eq) and ZnO (519.1 mg, 6.37 mmol, 0.1 eq) in anhydrous toluene (625 mL, 25V) was charged to the flask, followed by addition of pyridine-2-carboxaldehyde (341.51 mg, 3.18 mmol, 0.05 eq) under N_2 atmosphere. The reaction mixture was heated to 60 °C and stirred for 6 h, then cooled to 35 °C and stirred for 4 days. The mixture was cooled to 20 °C. The resulting solid product was collected by filtration and the filter cake was washed with cold toluene (250 mL (10V) × 2). The solid was dried under

vacuum at 25 °C overnight to afford **(*S*)-A1.5-NADL** as a white solid in 68% yield (30.6 g, 100% ee, 80 wt% purity by HPLC).

^{1}H NMR (600 MHz, DMSO-d6): δ 8.02 (d, *J* = 7.6 Hz, 1H), 7.95 (d, *J* = 8.3 Hz, 1H), 7.49 (d, *J* = 8.3 Hz, 1H), 7.02 (t, *J* = 9.4 Hz, 1H), 6.86 (d, *J* = 6.7 Hz, 2H), 4.52 – 4.37 (m, 1H), 4.18 (q, *J* = 7.7 Hz, 1H), 2.94 (dd, *J* = 13.3, 5.9 Hz, 1H), 2.87 (dd, *J* = 13.2, 7.9 Hz, 1H), 1.83 (s, 3H), 1.65 – 1.57 (m, 1H), 1.47 (t, *J* = 7.3 Hz, 2H), 0.88 (d, *J* = 6.6 Hz, 3H), 0.83 (d, *J* = 6.5 Hz, 3H).

^{13}C NMR (151 MHz, DMSO-d6): δ 174.9, 169.6, 163.3 (d, *J* = 13.4 Hz), 162.9, 161.7 (d, *J* = 13.4 Hz), 143.9, 143.6 (t, *J* = 9.4 Hz), 140.2, 128.7, 119.7, 112.9 (dd, *J* = 19.7, 4.6 Hz), 102.1 (t, *J* = 25.7 Hz), 55.9, 50.9, 42.5, 40.8, 24.8, 23.4, 22.8, 21.9.

^{19}F NMR (565 MHz, $CDCl_3$): δ -110.9.

Melting Point:164 °C

IR (ATR, DCM) ν_{max} = 3360, 3030, 3060, 1590, 1490, 1120, 1000, 830.

Diastereomeric excess (*de*): 100%, desired (SFC)

Specific rotation: $[\alpha]_D^{20}$ = +64.4 (deg·mL·g^{-1}·dm^{-1}) (measured in MeOH (10mg/mL) at 20 °C under 589nm)

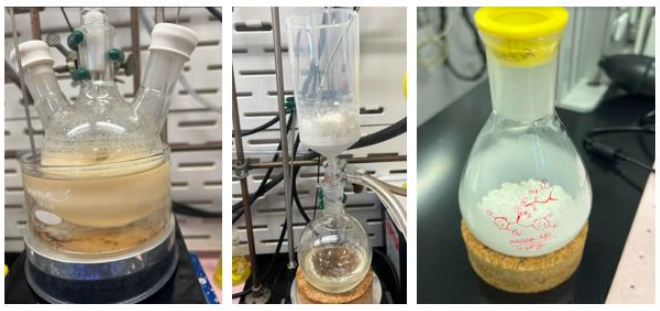

Figure 3.2.6. Representative pictures of scale-up synthesis of **(*S*)-A1.5-NADL** on 10 g scale

Synthesis of Frag A

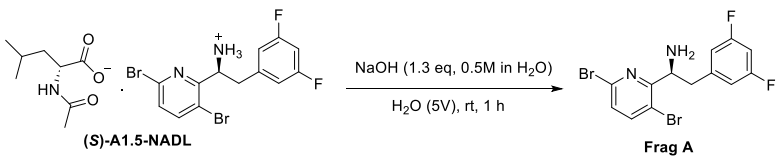

(*S*)-A1.5-NADL (10 g, 12.2 mmol, 1 eq, 80 wt% purity) and water (50 mL, 5V) were charged to a 250 mL three-necked round bottom flask equipped with overhead stirrer under N_2 atmosphere.

To this slurry aq. NaOH (16 mmol, 630 mg, 1.3 eq in 30 mL water, 3V) was added at 20 °C. The reaction mixture was stirred at the same temperature for 1 h. After 1 h, the solid obtained was filtered and dried under vacuum at 25 °C for overnight to afford white free amine **Frag A** (5.5 g, 96% isolated yield, 97% wt% by HPLC).

^{1}H NMR (600 MHz, $CDCl_3$): δ 7.65 (d, *J* = 8.3 Hz, 1H), 7.27 (t, *J* = 7.9 Hz, 1H), 6.75 (d, *J* = 6.3 Hz, 2H), 6.68 (dd, *J* = 12.5, 5.5 Hz, 1H), 4.56 (dd, *J* = 8.5, 5.3 Hz, 1H), 3.08 (dd, *J* = 13.5, 5.2 Hz, 1H), 2.78 (dd, *J* = 13.5, 8.6 Hz, 1H), 1.80 (s, 2H).

^{13}C NMR (151 MHz, $CDCl_3$): δ 162.9 (dd, *J* = 248.3, 12.9 Hz), 162.5 (s), 142.6 (s), 142.4 (t, *J* = 9.1 Hz), 140.5 (s), 128.1 (s), 118.9 (s), 112.2 (dd, *J* = 19.6, 5.1 Hz), 102.1 (t, *J* = 25.3 Hz), 56.0, 43.6.

^{19}F NMR (565 MHz, $CDCl_3$): δ -110.2.

Melting Point:114° C

IR (ATR, DCM) ν_{max} = 3360, 3030, 3060, 1623, 1453, 1123, 998, 857.

Enantiomeric excess (*ee*): 100% (SFC)

Optical rotation: $[\alpha]_D^{20}$ = +91.19 (deg·mL·g^{-1}·dm^{-1}) (measured in MeOH (10mg/mL) at 20 °C under 589nm)

Figure 3.2.7. Isolated enantiopure free amine **(S)-A1.5**

3.3 Copies of NMR spectra and analytical reports

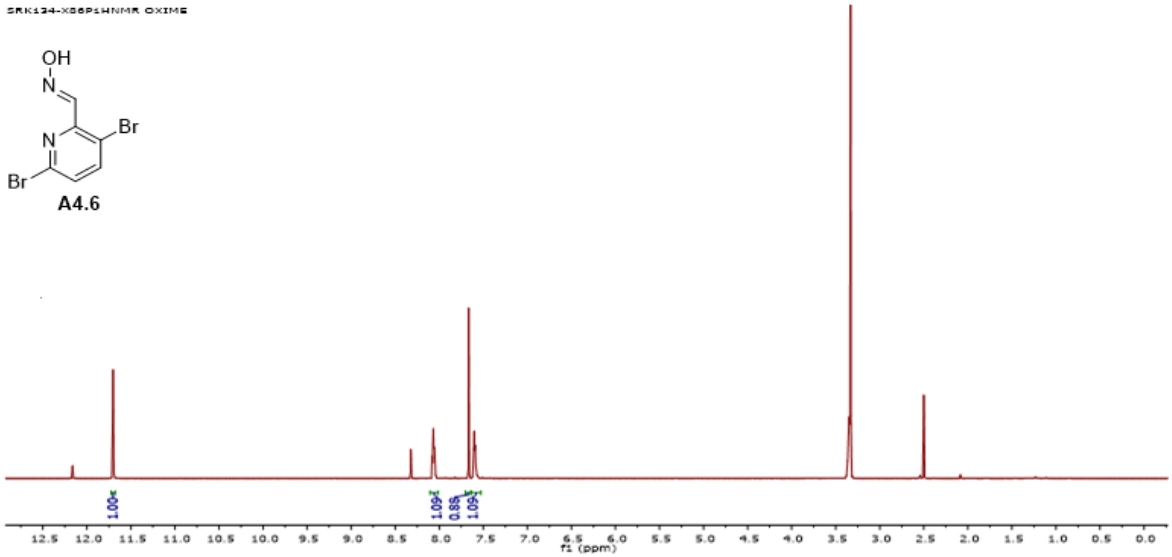

Figure 3.3.1 ^{1}H NMR for oxime **A4.6**

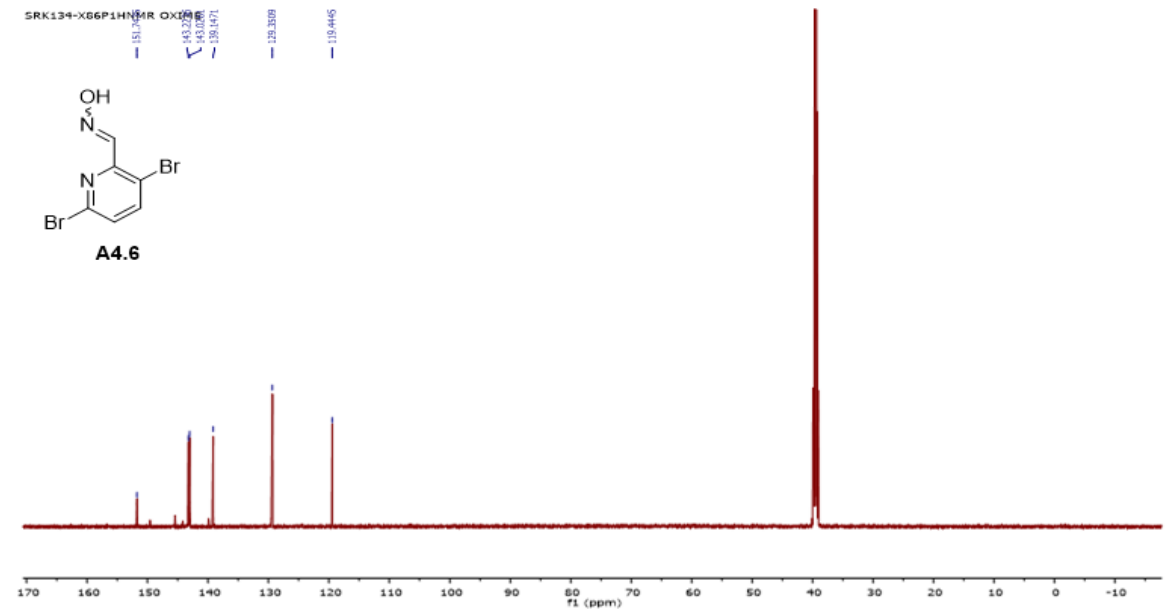

Figure 3.3.2 ^{13}C NMR for oxime **A4.6**

ID	Wt %	% RSD	210 nm Area %
PS136-X63	93.2%	0.6%	99.1%
PS136-X63-Aq	0.27 mg/mL	0.7%	5.7%

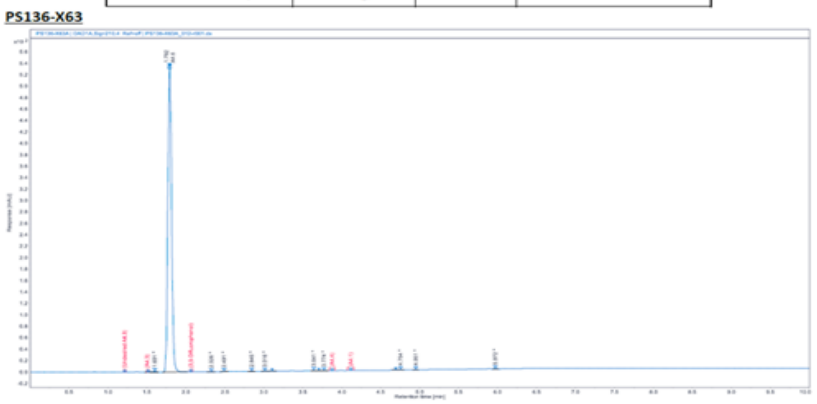

Figure 3.3.3 HPLC wt% analysis for oxime **A4.6**

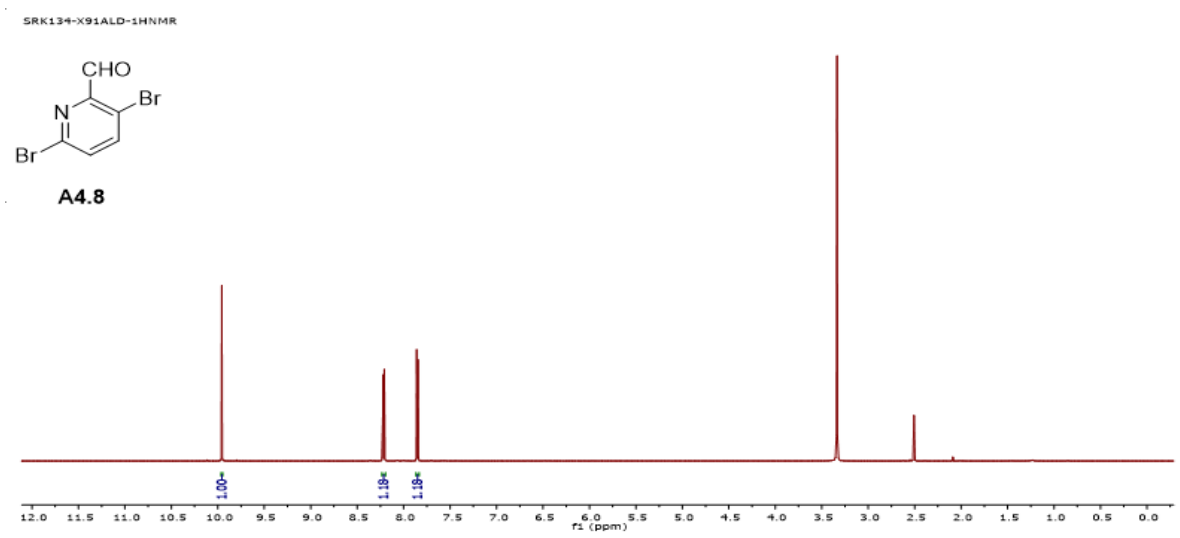

Figure 3.3.4 ^{1}H NMR for aldehyde **A4.8**

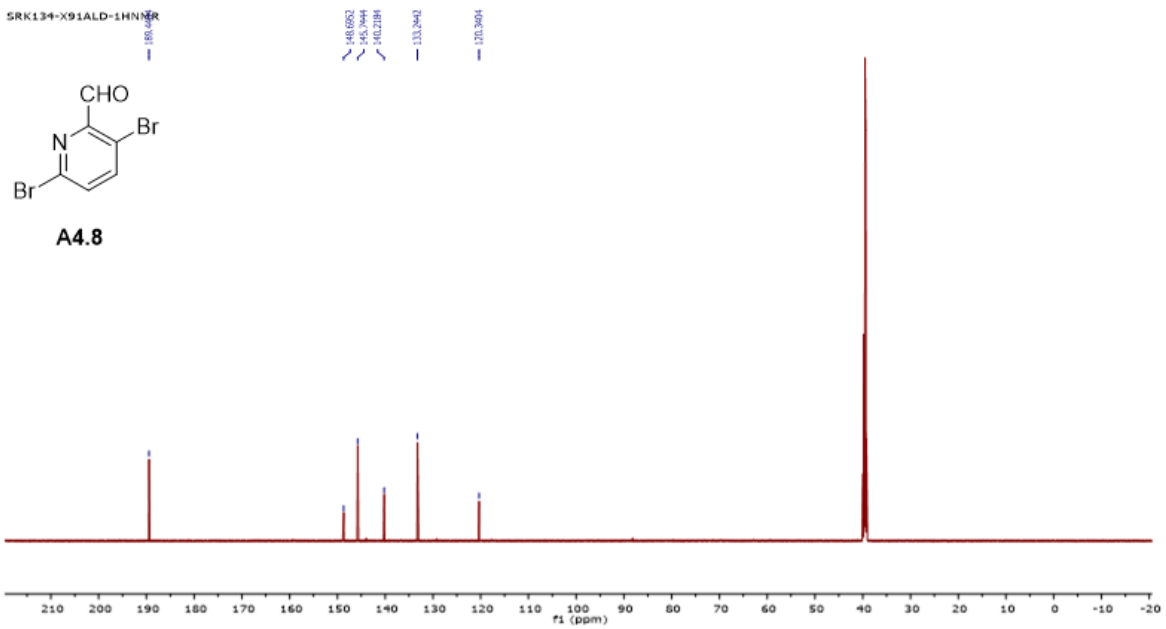

Figure 3.3.5 ^{13}C NMR for aldehyde **A4.8**

Summary of Results

GC-MS Weight Percent Assay			
ID	Wt %	% RSD	TIC Area %
SRK134-X96P	85.7%	1.0%	100%

SRK134-X96P

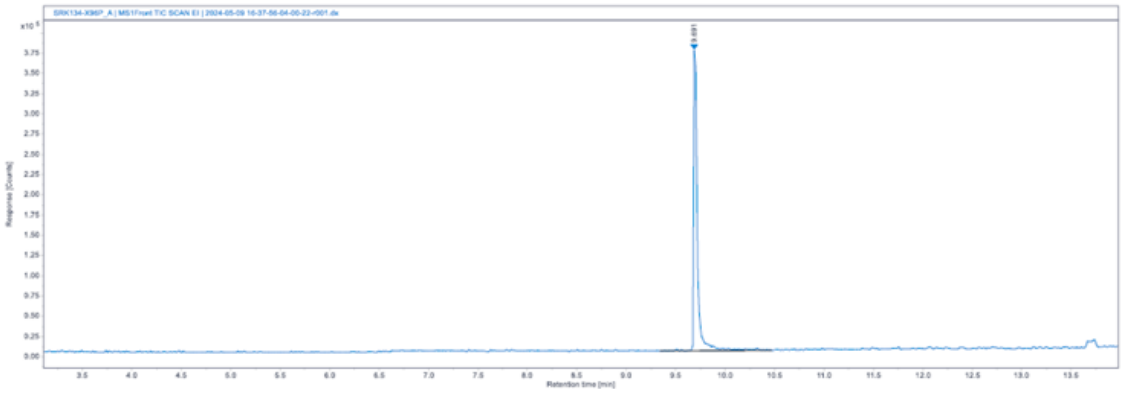

Figure 3.3.6 GCMS wt% analysis for isolated aldehyde **A4.8**

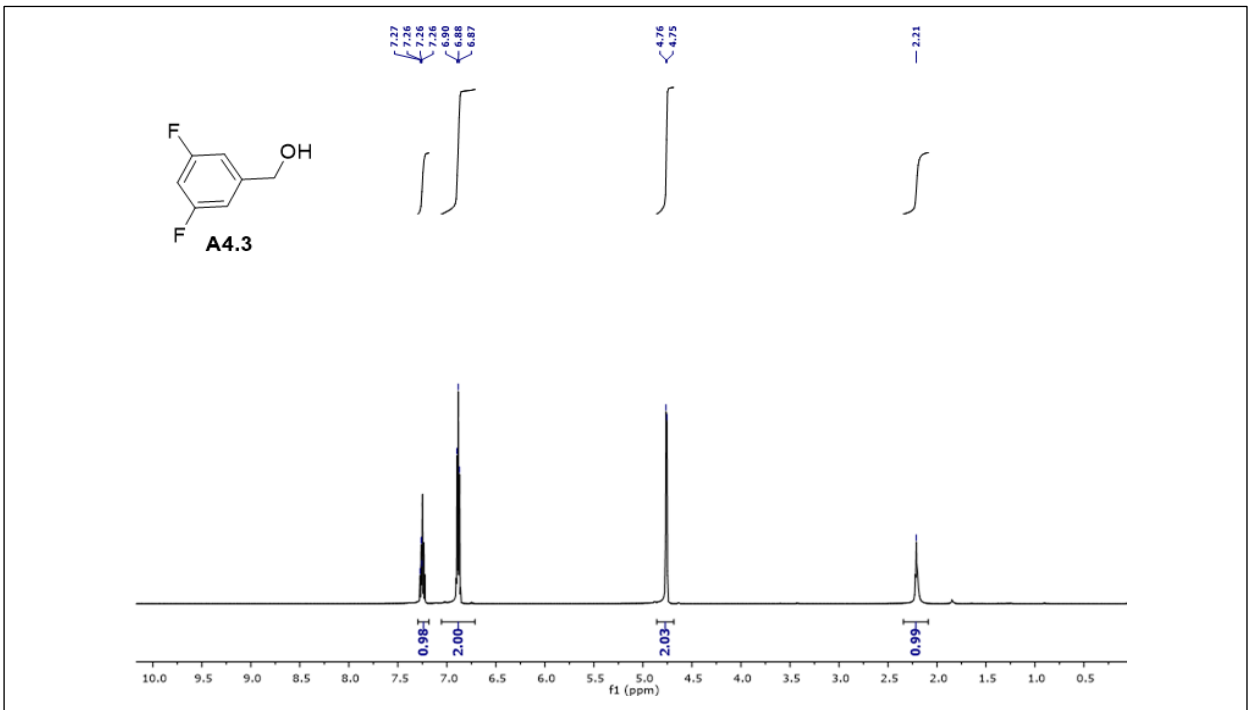

Figure 3.3.7 ^{1}H NMR for 3,5-difluorobenzyl alcohol **A4.3**

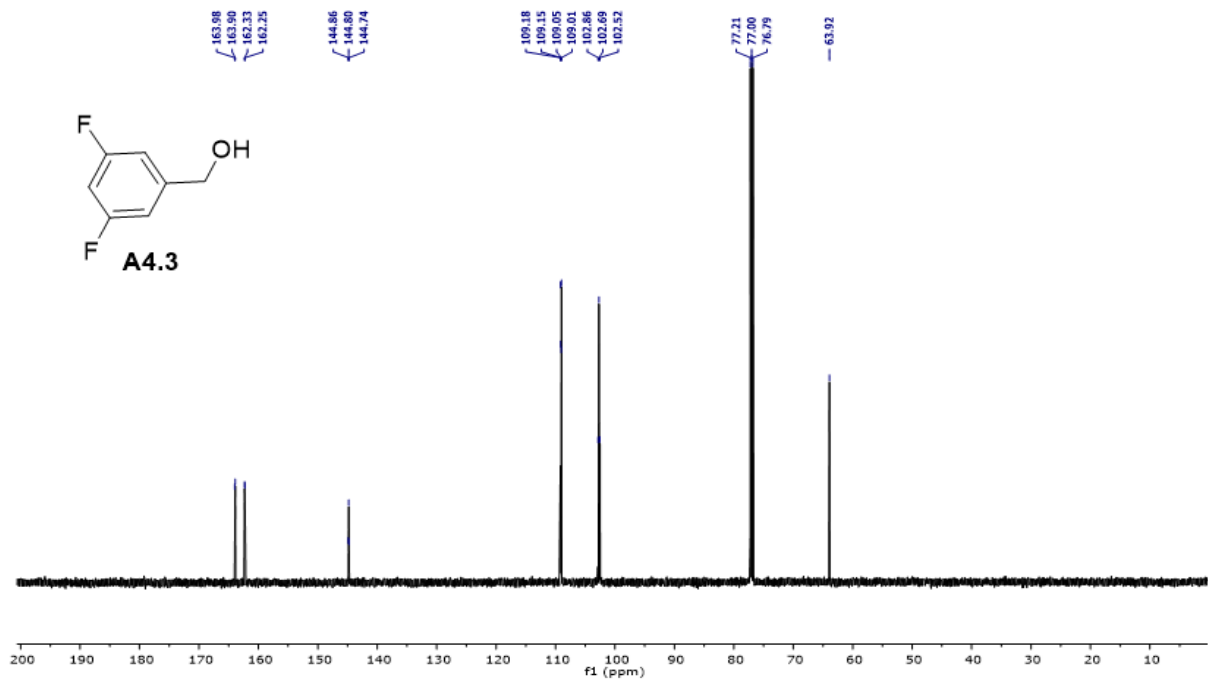

Figure 3.3.8 ^{13}C NMR for 3,5-difluorobenzyl alcohol **A4.3**

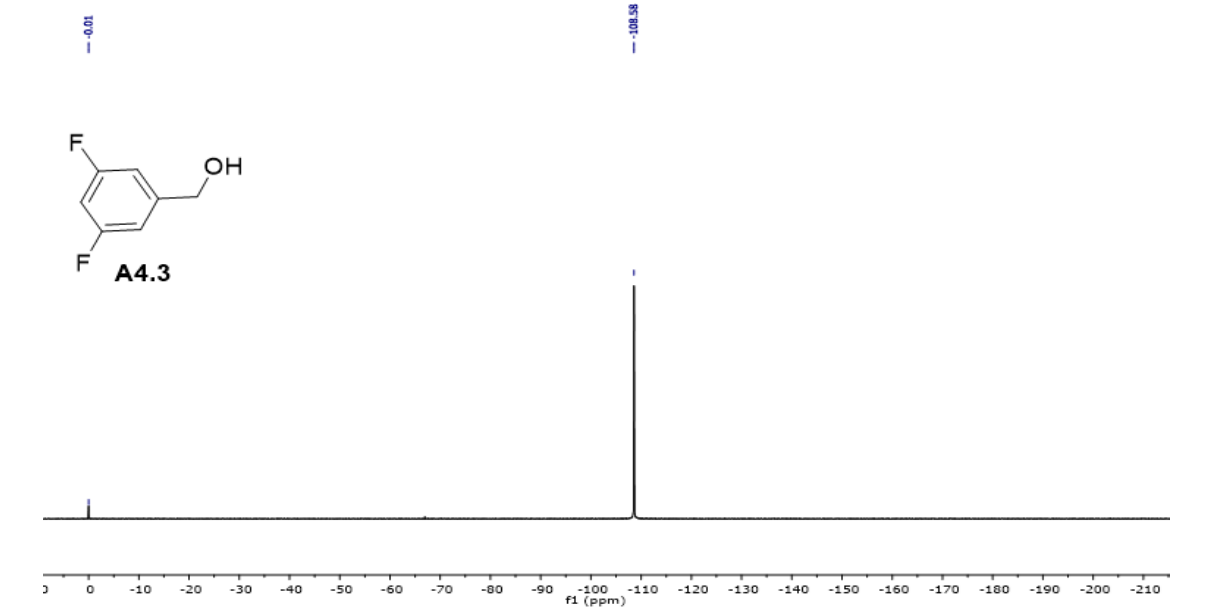

Figure 3.3.9 ^{19}F NMR for 3,5-difluorobenzyl alcohol **A4.3**

Summary of Results

LC-UV			
ID	**Wt %**	**% RSD**	**210 nm Area %**
SRK134-X83 Alcohol Crude	78.7%	1.02%	93.7%

LC-UV analysis

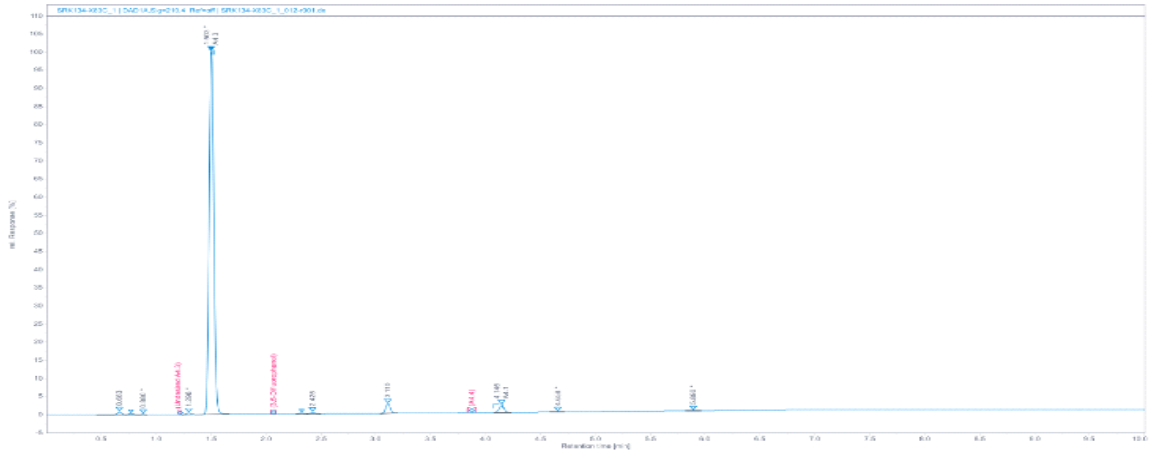

Figure 3.3.10 HPLC wt% analysis for isolated alcohol **A4.3**

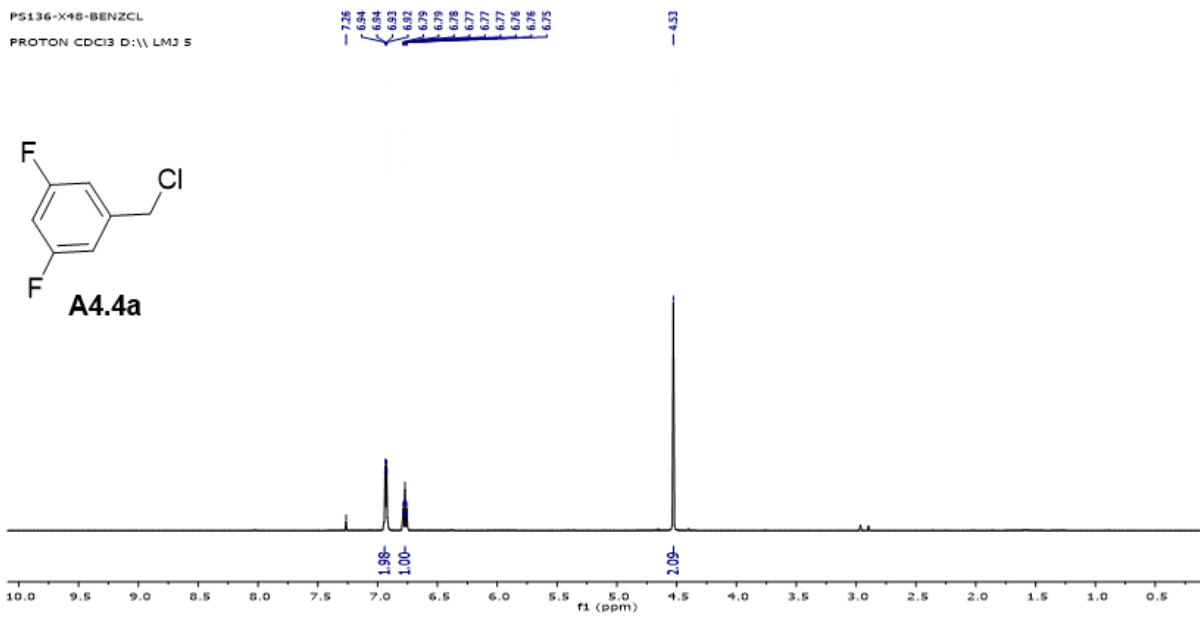

Figure 3.3.11 ^{1}H NMR for 3,5-difluorobenzyl chloride **A4.4a**

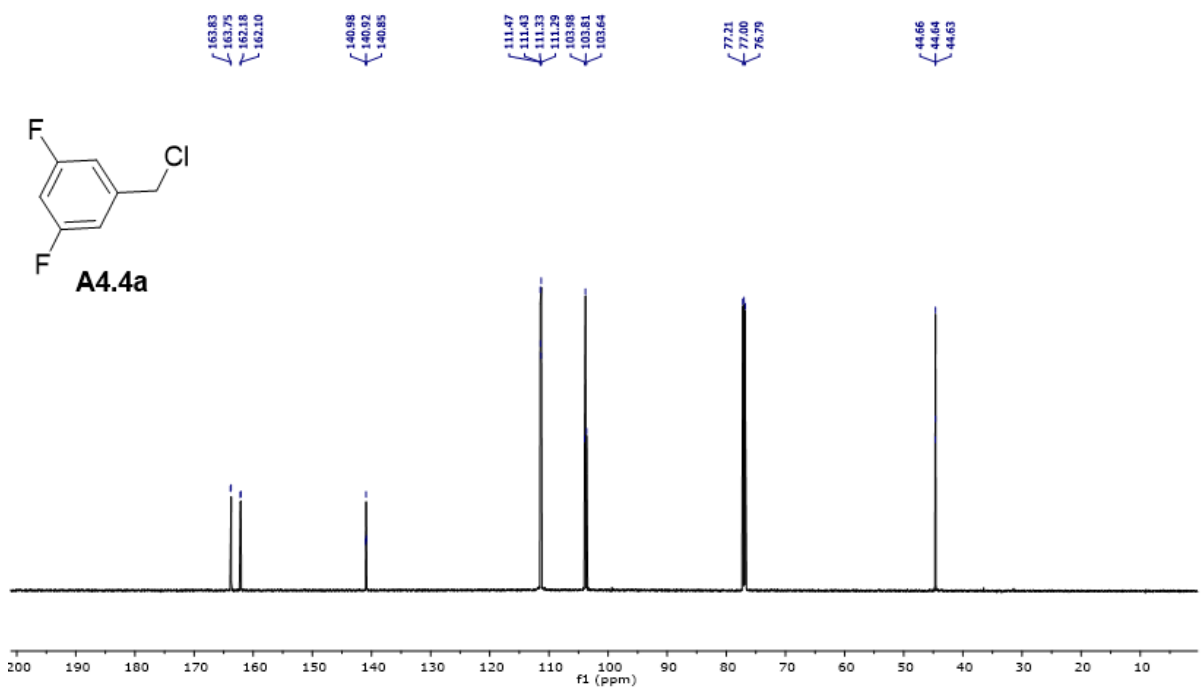

Figure 3.3.12 ^{13}C NMR for 3,5-difluorobenzyl chloride **A4.4a**

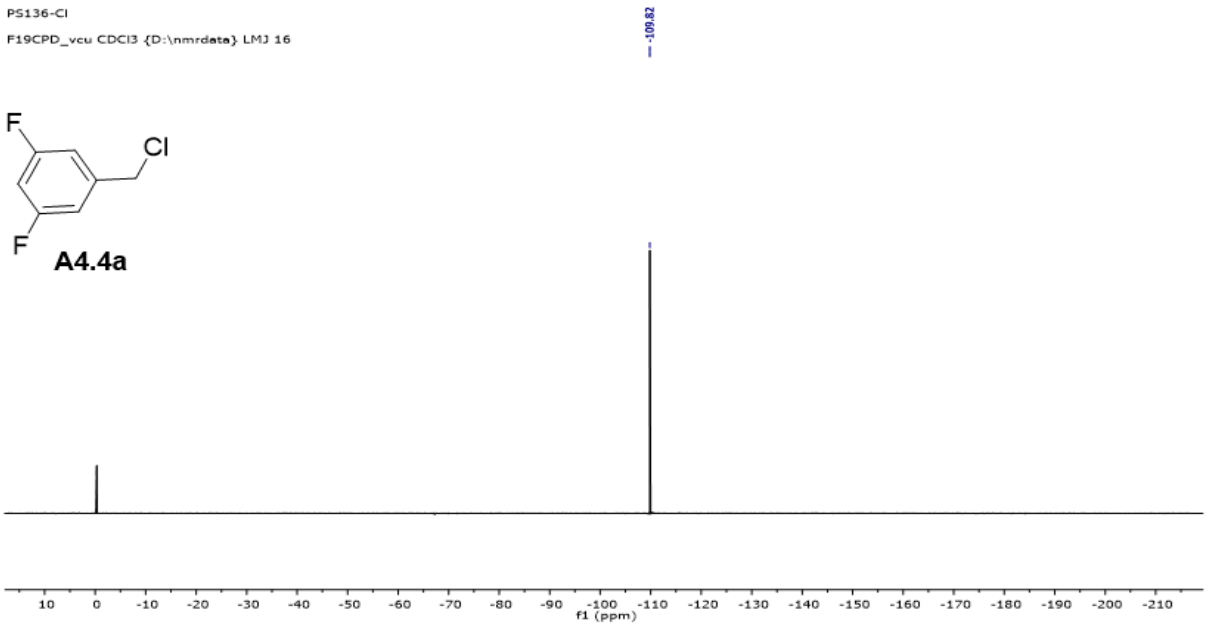

Figure 3.3.13 ^{19}F NMR for 3,5-difluorobenzyl chloride **A4.4a**

Summary of Results

Wt% of A4.4a by LC-UV		
ID	Wt % ±SD	225 nm Area %
PS136-X48	103.9 ± 7.0%	97.9%

LCUV Analysis

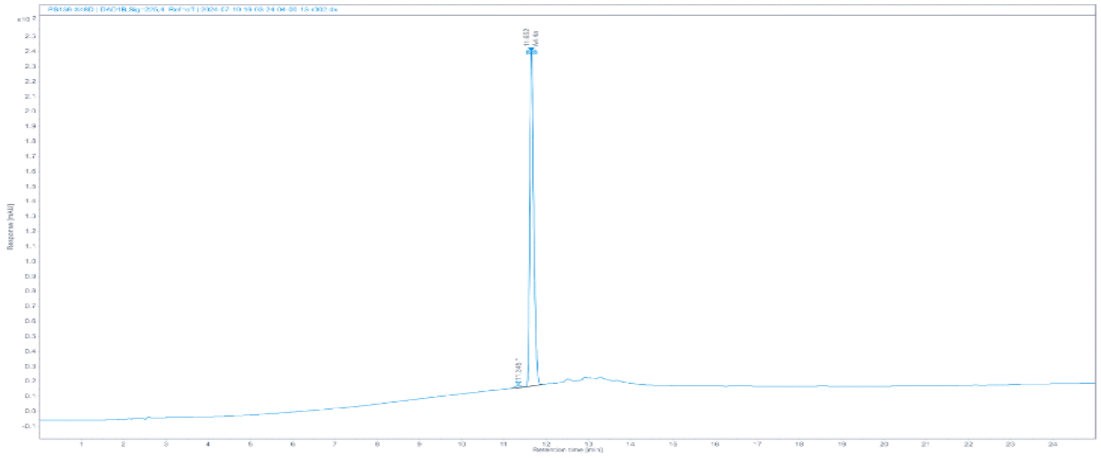

Figure 3.3.14 GCMS wt% analysis for isolated 3,5-diflurobenzyl chloride **A4.4a**

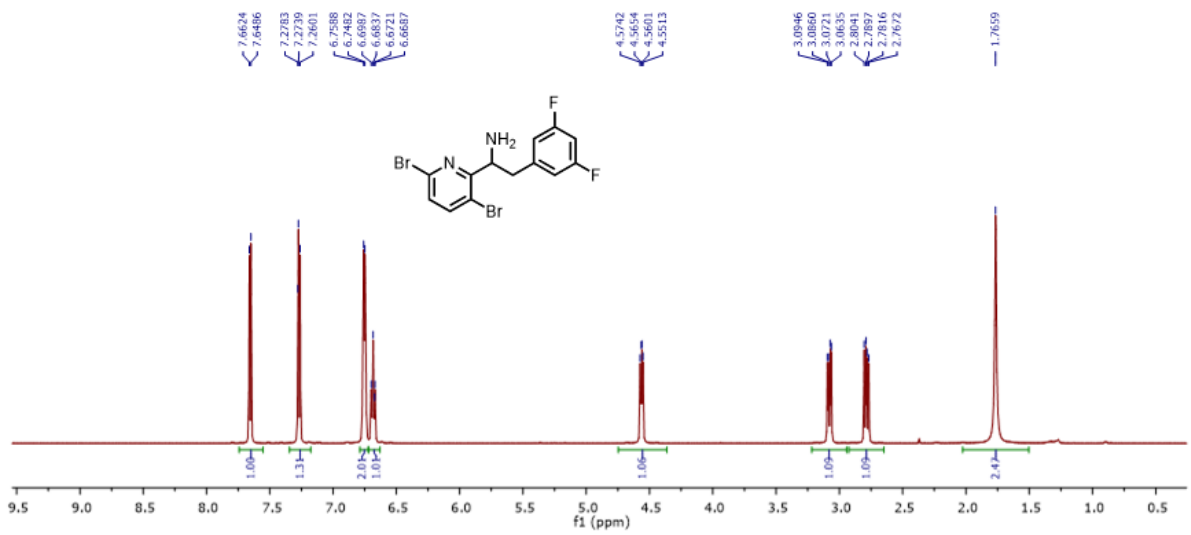

Figure 3.3.15 ^{1}H NMR for racemic amine **A1.5**

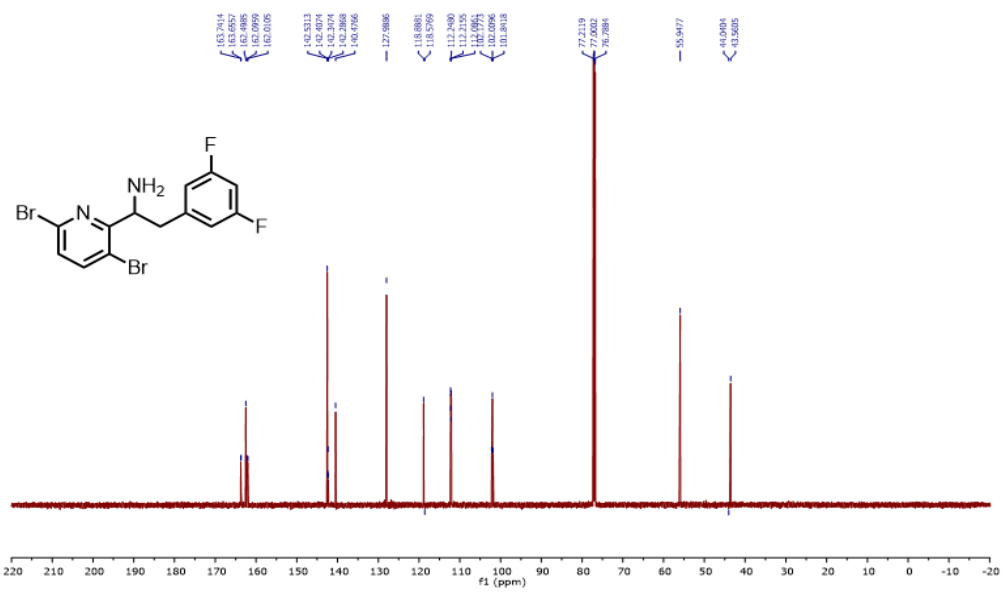

Figure 3.3.16 ^{13}C NMR for racemic amine **A1.5**

Wt % (±SD)	210 nm Area %	Water Content (w/w% ±SD)
94.1 ± 0.9%	97.4%	0.56 ± 0.10%

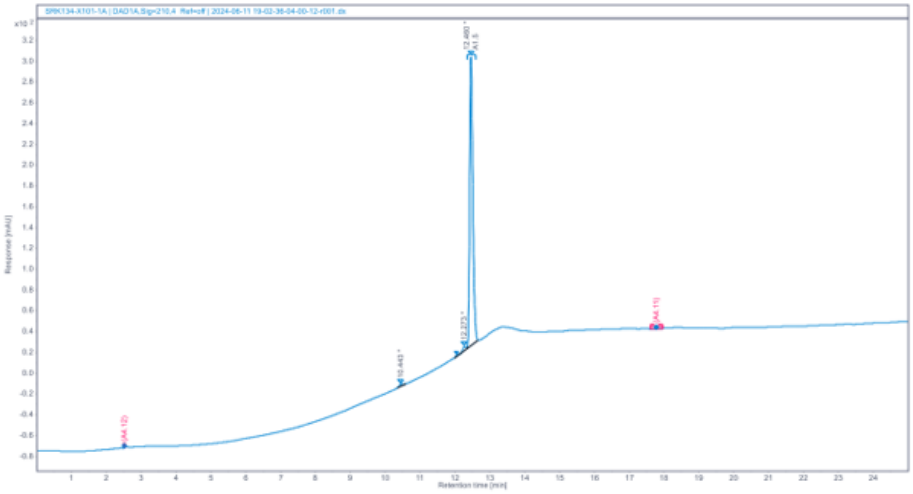

Figure 3.3.17 HPLC wt% analysis for isolated racemic amine **A1.5**

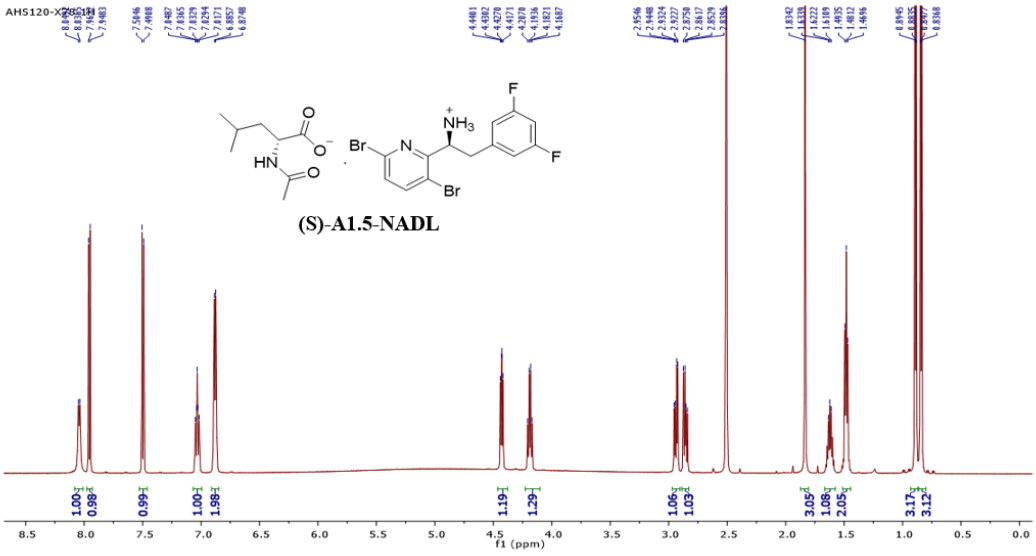

Figure 3.3.18 ^{1}H NMR for **(S)-A1.5-NADL**

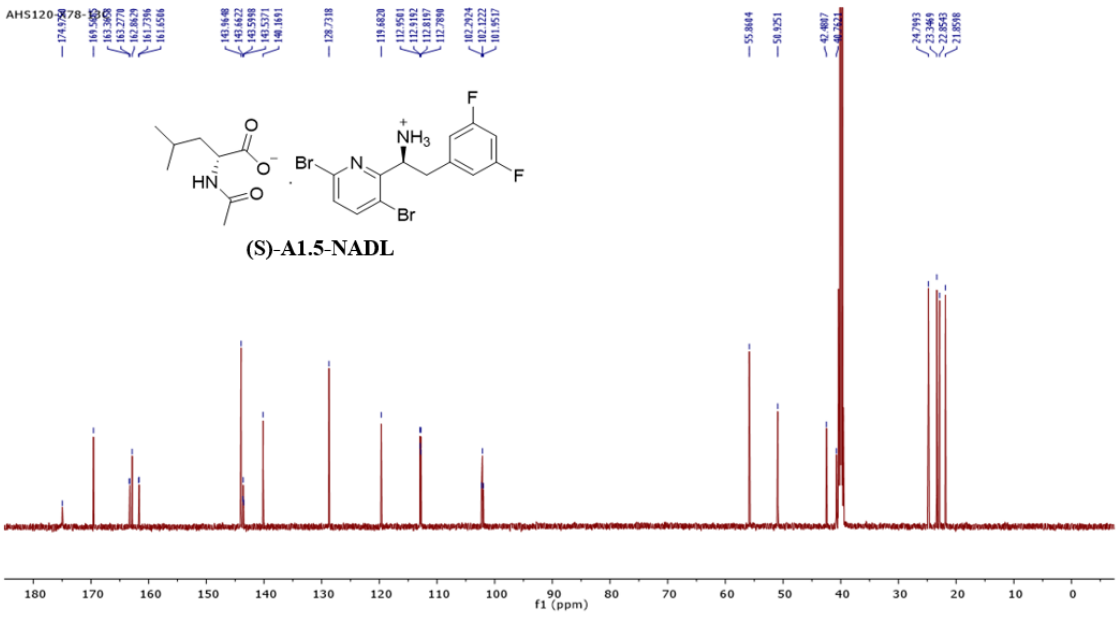

Figure 3.3.19 ^{13}C NMR for **(S)-A1.5-NADL**

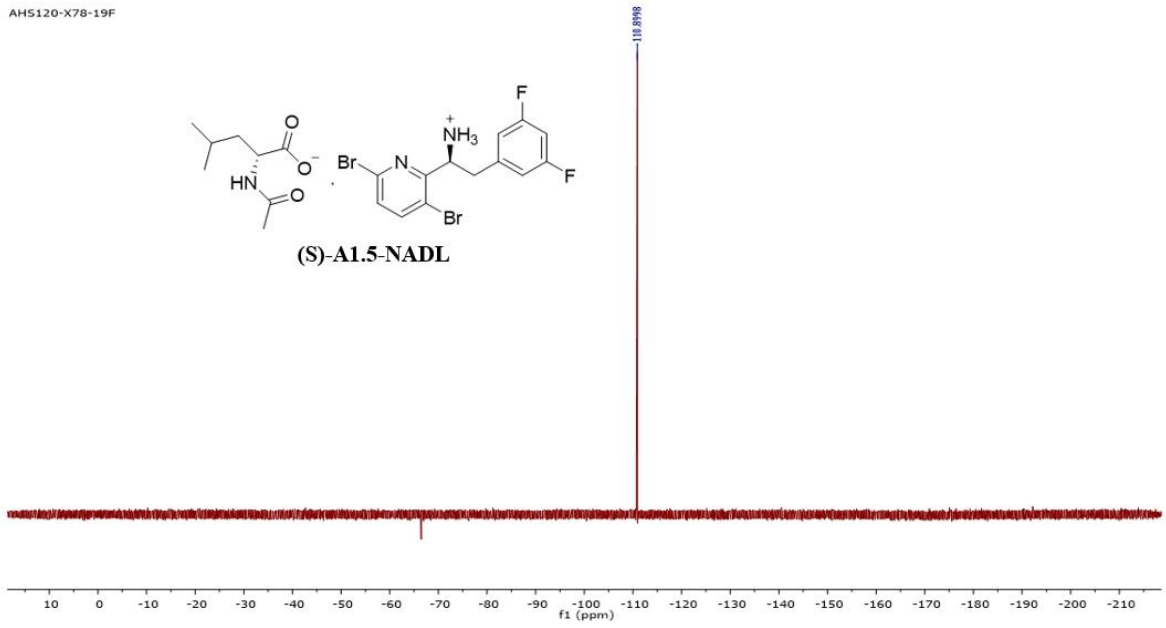

Figure 3.3.20 ^{19}F NMR for **(S)-A1.5-NADL**

Wt% Assay by LC-UV			
ID	Wt % ± % SD*	225 nm Area %	Water Content (w/w%)
SRK134-X103	80.5% ± 2.9%	96.1%	1.12% ± 0.02%

*Wt % calculated as free base, SD = standard deviation

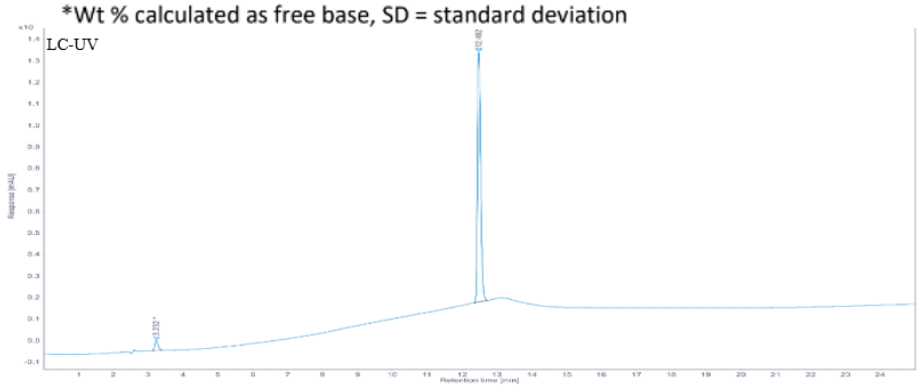

Figure 3.3.21 HPLC wt% analysis of **(S)-A1.5-NADL**

Chiral Analysis by SFC-UV of A1.5		
ID	Area % @ 210 nm	
	(R)-Isomer	*(S)-Isomer*
SRK134-X103	0%	100%

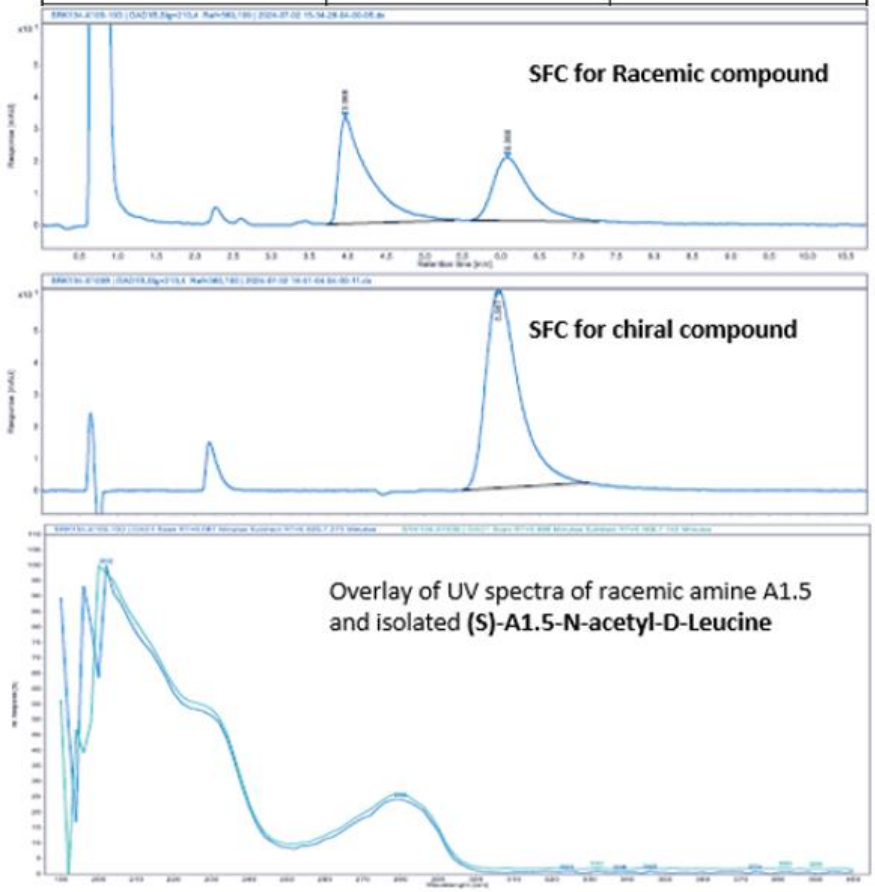

Figure 3.3.22 SFC of **(*S*)-A1.5-NADL**

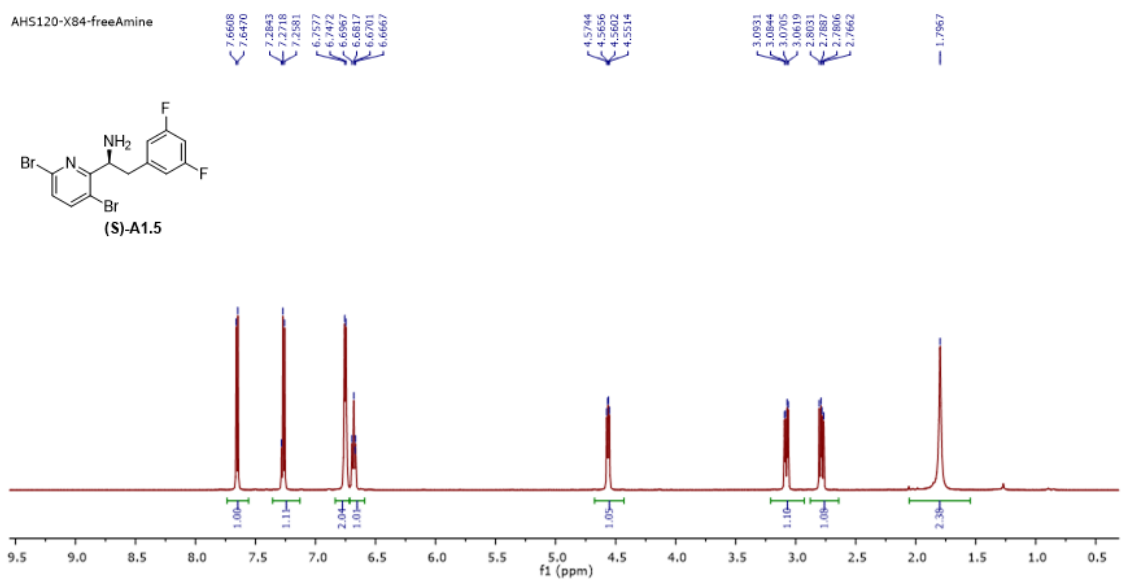

Figure 3.3.23 ^{1}H NMR for enantiopure free amine **Frag A ((*S*)-A1.5)**

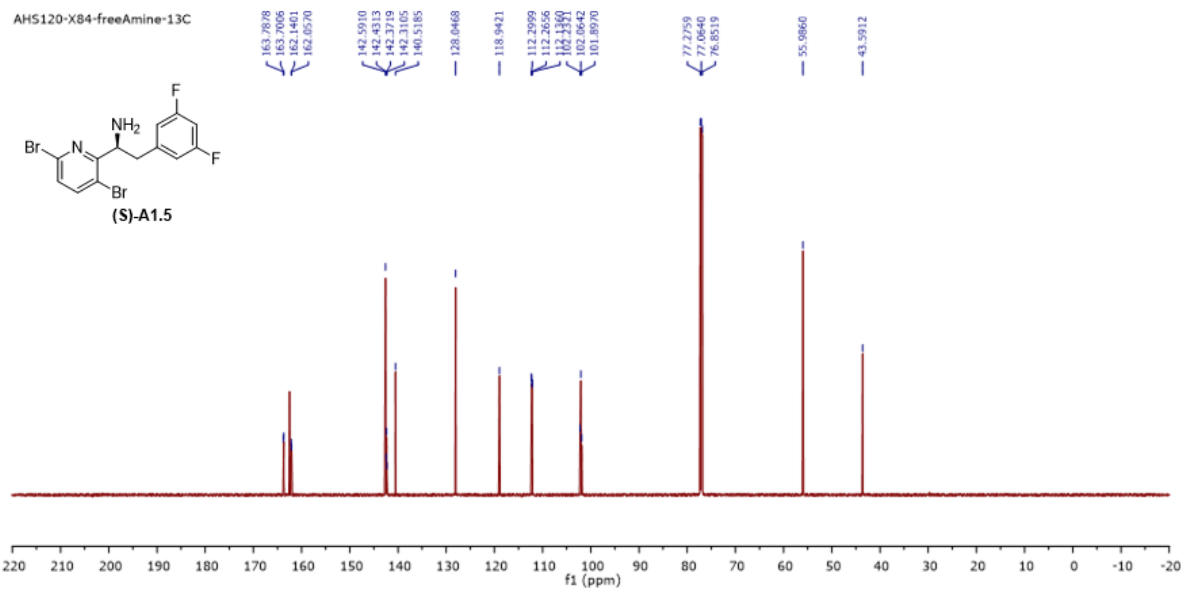

Figure 3.3.24 ^{13}C NMR for enantiopure free amine **Frag A ((*S*)-A1.5)**

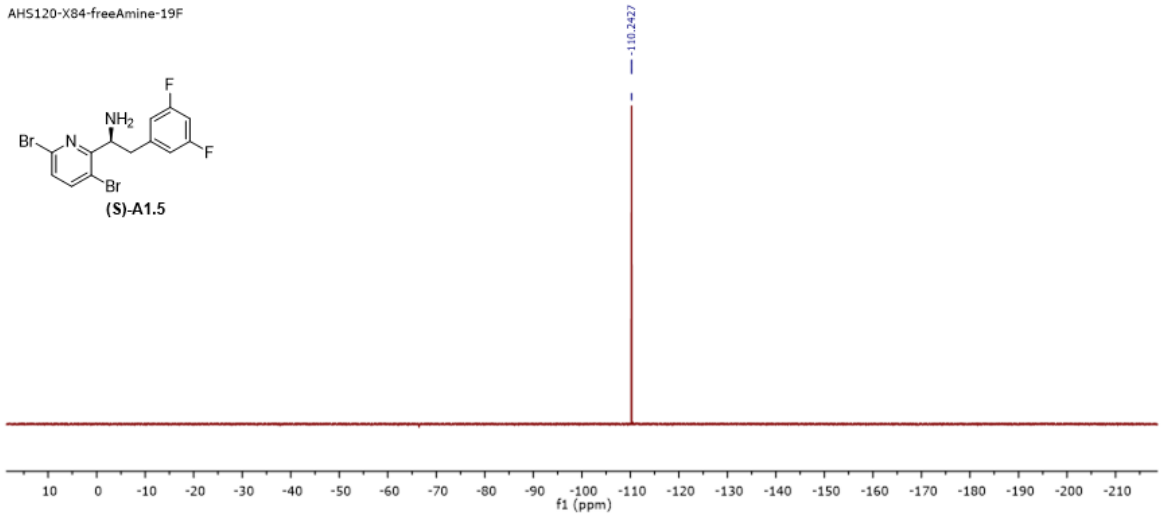

Figure 3.3.25 ^{19}F NMR for enantiopure free amine **Frag A ((*S*)-A1.5)**

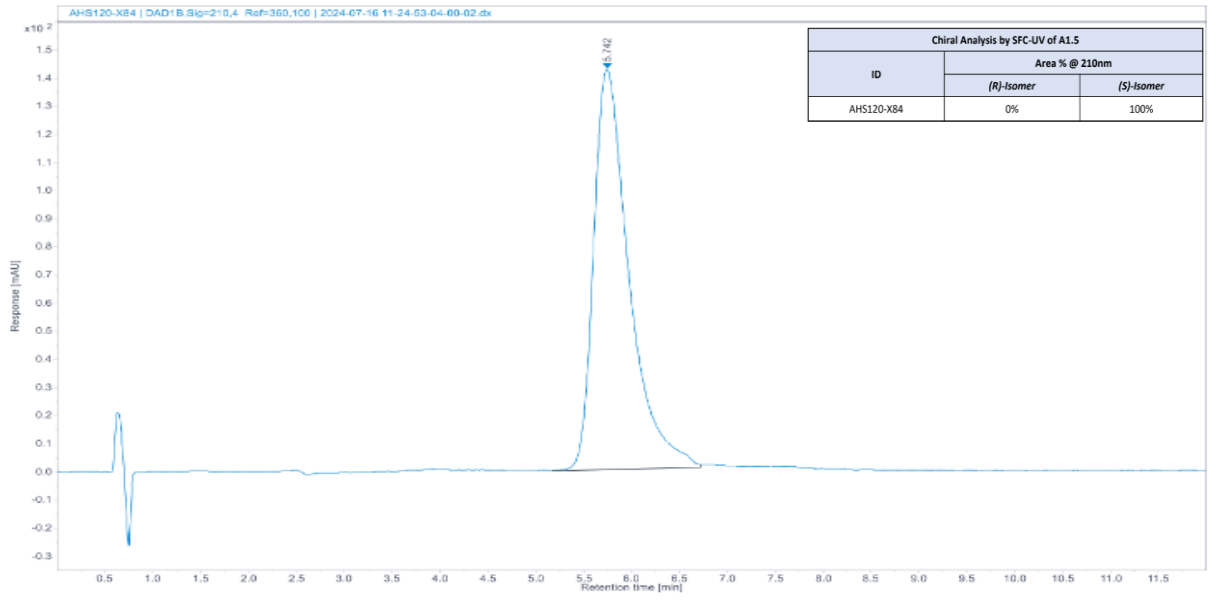

Figure 3.3.26 SFC analysis of free enantiopure amine **Frag A ((*S*)-A1.5)**

Weight Percent Assay by LC-UV		
ID	Wt % A1.5	225 nm Area %
AHS120-X84	97.0 ± 1.0%	99.7%

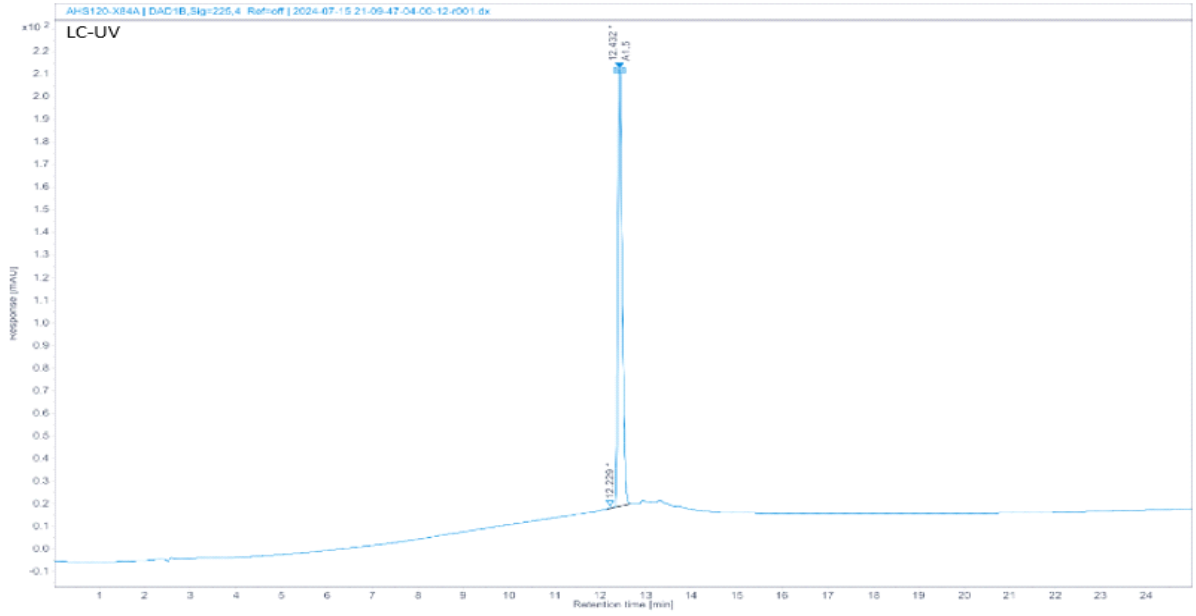

Figure 3.3.27 HPLC Wt% analysis for isolated free enantiopure amine **Frag A ((*S*)-A1.5)**

4 Appendix

4.1 Synthesis of 3,5-difluorobenzyl chloride **A4.4a** (Milestone 4 in LenA 4)

4.1.1 Optimization of the synthesis of 3,5-difluorobenzyl chloride **A4.4a**

*4.1.1.1 2.2.1.1 Synthesis of 3,5-difluorobenzyl alcohol **A4.3***

3,5-Difluorobenzyl chloride **A4.4a**, an alkylating reagent in the **A4.11** synthesis, was expensive and one of the cost drivers in LenA 4 route. To achieve a more cost-effective route for **Frag A**, we developed a two-step route to synthesize 3,5-difluorobenzyl chloride from commercially available 3,5-difluorobenzoic acid **A4.2** (Scheme 4.1.1). The key transformation was $NaBH_4/I_2$-based carboxylic acid reduction to afford alcohol **A4.3** and the subsequent

chlorination with $SOCl_2$/DMF. Herein, we describe detailed results of the synthesis of 3,5-difluorobenzyl chloride.

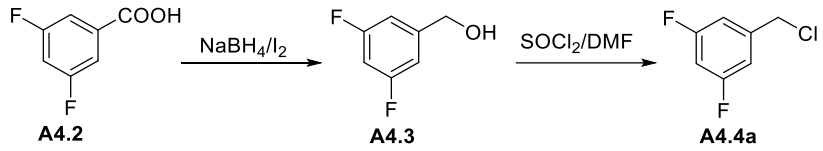

Scheme 4.1.1 Two-step approach for synthesis of 3,5-difluorobenzyl chloride (**A4.4a**)

The synthesis of 3,5-difluorobenzyl alcohol (**A4.3**) is imperative to access **A4.4a**. Our initial efforts to make **A4.3** focused on the reaction of 1-bromo-3,5-difluorobenzene (**A1.1**) with paraformaldehyde. Commencing from the halo-exchange reaction of A1.1 (1 eq) and Mg (5 eq) in THF, the resulting Grignard reagent reacted with paraformaldehyde (3.3 eq) to afford **A4.3** in 40 A% (LCAP, 210 nm), and debromination was the major side-product (Table 4.1.1, Entry 1). Attempts to improve the yield failed. We envisioned that reduction of 3,5-difluorobenzoic acid would provide an effective way to access **A4.3**. The reduction proceeded smoothly with $NaAlH_4$ as the reducing reagent. The reaction of **A4.2** with $NaAlH_4$ (1.1 eq) in THF (10V) at 0 °C afforded **A4.3** in 99 A% (LCAP, 210 nm) (Table 4.1.1, Entry 2). Unexpectedly, the cost of $NaAlH_4$ increased dramatically in recent years due to its low market volumes. Thus, we screened other cheap reducing reagent for the reduction. Red-Al was tried but only 74 A% (LCAP, 210 nm) of **A4.3** was obtained (Table 4.1.1, Entry 3). To our delight, initial results showed that **A4.3** was obtained in 86 A% (LCAP, 210 nm) with $NaBH_4$ (1.2 eq) /I_2 (0.5 eq)[21] as the reducing reagent in THF (60V) at 25 °C (Table 2.2.1, Entry 4). Thus, $NaBH_4$ (1.2 eq) /I_2 (0.5 eq) was chosen for further optimization to improve the yield at scale. Concentration of the reaction mixture and the reaction temperature were critical to afford a full conversion of the reaction. Increase of the reaction temperature to 65 °C enabled the formation of **A4.3** up to 96 A% (LCAP, 210 nm) in THF (5V) (Table 4.1.1, Entry 5). Among various solvent screening, it was found that the solvent volume from 5V to 15V afforded a similar yield of **A4.3** (93-96 A%) when the reactions were carried out at 65 °C (Table 4.1.1, Entries 6-8). It should be noted that an exotherm was observed in the reaction with 5V of THF as solvent during the addition of $NaBH_4$. No obvious exotherm was observed in a more dilute reaction medium (i.e. THF (10V)).

Table 4.1.1 Initial screen of synthesis of 3,5-difluorobenzyl alcohol **A4.3**

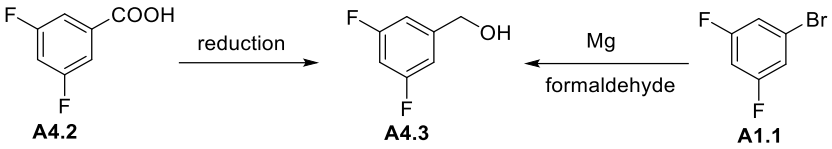

Entry[1]	SM (g)	Condition	**A4.3** (A%)[2]
1	**A1.1** (40)	Mg (5 eq), HCHO (3.3 eq), THF (10V), 25 °C, 8 h	40
2	**A4.2** (2)	Red Al (60% in toluene, 1 eq), THF (10V), 0 °C to 25 °C, 1 h	74
3	**A4.2** (50)	$NaAlH_4$ (1.1 eq), THF (10V) 0 °C to 25 °C, 2 h	99
4	**A4.2** (1)	$NaBH_4$ (1.2 eq), I_2 (0.5 eq), THF (60V), 0 to 25 °C, 21 h	86
5	**A4.2** (2)	$NaBH_4$ (1.2 eq), I_2 (0.5 eq), THF (5V), 0 °C to 65 °C, 18 h	96
6	**A4.2** (2)	$NaBH_4$ (1.2 eq), I_2 (0.5 eq), THF (7.5V), 0 °C to 65 °C, 18 h	93
7	**A4.2** (2)	$NaBH_4$ (1.2 eq), I_2 (0.5 eq), THF (10V), 0 °C to 65 °C, 15 h	94
8	**A4.2** (2)	$NaBH_4$ (1.2 eq), I_2 (0.5 eq), THF (15V), 0 °C to 65 °C, 16 h	94
9	**A4.2** (25)	$NaBH_4$ (1.2 eq), I_2 (0.5 eq), THF (10V), 0 °C to 65 °C, 17 h	91

[1]Typical reduction with $NaBH_4/I_2$: reactions conducted with **A4.2** (1 eq), $NaBH_4$ (1.2 eq), I_2 (0.5 eq) at 0 °C then heated to 65 °C in THF under conditions as shown in the table unless otherwise stated. [2]A% of **A4.3** was obtained by HPLC (210 nm).

Optimal reduction conditions were identified as: $NaBH_4$ (1.2 eq), I_2 (0.5 eq), THF (10V), 0 °C to 65 °C, 15-18 h. This optimized condition was verified with a 25g-scale reaction, and 91 A% (LCAP, 210 nm) of **A4.3** was obtained (Table 4.1.1, Entry 9).

*4.1.1.2 Synthesis of 3,5-difluorobenzyl chloride **A4.4a***

To complete the synthesis of 3,5-difluorobenzyl chloride (**A4.4a**), alcohol **A4.3** was subject to the traditional chlorination condition [oxalyl chloride $(COCl)_2$, cat. DMF].[22] Unexpectedly, the reaction of **A4.3** with $(COCl)_2$ resulted in a complex mixture and no significant amount of **A4.4a** was observed (Table 4.1.2, Entry 1). The chlorination of **A4.3** with conc HCl afforded **A4.4a** in 63 A% (LCAP) and main starting material **A4.3** remained (26 A%) (Table 4.1.2, Entry 2). Chlorination with conc. HCl provided a cleaner reaction profile compared to $(COCl)_2$, unfortunately, further attempts (increase temperature, increase eq of conc. HCl, elongation of reaction time, etc.) to improve the yield resulted in poorer reaction profiles. To our delight, chlorination with thionyl chloride [23] afforded better conversion and cleaner reaction profiles. Initially, the reaction of the alcohol **A4.3** with thionyl chloride without DMF afforded

incompletion of the chlorination. The addition of catalytic amount of DMF (5 mol%) is critical to afford a full conversion of the chlorination. For example, **A4.3** with thionyl chloride (1.5 eq) and DMF (0.05 eq) in DCM (6V) at 25 °C afforded **A4.4a** in 100 A% (LCAP) (Table 4.1.2, Entry 3). The screen of equivalents of thionyl chloride showed that the chlorination proceeded smoothly with thionyl chloride from 1.2 eq to 1.5 eq (Table 4.1.2, Entries 4-5). Thus, 1.2 eq of thionyl chloride was used for scale-up in this chlorination. The condition was verified with a 29g-scale reaction and the conversion was >98 A%, however A% of **A4.4a** in the crude was 82 A% (LCAP). After distillation (80 °C/42 mmHg) the product **A4.4a** was obtained in 59% isolated yield with 81wt% (HPLC) (Table 4.1.2, Entry 6).[s]

Table 4.1.2 Synthesis of 3,5-difluorobenzyl chloride **A4.4a**

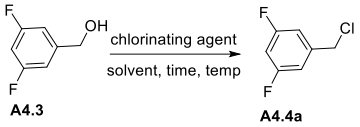

A4.3 **A4.4a**

Entry[1]	Input (**A4.3**)	Condition	IPC (A%)[2]		Comment
			A4.3	**A4.4a**	
1	1.0 g	$(COCl)_2$ (1.5 eq), DMF (0.05 eq), DCM (2V), 25 °C, 4 h	-	-	Decomposition was observed
2	0.5 g	conc. HCl (12V), 110 °C, 4 h	26 %	63 %	Low conversion
3	1.0 g	$SOCl_2$ (1.5 eq), DMF (0.05 eq), DCM (6V), 17 h, 25 °C	-	100 %	-
4	1.0 g	$SOCl_2$ (1.3 eq), DMF (0.05 eq), DCM (6V), 17 h, 25 °C	-	100 %	-
5	1.0 g	$SOCl_2$ (1.2 eq), DMF (0.05 eq), DCM (6V), 17 h, 25 °C	-	100 %	-
6	29 g	$SOCl_2$ (1.2 eq), DMF (0.05 eq), DCM (6V), 17 h, 25 °C	2 %	82 %	output[2]: 24 g, 82 wt%[3]

[1]All reactions conducted with **A4.3** (1 eq) under conditions as shown in the table unless otherwise stated; [2]HPLC A% measured at 210 nm; [3]Product **A4.4a** was isolated using distillation at 80 °C with 42 mmHg; [4]Purity measured by HPLC wt% compared to a known standard.

[s] The chlorination with $SOCl_2$ was used for scale-up without further optimization due to the limited timeline of the project.

4.1.2 Scale-up of 3,5-difluorobenzyl chloride **A4.4a**

*4.1.2.1 Scaleup synthesis of alcohol **A4.3***

The optimized condition of reduction of 3,5-difluorobenzoic acid **A4.2** to afford alcohol **A4.3** was conducted on 100 g-scale (Table 4.1.3). Firstly, $NaBH_4$ was dissolved in THF (4V), 3,5-difluorobenzoic acid **A4.2** was dissolved in THF (3V) and iodine was dissolved in THF (3V). The solution of $NaBH_4$ was then added to the solution of **A4.2** at 0º C followed by addition of the iodine solution. The reaction mixture was heated at 65 °C for 18h and the IPC showed 97 A% **A4.3** (LCAP, 210 nm). After workup (see experimental section for details section 3.), **A4.3** was obtained in 90% isolated yield with 94 wt% (HPLC). The obtained alcohol **A4.3** was used for next step without further purification.

Table 4.1.3 Scale up synthesis of 3,5-difluorobenzyl alcohol **A4.3**

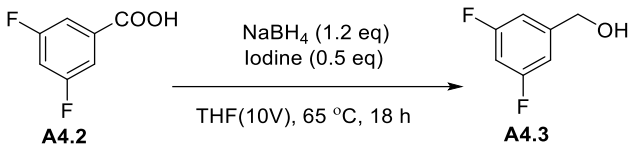

Entry[1]	Input (**A4.2**)	IPC[2]	Output after purification[1]		
		A4.3 (A%)	Yield[3]	mass	wt%[4]
1	100 g	97 %	90 %	87 g	94

[1]See experimental section for details; [2]A% was obtained by LCAP (210 nm); wt% with reference to known standard; [2]Corrected yield based on HPLC wt% purity; [3]Corrected yield based on wt%; [4]Wt% was measured by HPLC (210 nm) with a known standard.

*4.1.2.2 Scale-up synthesis of chloride **A4.4a***

The scale-up of 3,5-difluorobenzyl chloride **A4.4a** was demonstrated on a 40 g-scale of 3,5-difluorobenzyl alcohol **A4.3** under the optimized condition (Table 4.1.4). The reaction of alcohol **A4.3** and thionyl chloride with a catalytic amount of DMF (5 mol%) afforded **A4.4a** in 99 A% (LCAP, 210 nm). After distillation 3,5-difluorobenzyl chloride **A4.4a** was obtained in 71% isolated yield with >99 wt% purity (HPLC, 210 nm).

Table 4.1.4 Scale-up of 3,5-difluorobenzyl chloride **A4.4a**

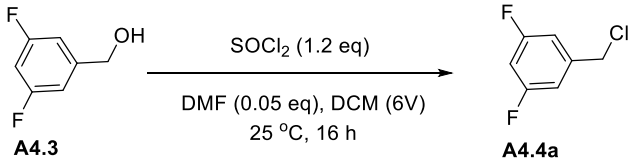

Entry	Input (**A4.3**)	Output (**A4.4a**)	Wt%[1]	Yield[2]
1	40 g	33 g	>99	71 %

[1]Wt% was obtained by HPLC (210 nm); [2]Corrected yield based on HPLC purity.

4.1.3 Synthesis of 3,5-difluorobenzyl bromide **A4.4**

Similarly, 3,5-difluorobenzyl bromide **A4.4** was also prepared by bromination of 3,5-difluorobenzyl alcohol **A4.3**. To identify a reliable bromination, various conditions such as TMSBr,[24] aq. HBr/acetic acid,[25] aq. HBr/H_2SO_4 and PBr_3 [26] were investigated (Table 4.1.5).

Table 4.1.5 Synthesis of 3,5-difluorobenzyl bromide **A4.4**

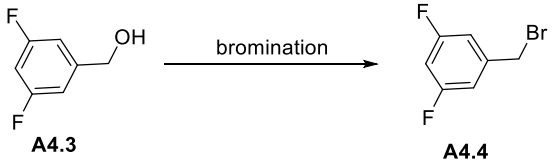

A4.3 **A4.4**

Entry	**A4.3** (g)	Condition	IPC (A%)[2]	
			A4.3	**A4.4**
1	0.25	TMSBr (1 eq), $CHCl_3$ (2V), 45 °C, 16 h	10	90
2	0.25	48% HBr (1.2 eq) / acetic acid (1.2V), 100 °C, 6 h	<5	>95
3	0.45	48% HBr (2.0 eq) / H_2SO_4 (3.5 eq), 33 °C, 24 h	42	58
4	0.2	PBr_3 (0.7 eq), THF, 0 °C to rt, 24 h	50	50
5[3]	42	48% HBr (3 eq) / acetic acid (1.2V), 100 °C, 6 h	<5	>95

[1]The bromination was conducted with: **A4.3** (1 eq), brominating reagent under the condition as shown in the table unless otherwise stated; [2]A% was obtained by HPLC (210 nm); [3]3,5-difluorobenzyl bromide **A4.4** (52.8 g) was obtained after purification in 87% isolated yield with ~80 wt% purity (HPLC).

Among all these screened conditions, bromination with 48% HBr (1.2 eq) in acetic acid (1.2V) afforded **A4.4** in >95 A% (HPLC). This approach was chosen for bromination and it was verified with a 42 g-scale of **A4.3**. Thus, the reaction of **A4.3** with 48% HBr (3 eq) afforded **A4.4** in 87% isolated yield with ~80 wt% purity (HPLC).[t]

[t] It was found that excess (3 eq) of 48% HBr was required to afford a full conversion of the **A4.3**. It should be noted that **A4.4** is extremely lachrymatory and all the bromination must be done in fume-hood with proper PPE.

4.2 Route scouting of **LenA 1**

LenA 1 is a 7-step approach to prepare **Frag A**.[27] The key step in the sequence is the Weinreb amide-based ketone synthesis, which provides an alternative entry point to the core structural component. Starting from the inexpensive 2-(3,5-difluorophenyl)acetic acid, the Weinreb amide synthesis and the followed nucleophilic substitution afford the ketone in 47% yield. The subsequent functional group manipulation delivers the racemic amine which was then resolved with N-acetyl-D-leucine (NADL) under the DKR approach as discussed in section 2.3. This synthetic route was demonstrated on decagram scale and affords the enantiopure amine in an overall isolated yield of 15-20% (Scheme 4.2.1).[u]

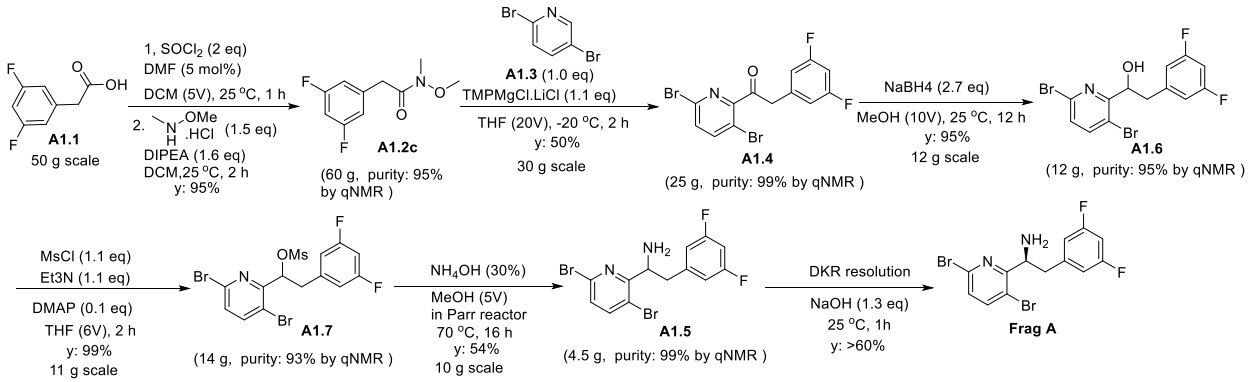

Scheme 4.2.1. Route LenA 1 for the synthesis of **LenA**

To initiate the synthesis of LenA 1, effort was focused on the ketone **A1.4** synthesis. The reaction of 3,5-difluorophenylacetonitrile (**A1.2a**) with **A1.3** with different organometallic reagents failed to generate the desired product (Table 4.2.1, Entries 1-4). We assumed that the lower pKa (~19)[28] of **A1.2a** mainly caused the protonation of Grignard reagent (quenching) rather than addition to nitrile. We envisioned that decreased acidity of the benzylic C-H bonds of the electrophile might mitigate deprotonation and thus favor the addition reaction. In this regard, the reaction of **A1.3-Mg** with ester **A1.2b** (pKa ~ 22 -23)[28] afforded the desired product in 15% isolated yield (Table 4.2.1, Entry 5). The positive results inspired us to investigate other electrophiles. Weinreb amide **A1.2c** (pKa ~ 26) was identified as the optimal electrophile to afford ketone **A1.4** (Table 4.2.1, Entry 6). Among all condition tested for Weinreb amide, the condition using 1 eq of each Knochel-Hauser base and Weinreb amide **A1.2c** at -20 °C delivered the best

[u] This route was not chosen for scale-up because of its high RMC.

result of ketone **A1.4** (Table 4.2.1, Entries 7-8). The protocol was demonstrated on a 30 g scale, affording **A1.4** in 50% of isolated yield with 93% purity (qNMR) after a process of an extractive workup and subsequent trituration (Table 4.2.1, Entry 9). Weinreb amide **A1.2c** was readily synthesized from commercial acid **A1.1** in a one-pot process as shown in **Error! Reference source not found.**.

Table 4.2.1 Optimizations for the synthesis of ketone **A1.4**

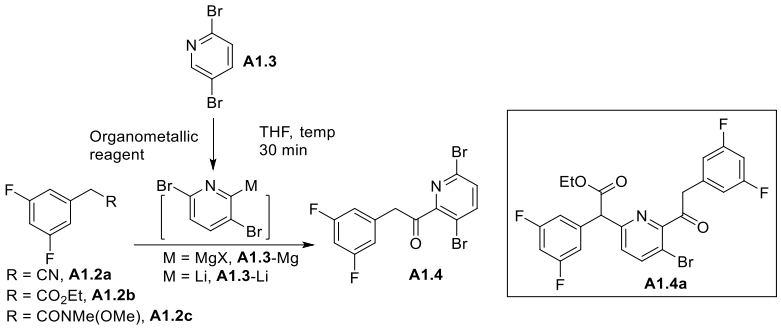

Entry[1]	Organometallic reagent (eq)	Electrophile (eq)	Temp (°C)	GC-MS analysis (TIC A%)[2]		
				A1.4	**A1.2*a*/ A1.2*b*/ A1.2*c***	**A1.3**
1	TMPMgCl·LiCl (1.5)	**A1.2a** (1.5)	-20	ND	50	45
2	TMPMgCl·LiCl (2.5) / $ZnCl_2$ (1.1)	**A1.2a** (1.1)	-20	ND	30	60
3[3]	LDA (1.0) / HMPA (10%)	**A1.2a** (1.2)	-40	ND	57	2
4	LiHMDS (1.0) / HMPA (10%)	**A1.2a** (1.2)	-40	ND	31	50
5[4]	TMPMgCl·LiCl (1.5)	**A1.2b** (1.5)	-20	20	31	30
6	TMPMgCl·LiCl (1.1)	**A1.2c** (1.1)	-10	51	-	40
7	TMPMgCl·LiCl (1.0)	**A1.2c** (1.1)	-20	67	-	25
8	TMPMgCl·LiCl (1.1)	**A1.2c** (1.1)	-20	85	-	10
9[5]	TMPMgCl·LiCl (1.1)	**A1.2c** (1.1)	-20	68[6]	5	10

[1]All reactions were carried out with **A1.3** (0.25 g, 1 eq) and organometallic reagent in THF (10V) for 30 min, followed by addition of electrophile and stirring at the same temperature for 2 h under the condition shown in the table unless otherwise stated, solvent volume (V) = mL/g of **A1.3**; [2]All these data were IPC of crude reaction mixtures obtained

by GC-MS total ion chromatogram (TIC) and reported as A% unless otherwise stated; [3]Impurity with m/z 179 was observed in 42A%; [4]4 h [5]Reaction was conducted on 30 g scale; [6]Extractive workup and sub sequential trituration for purification, 50% yield of the product was obtained with 93% purity (qNMR) after trituration from 5% ethyl acetate in heptane. ND: the desired product was not detected.

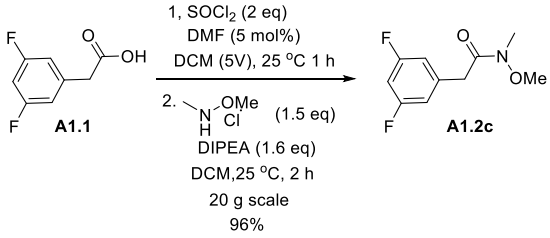

Scheme 4.22.2. Synthesis of Weinreb amide **A1.2c**

With ketone **A1.4** in hand, our effort was shifted to the synthesis of racemic amine **A1.5**. Leuckart amination of **A1.4** with NH_4HCO_2 was conducted,[29] but resulted in decomposition. Other amines, such as Boc-NH_2[30]/*t*-BuS(O)NH_2[31] also failed to react with ketone **A1.4**. Ultimately, the reduction of ketone **A1.4**, mesylation of the incipient alcohol, then amination of mesylate **A1.7** successfully afforded **A1.5** in overall ~51% yield over 3 steps with 99% purity (Scheme 4.2.3).

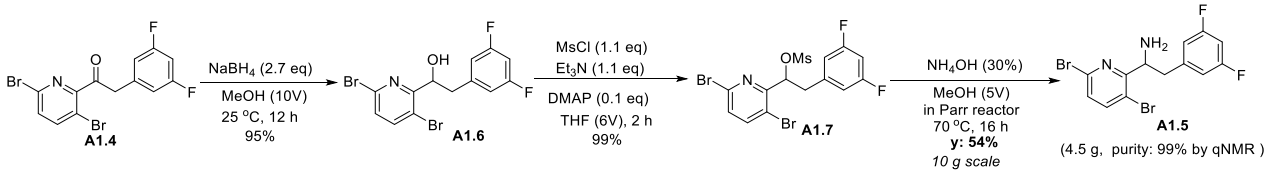

Scheme 4.2.3. Synthesis racemic amine **A1.5** from **A1.4**

To finish up the synthesis of **Frag A**, the obtained racemic amine **A1.5** was then subject to DKR with N-Acetyl-D-Leucine in the presence of 2-PyCHO (5 mol%) and ZnO (10 mol%), and the salt of the desired Frag A enantiomer with N-Acetyl-D-Leucine was obtained in 70-80% isolated yield. The treatment of the salt with aq NaOH afforded the free enantiopure amine in >97% isolated yield. In summary, this strategy (LenA 1) featured ketone synthesis, nucleophilic amination and dynamic kinetic resolution as key steps. These findings provide an efficient approach to make ketone **A1.4** from inexpensive raw materials. This route also provides an alternative way to prepare enantiopure amine ***(S)*-4** in the synthesis of lenacapavir. However, two steps with ~50% yield (synthesis of **A1.4** and **A1.5**) resulted in a high RMC of LenA 1 and make this route less

competitive compared to the route LenA 4. Thus, this route was not considered for further scale-up.

4.3 Route scouting of **LenA 3**

LenA 3 involves a 4-5-step route to **Frag A** (Scheme 4.3.1). The proposed sequence commences with formylation of **A1.3** with TMPMgCl·LiCl/DMF. The resulting aldehyde **A3.2** is subject to asymmetric epoxidation to form epoxide **A3.3**. Alternatively, **A3.2** can be converted to olefin **A3.3a** through a Wittig reaction, followed by epoxidation to afford **A3.3**. The epoxide **A3.3** reacts with 3,5-difluorophenylmagnesium bromide then MsCl to give **A3.4**. Finally, amination of **A3.4** affords **Frag A**. The key step is the asymmetric synthesis of epoxide **A3.3**. There are two possible pathways to prepare the epoxide: 1) asymmetric Corey-Chaykovsky epoxidation [32] of aldehyde **A3.2** or 2) asymmetric- or biocatalytic-epoxidation of olefin.[33]

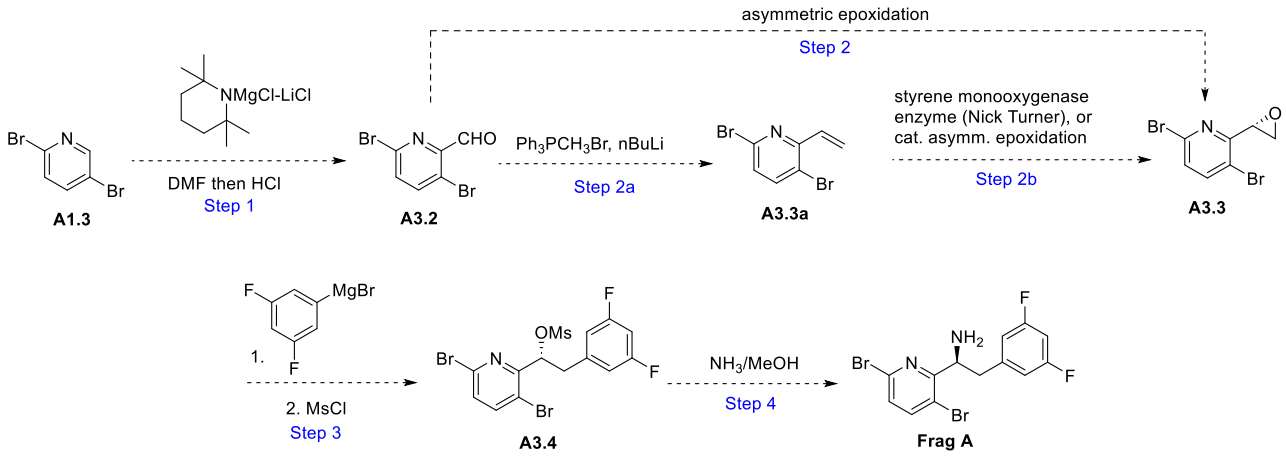

Scheme 4.3.1. Epoxide approach to **Frag A**

Initially, in accord with the literature,[13] aldehyde **A3.2** was prepared by formylation of 2,3-dibromopyridine **A1.3** (1.0 eq) with TMPMgCl.LiCl (1.5 eq) and DMF (4.8 eq) in 45% yield (**Error! Reference source not found.**).

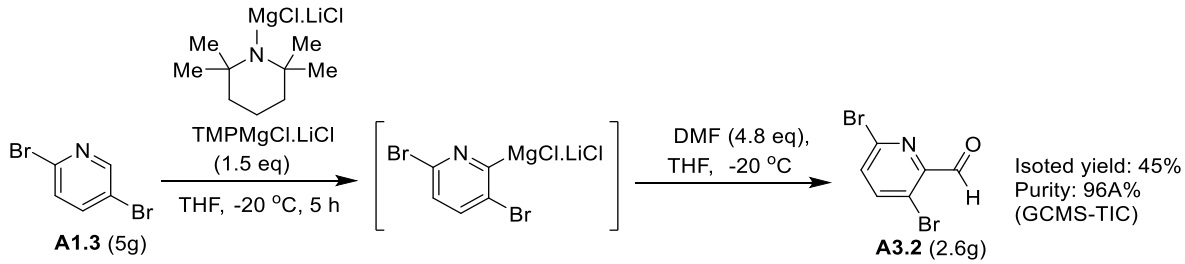

Scheme 4.3.2 Synthesis of aldehyde **A3.2**

With aldehyde **A3.2** in hand, Corey-Chaykovsky epoxidation was first tried to obtain racemic epoxide *rac*-**A3.3** (Scheme 4.3.3). Under a typical Corey-Chaykovsky condition, the reaction of **A3.2** with trimethylsulfoxonium iodide (1.1 eq) in the presence of NaH (1.1 eq) afforded the epoxide *rac*-**A3.3** in < 17% yield. Attempts to improve the yield failed. With the *rac*-**A3.3** in hand, the ring-opening reaction with 3,5-difluorophenylmagnesium bromide was tried and it failed to produce any desired product.

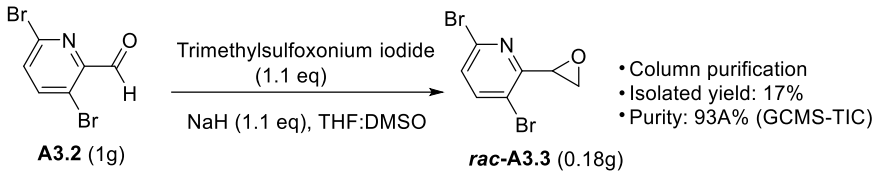

Scheme 4.3.3 Synthesis of epoxide *rac*-**A3.3**

We also tried the alternative two-step route to access **A3.3** (from aldehyde to olefin then epoxide). It turned out the methylenation of aldehyde **A3.2** was problematic. The Witting reaction with various bases such as *n*-BuLi, LiHMDS or *t*-BuOK failed to afford olefin **A3.3a** (**Error! Reference source not found.**).

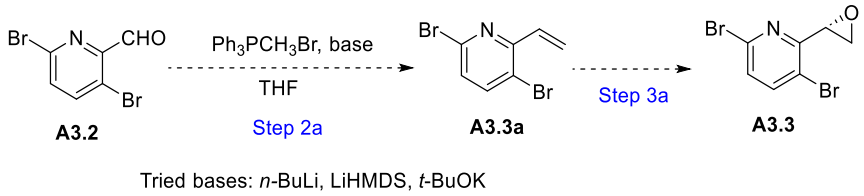

Scheme 4.3.4 Synthesis of epoxide *rac*-**A3.3**

All the failed results indicated the challenges for the LenA 3 route. Considering the limited timeline of the project, this approach was abandoned and our focus turned to LenA 4.

4.4 Acquisition Methods, Retention Times, Chromatograms, and Spectra

4.4.1 LenA-4 (LC-UV)

Structures & IDs:

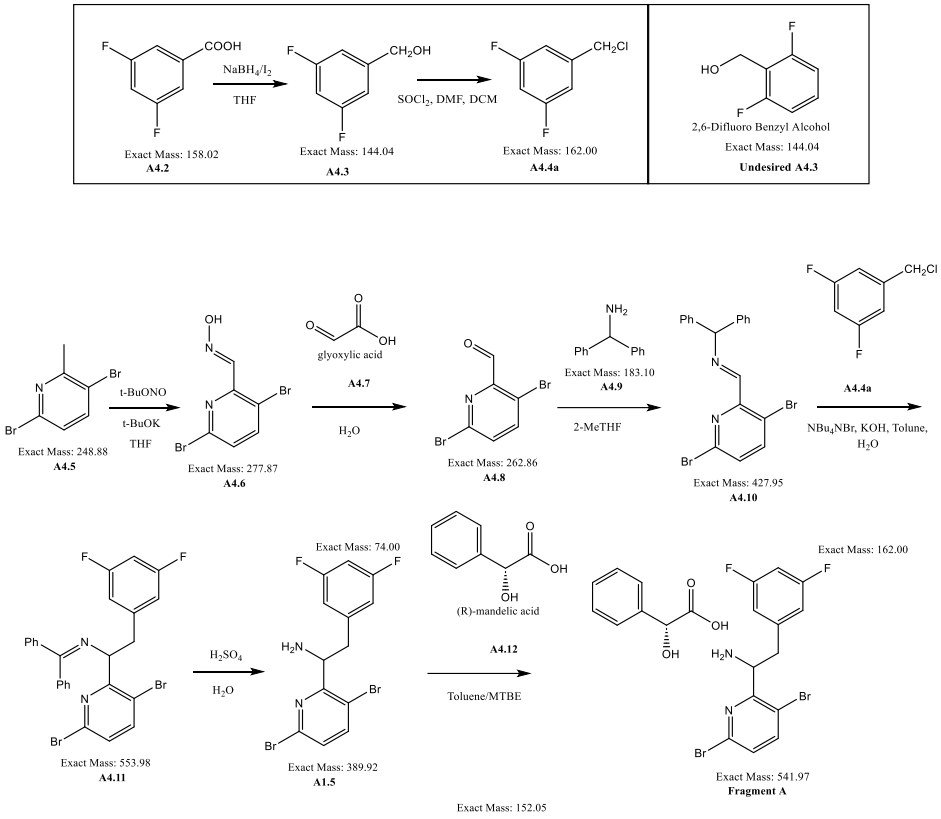

Instrument Type: Agilent 1100 liquid chromatograph (LC) with diode array detector (DAD)

Conditions:

Column: Agilent ZORBAX Extend-C18, 4.6 x 250 mm, 5 µm

Mobile Phase A: 25 mM potassium phosphate buffer, pH 8.5

(4.222 g K_2HPO_4 + 0.103 g KH_2PO_4 in 1 L 18 M·Ω water, adjust pH between 8.4-8.5)

Mobile Phase B: Methanol

Injection volume: 1 µL Column temp: 30°C Flow rate: 1.0 mL/min

Detector wavelength(s): 210 nm (SM and Steps 1 and 2), 225 nm (Steps 3,4,5,6)

LC Gradient Table:

Time (min)	%A	%B
0	60	40

Sample preparation: Prepare samples at 1 mg/mL in acetonitrile

0.5	60	40
10	10	90
25	10	90

Post-run equilibration: 4 minutes

Retention Times			
A4.4a Starting Material Step 1 (210 nm)			
Compound	**Time (min)**	**Relative RF (mg/mL)***	**Relative RF (M)***
A4.2	4.4	0.93	1.0
Undesired A4.3	6.3	1.1	1.1
A4.3	7.8	1.0	1.0
A4.4a Starting Material Step 2 (210 nm)			
Undesired A4.3	6.3	1.1	1.1
A4.3	7.8	0.83	0.73
A4.4a	11.7	1.0	1.0
Step 1 (210 nm)			
A4.6	7.4 8.4	-	-
A4.5	11.9	-	-
Step 2 (210 mm)			
A4.7	2.1	0.05	0.01
A4.6	7.4 8.4	-	-
A4.8	8.0	1.0	1.0
Step 3 (225 nm)			
A4.8	8.0	1.0	0.61
A4.9	10.5	0.25	0.11
A4.10	14.9	1.0	1.0
Step 4 (225 nm)			
A4.4a	11.7	0.61	0.18
A4.10	14.9	1.3	1.0

A4.11	17.8	1.0	1.0
Step 5 (225 nm)			
A1.5	12.5	1.0	1.0
A4.11	17.8	1.1	1.5
Step 6 (225 nm)			
A4.12	2.5	0.68	0.26
A1.5 (**Frag A**)	12.5	1.0	1.0

Note: A4.6 has been observed as the E and the Z isomers by NMR.

$$*Relative\ RF = \frac{\left(Analyte\ 2\ Peak\ Area / Analyte\ 2\ Conc.\right)}{\left(Analyte\ 1\ Peak\ Area / Analyte\ 1\ Conc.\right)}$$

Representative Chromatograms

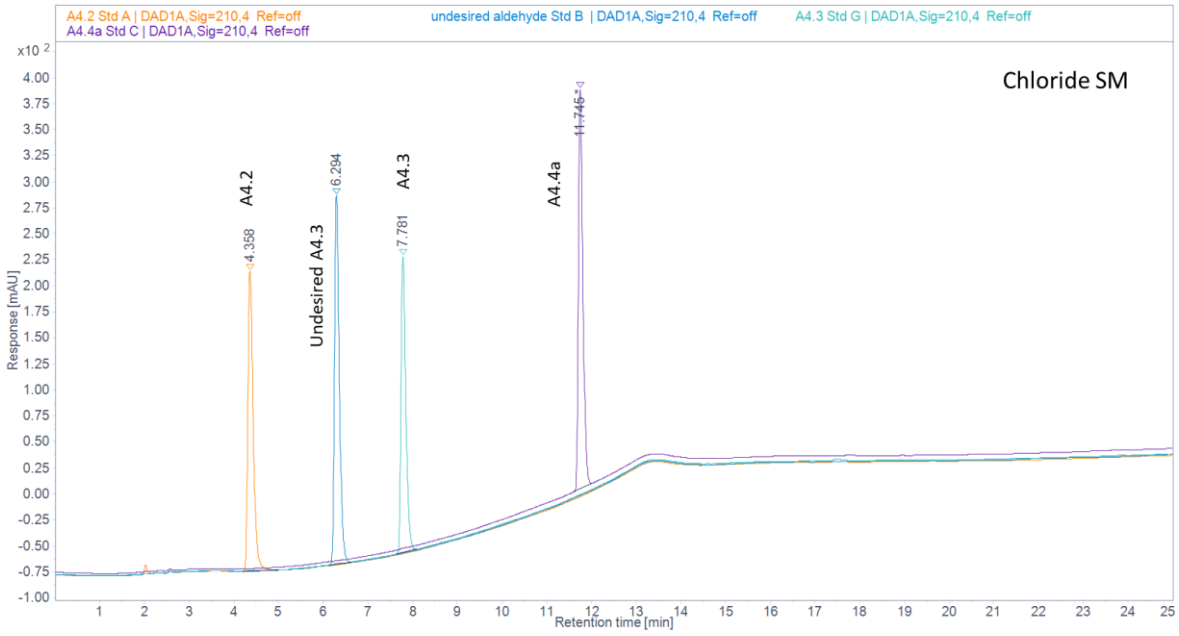

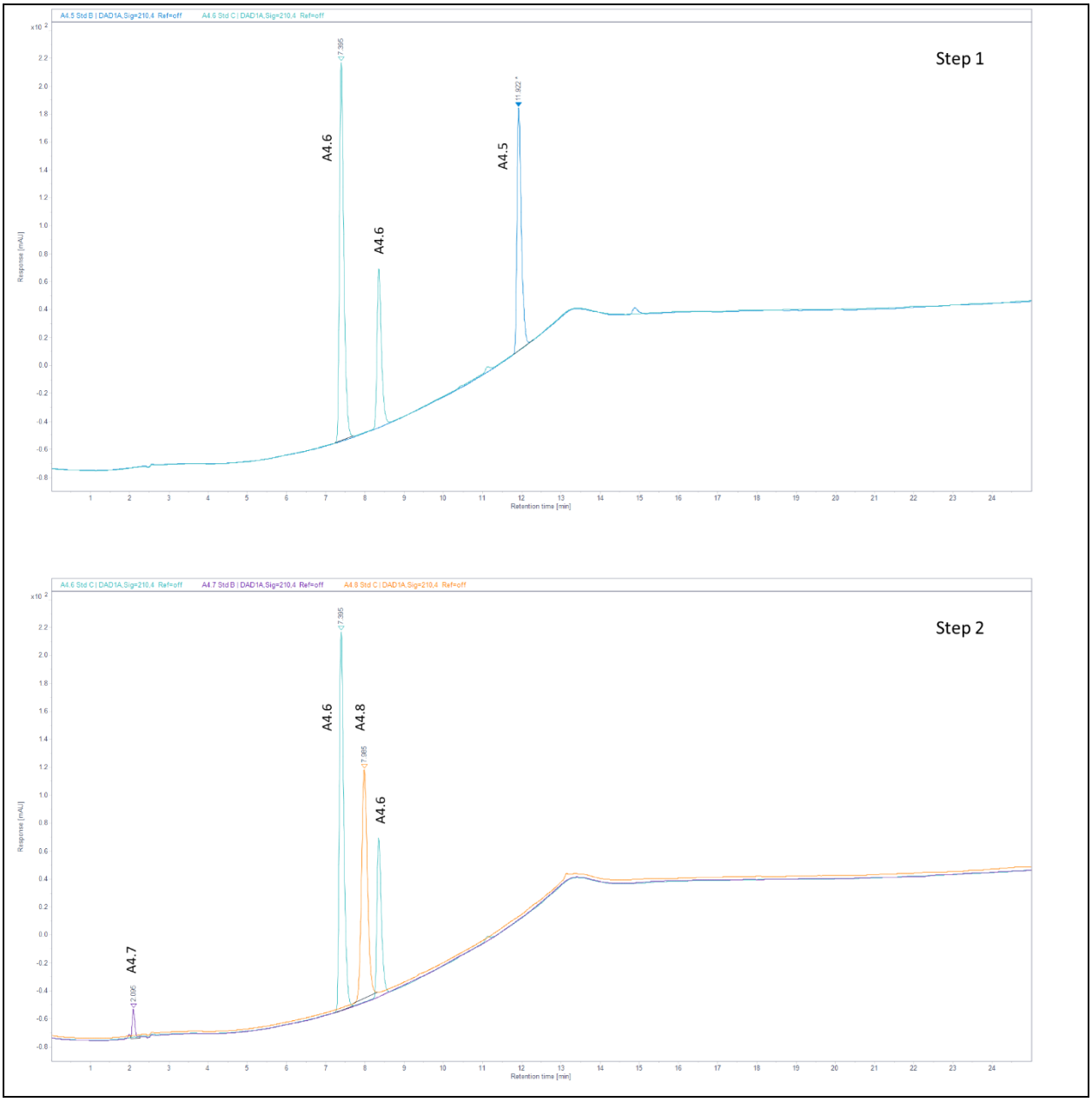
Step 1
A4.6
A4.6
A4.5
Step 2
A4.6
A4.8
A4.6
A4.7

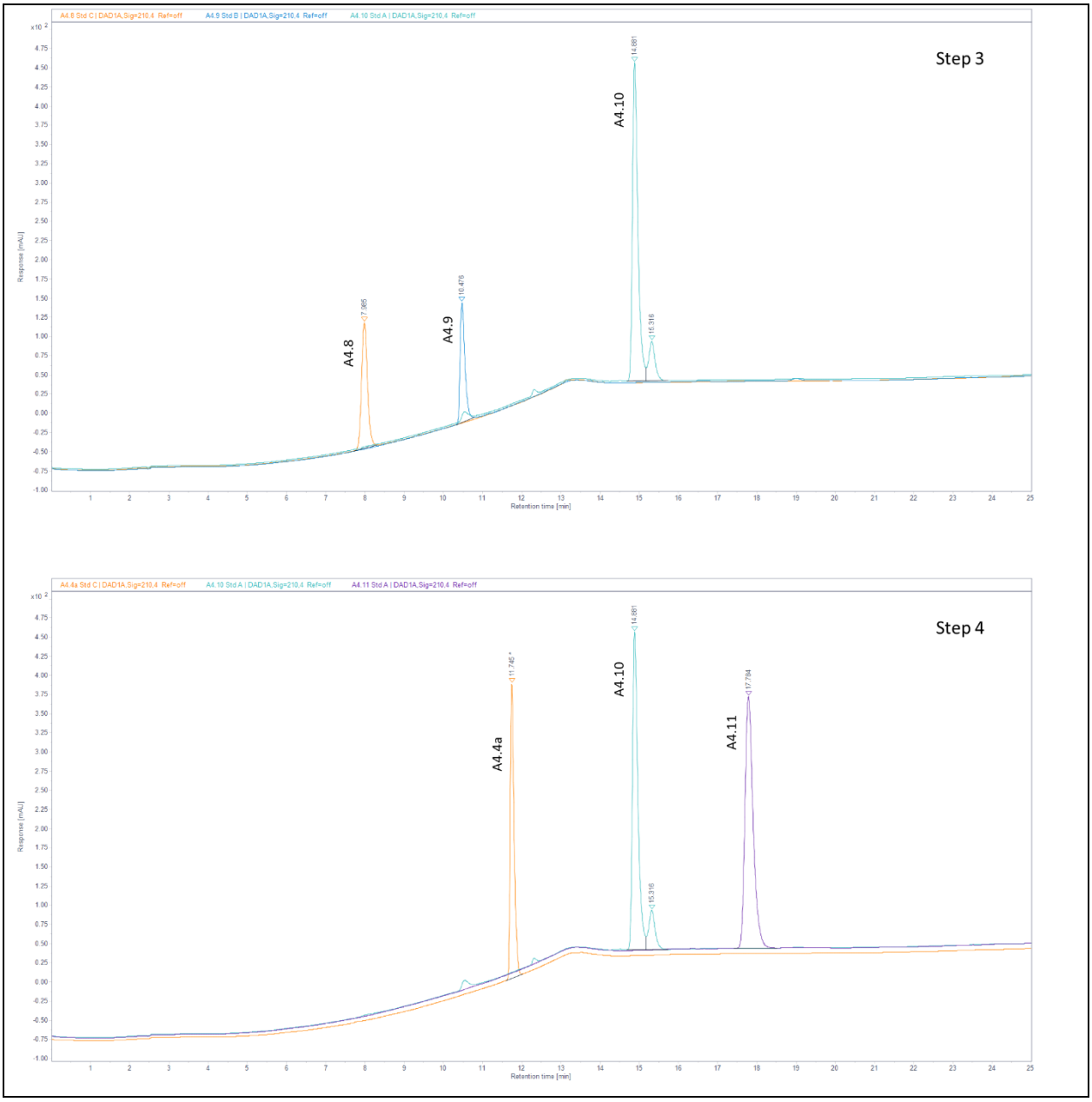
Step 3
A4.8
A4.9
A4.10
Retention time [min]
Response [mAU]
Step 4
A4.4a
A4.10
A4.11
Retention time [min]
Response [mAU]

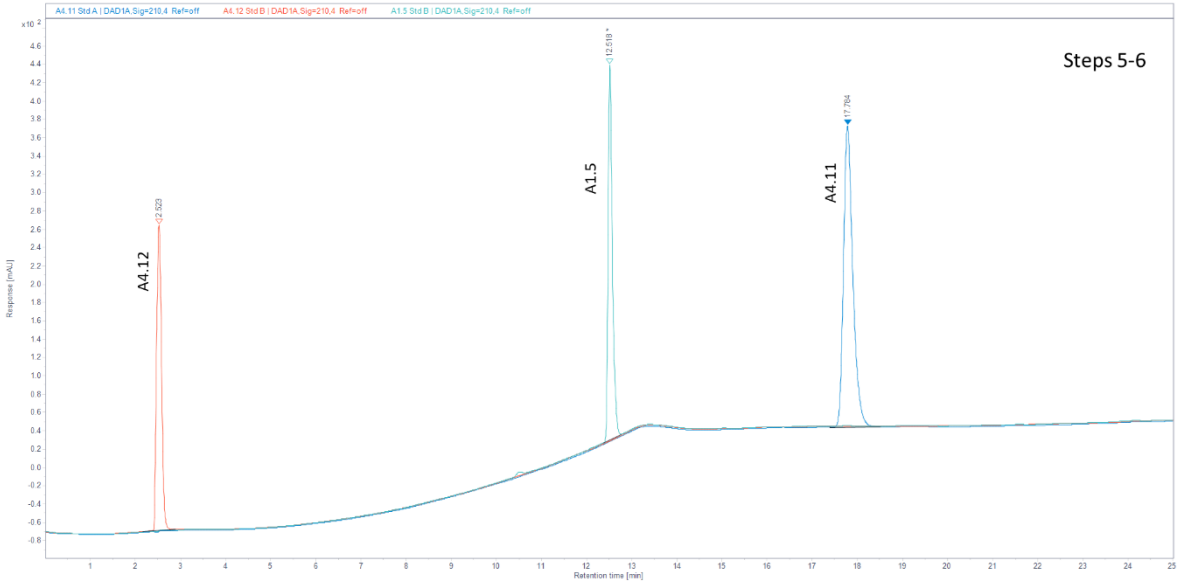
Steps 5-6
A4.12
A1.5
A4.11
Retention time [min]

UV Spectra

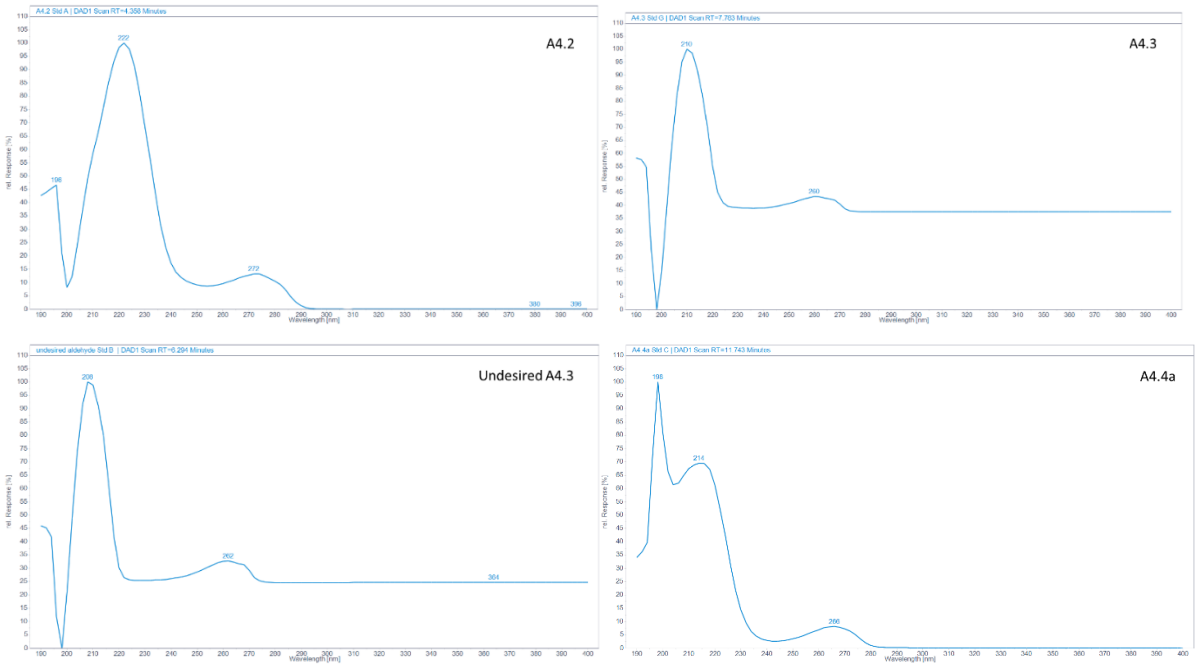
A4.2
A4.3
Undesired A4.3
A4.4a

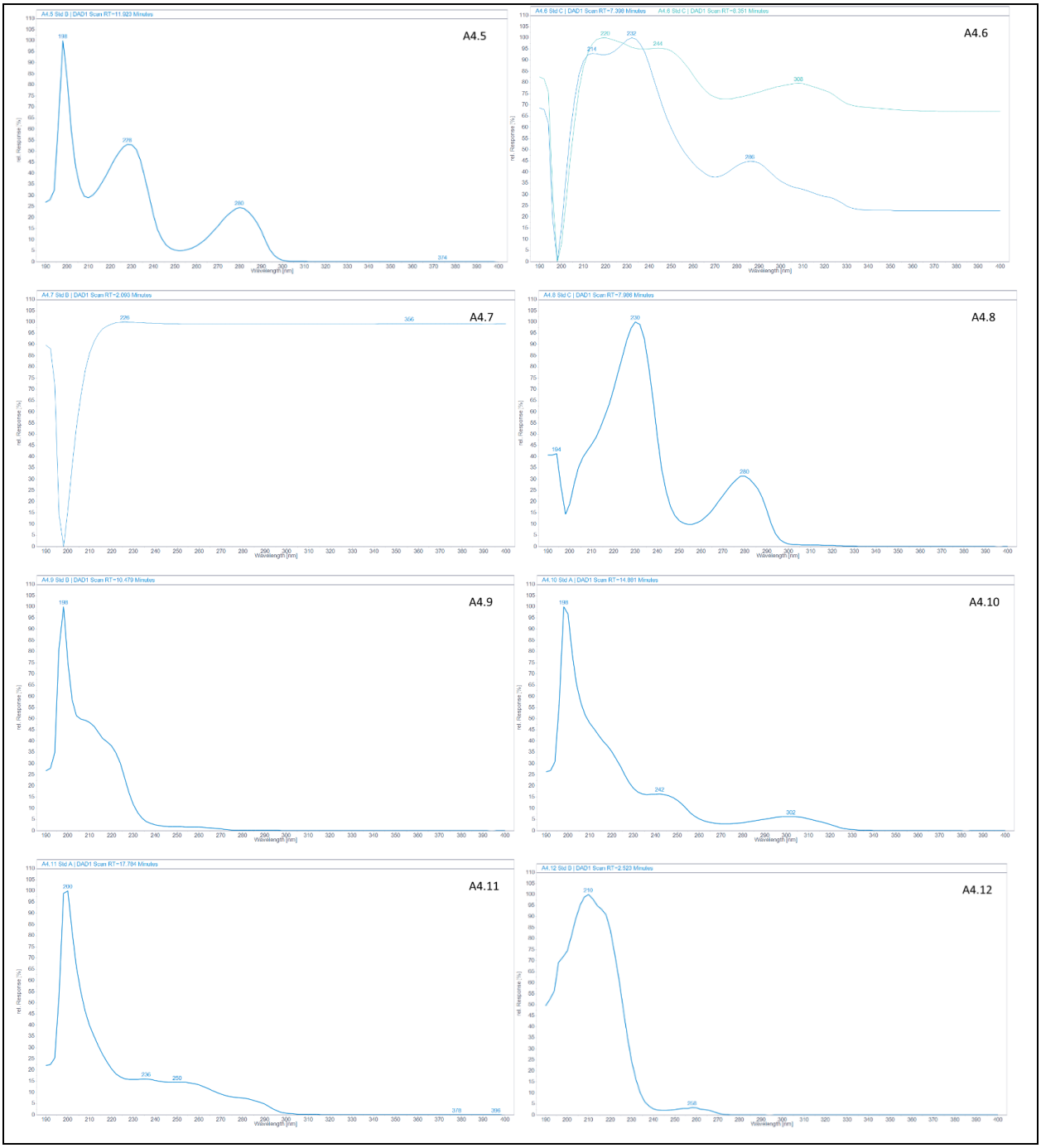
A4.5
A4.6
A4.7
A4.8
A4.9
A4.10
A4.11
A4.12

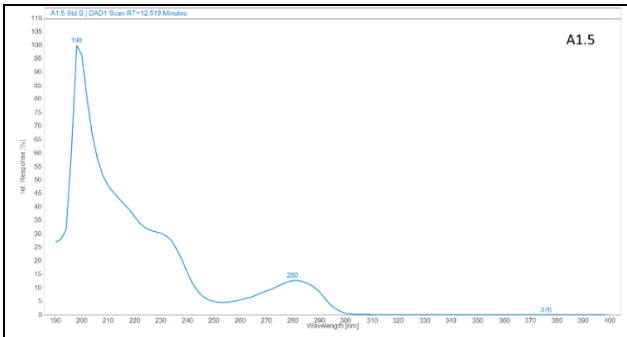

4.4.2 LenA-4 (SFC, Chiral)

Structures & IDs:

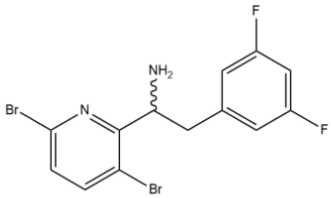

1-(3,6-dibromopyridin-2-yl)-2-(3,5-difluorophenyl)ethan-1-amine
Exact Mass: 389.92

Instrument Type: Agilent 1260 Infinity super critical fluid chromatograph (SFC) with diode array detector (DAD)

Conditions:

Column: Chiral Technologies CHIRALPAK IA SFC, 4.6 x 250 mm, 3 µm

Mobile Phase A: CO_2

Mobile Phase B: Methanol

Injection volume: 5 µL Column temp: 25°C Flow rate: 2.0 mL/min

BPR Pressure: 100 bar BPR temp: 60°C

Detector wavelength(s): 210 nm

Gradient Table:

Time (min)	%A	%B
0	90	10
10	90	10

Post-run equilibration: NA

Sample preparation: Prepare samples at 1 mg/mL in acetonitrile

Retention Times

Compound	Time (min)	Relative RF (mg/mL)*	Relative RF (M)*
(R) A1.5	4.2	-	-
(S) A1.5	6.8	-	-

Representative Chromatogram

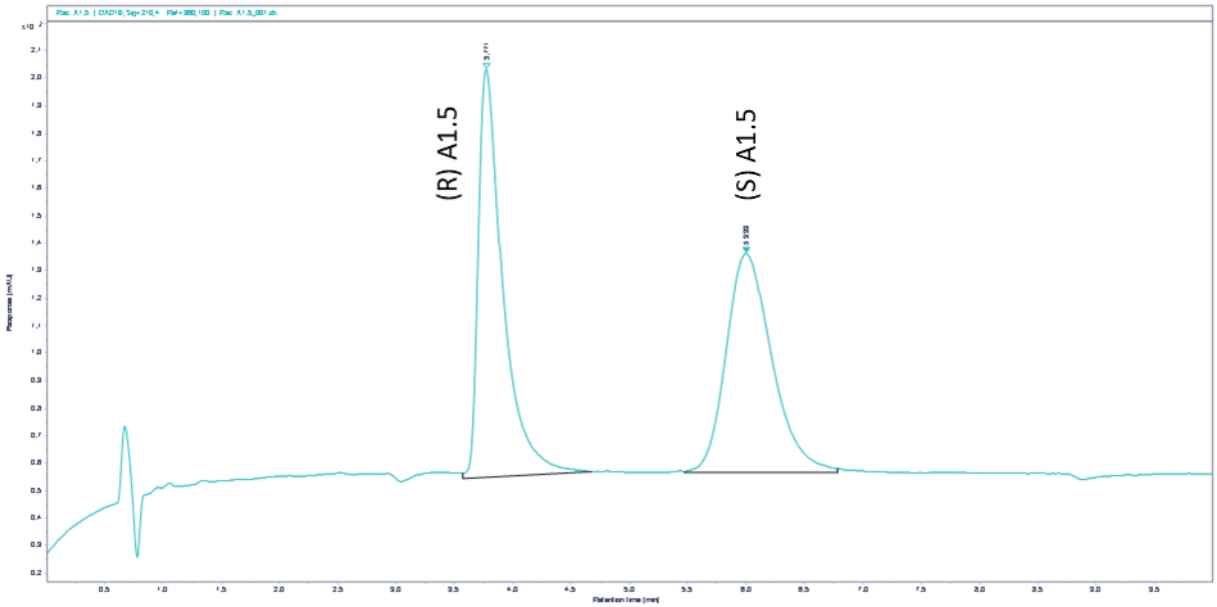

UV Spectra

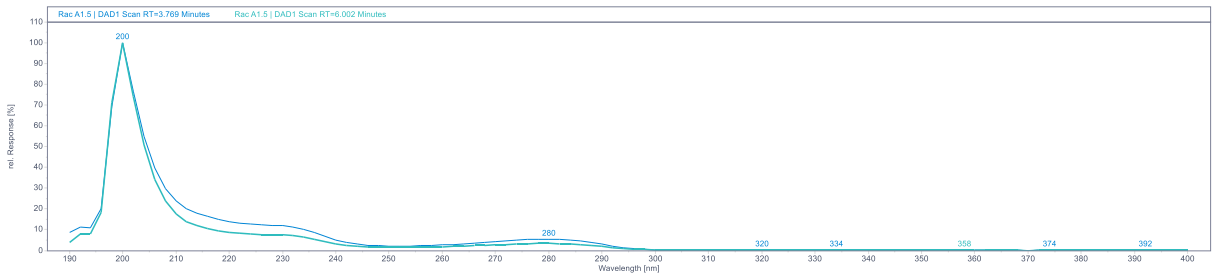

4.4.3 GC Solvents (GC-MS)

Instrument Type: Agilent 6890 gas chromatograph (GC) with a 5977 mass spectrometer detector (MSD)

Conditions:

Column: HP-1; 30M X 0.320 mm; 5 µM film

Inlet Pressure: 4.8 psi	Split Ratio: 50:1	Split Flow: 39.439 mL/min
Column flow: 0.787 mL/min	Injection Temp: 260 ºC	Injection volume: 1 µL
Solvent Delay: 3 min	Runtime: 20 min	

Temperature Program:

Time (min)	Temp (˚C)	Ramp (˚C/min)	Hold (min)
0	50	0	5
20	235	20	5.75

MS Parameters:

Transfer Line Temp (˚C)	250
Source Temp (˚C)	230
Quad Temp (˚C)	150
Electron Energy (eV)	70

Sample preparation: Prepare samples at 5-10 mg/mL in acetonitrile or other suitable solvent.

Retention Times

Compound	*m/z*	Time (min)
Dichloromethane	84	3.75
Heptane	100	8.55
Toluene	91	9.63

Representative Chromatogram

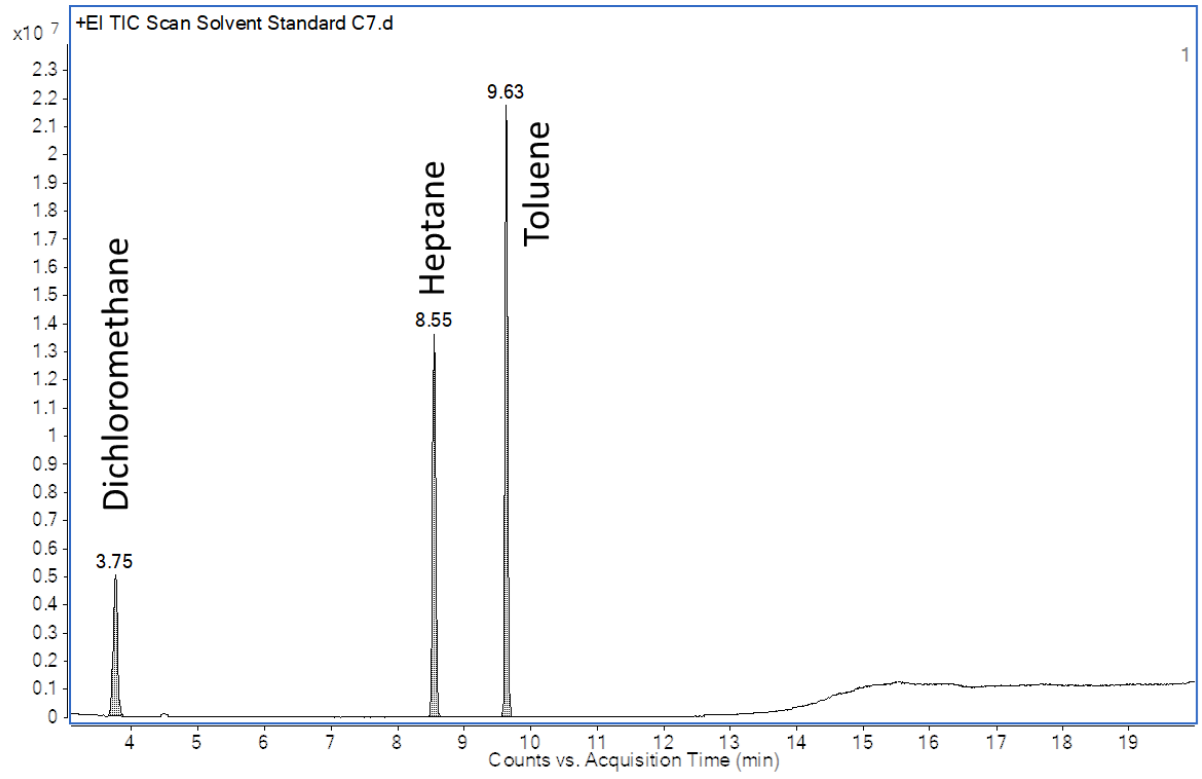

Mass Spectra

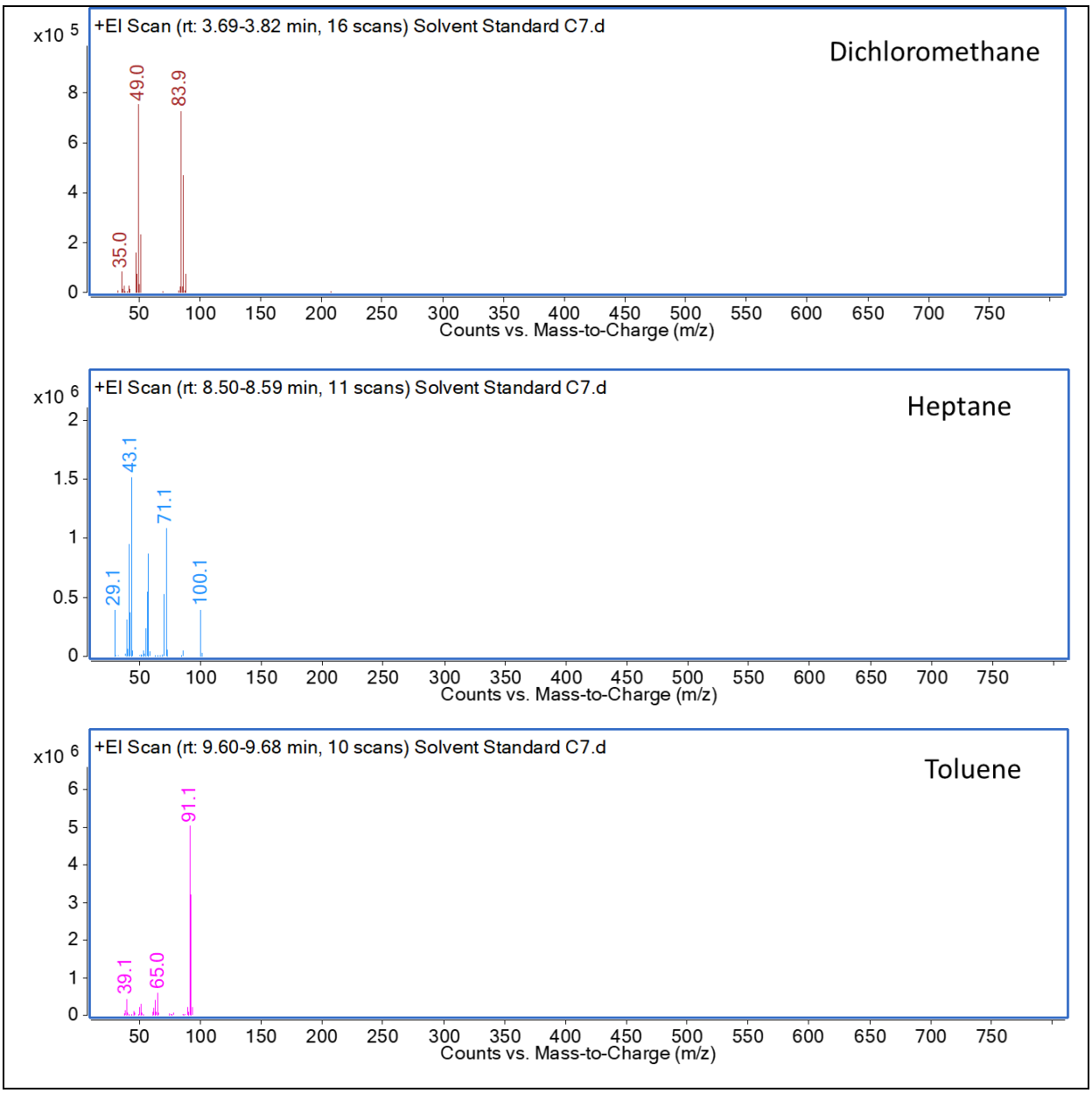
+EI Scan (rt: 3.69-3.82 min, 16 scans) Solvent Standard C7.d
Dichloromethane
x10 5
49.0
83.9
35.0
Counts vs. Mass-to-Charge (m/z)
+EI Scan (rt: 8.50-8.59 min, 11 scans) Solvent Standard C7.d
Heptane
x10 6
43.1
71.1
29.1
100.1
Counts vs. Mass-to-Charge (m/z)
+EI Scan (rt: 9.60-9.68 min, 10 scans) Solvent Standard C7.d
Toluene
x10 6
91.1
39.1
65.0
Counts vs. Mass-to-Charge (m/z)

4.5 Single X-ray crystal structure of **Frag A**

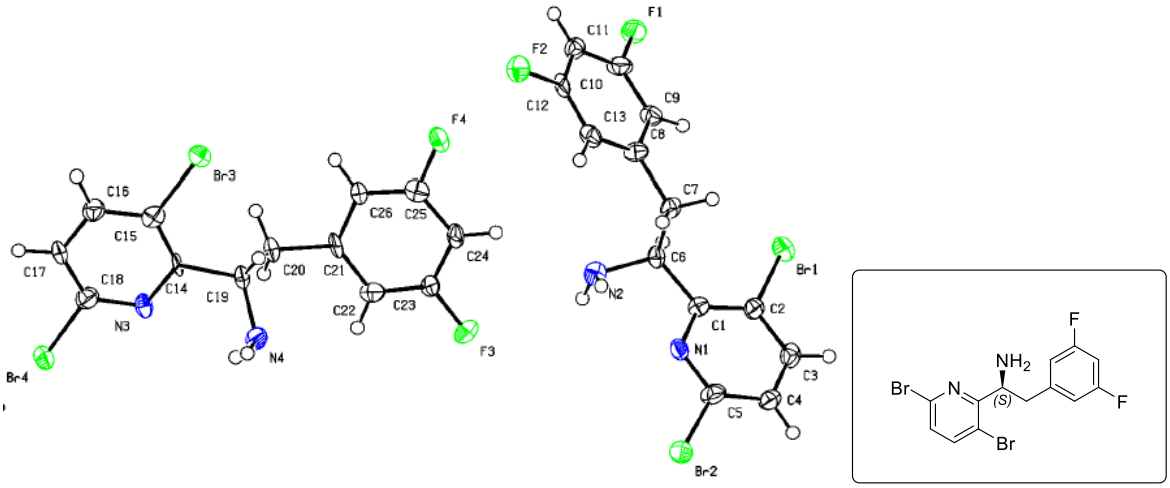

Figure 4.5.1 Single-crystal X-ray structure of **Frag A** (**(*S*)-A1.5)** with thermal ellipsoids drawn at 50% probability.

Table 4.5.1 Crystal data for **Frag A**

```
Bond precision:   C-C = 0.0198 A          Wavelength=1.54184

Cell:             a=4.4017(1)     b=35.5653(6)     c=17.0644(3)
                  alpha=90        beta=90          gamma=90
Temperature:      100 K

                  Calculated                  Reported
Volume            2671.39(9)                  2671.39(9)
Space group       P 21 21 21                  P 21 21 21
Hall group        P 2ac 2ab                   P 2ac 2ab
Moiety formula    C13 H10 Br2 F2 N2           2(C13 H10 Br2 F2 N2)
Sum formula       C13 H10 Br2 F2 N2           C26 H20 Br4 F4 N4
Mr                392.03                      784.10
Dx,g cm-3         1.949                       1.950
Z                 8                           4
Mu (mm-1)         7.821                       7.821
F000              1520.0                      1520.0
F000'             1512.60
h,k,lmax          5,43,21                     5,43,21
Nref              5292[ 3130]                 5256
Tmin,Tmax         0.363,0.661                 0.561,1.000
Tmin'             0.059

Correction method= # Reported T Limits: Tmin=0.561 Tmax=1.000
AbsCorr = MULTI-SCAN

Data completeness= 1.68/0.99        Theta(max)= 72.098

R(reflections)= 0.0685( 5139)                wR2(reflections)=
                                             0.1556( 5256)
S = 1.092                  Npar= 356
```

Table 4.5.2 Fractional Atomic Coordinates (×10^4) and Equivalent Isotropic Displacement Parameters (Å^2×10^3) for **Frag A**. U_{eq} is defined as 1/3 of the trace of the orthogonalised U_{ij}.

Atom	x	y	z	U_{eq}
Br4	-3974(4)	6224.0(4)	7983.6(8)	27.4(4)
Br3	4037(4)	7330.6(4)	5787.7(9)	28.8(4)
Br1	11689(4)	5449.6(4)	-1180.9(9)	29.9(4)
Br2	18148(4)	4703.9(4)	1857.5(9)	35.0(4)
F2	11650(20)	7277(2)	1758(5)	33(2)
F4	7390(20)	6901(2)	2715(5)	35(2)
F1	6550(20)	7011(2)	-591(5)	34(2)
F3	6150(30)	5601(2)	3035(6)	44(2)
N1	14750(30)	5222(3)	1059(7)	23(3)
N2	10530(30)	5767(4)	1448(8)	27(3)
N3	-270(30)	6406(3)	6752(7)	22(2)
N4	3950(40)	6050(3)	5778(7)	29(3)

Atom	x	y	z	U_{eq}
C23	5540(40)	5959(4)	3274(8)	26(3)
C1	13350(30)	5382(4)	447(8)	23(3)
C6	11560(30)	5742(4)	624(7)	21(3)
C20	1130(30)	6456(4)	4861(7)	24(3)
C19	3080(40)	6437(4)	5616(7)	22(3)
C10	8570(40)	6907(4)	-19(9)	30(3)
C25	6130(40)	6606(4)	3109(9)	28(3)
C13	12500(30)	6696(4)	1127(8)	25(3)
C12	11060(40)	7034(4)	1148(7)	23(3)
C14	1480(30)	6632(4)	6289(7)	19(3)
C17	-1260(40)	6931(4)	7599(8)	26(3)
C18	-1600(40)	6561(4)	7371(9)	30(3)
C22	3680(40)	6011(4)	3912(8)	27(3)
C24	6830(40)	6248(4)	2840(7)	25(3)
C2	13560(30)	5228(4)	-303(8)	26(3)
C11	9020(40)	7155(4)	585(8)	24(3)
C15	1790(30)	7007(4)	6456(8)	24(3)
C3	15360(30)	4904(4)	-411(9)	28(3)
C21	3030(30)	6377(4)	4148(7)	21(3)
C8	12000(40)	6456(4)	504(9)	25(3)
C26	4310(30)	6682(4)	3734(8)	24(3)
C7	13630(30)	6080(4)	439(9)	27(3)
C9	9990(30)	6565(4)	-88(9)	24(3)
C4	16730(40)	4734(4)	223(8)	27(3)
C16	430(40)	7161(4)	7120(8)	28(3)
C5	16310(40)	4909(4)	948(9)	32(4)

Table 0.3 Anisotropic Displacement Parameters ($\times 10^4$) **Frag A**. The anisotropic displacement factor exponent takes the form: $-2\pi^2[h^2a^{*2} \times U_{11} + \ldots + 2hka^* \times b^* \times U_{12}]$

Atom	U_{11}	U_{22}	U_{33}	U_{23}	U_{13}	U_{12}
Br4	30.9(8)	32.1(7)	19.2(7)	0.5(5)	1.5(7)	-2.3(7)
Br3	33.2(9)	27.1(7)	26.0(7)	3.2(6)	1.6(7)	-0.9(7)
Br1	31.1(9)	36.7(8)	22.0(7)	1.8(6)	-0.7(7)	-1.2(7)
Br2	43.7(10)	33.7(8)	27.5(8)	5.5(6)	0.9(8)	11.8(7)
F2	44(5)	33(4)	22(4)	-9(3)	-9(4)	-3(4)
F4	46(6)	36(5)	22(4)	1(4)	10(4)	-2(4)
F1	39(5)	36(5)	28(4)	4(3)	-7(4)	12(4)
F3	69(7)	24(4)	39(5)	-7(4)	9(6)	11(5)
N1	24(6)	25(6)	19(6)	1(5)	5(5)	-2(5)
N2	21(7)	29(6)	30(7)	-3(5)	1(6)	-3(5)
N3	18(6)	32(6)	15(5)	-3(5)	-1(5)	-2(5)
N4	39(8)	28(6)	20(6)	-4(5)	-7(6)	8(6)
C23	43(9)	25(7)	10(6)	-4(5)	-7(6)	6(6)
C1	23(7)	21(6)	25(7)	0(5)	-1(6)	2(6)
C6	20(7)	28(7)	16(6)	-3(5)	0(6)	1(6)
C20	21(7)	33(7)	17(6)	-2(5)	6(6)	-2(6)
C19	24(7)	29(7)	14(6)	-2(5)	4(6)	1(6)
C10	37(9)	23(7)	30(8)	6(6)	-5(8)	4(7)
C25	27(8)	29(7)	28(7)	2(6)	-6(7)	-3(6)

Atom	U_{11}	U_{22}	U_{33}	U_{23}	U_{13}	U_{12}
C13	31(8)	31(7)	15(6)	1(5)	-6(6)	-4(6)
C12	37(8)	27(7)	6(5)	-7(5)	-1(6)	-10(6)
C14	8(6)	37(7)	11(6)	3(5)	8(5)	7(5)
C17	34(9)	31(7)	13(6)	0(5)	7(7)	1(7)
C18	37(9)	25(7)	27(7)	-2(6)	-4(7)	4(7)
C22	36(9)	20(6)	25(7)	0(5)	-10(7)	-1(6)
C24	27(7)	37(7)	11(6)	-4(5)	-2(6)	6(7)
C2	23(7)	22(7)	32(8)	0(5)	11(7)	-2(6)
C11	22(7)	23(6)	28(7)	-2(5)	4(6)	0(6)
C15	15(7)	29(7)	27(7)	0(5)	-9(6)	6(6)
C3	23(8)	29(7)	31(8)	-4(6)	8(7)	-3(6)
C21	18(6)	41(8)	3(5)	-1(5)	-4(5)	1(6)
C8	26(7)	18(6)	31(8)	0(5)	-4(7)	-4(6)
C26	27(7)	27(7)	16(6)	-1(5)	6(6)	1(6)
C7	19(7)	23(7)	39(8)	0(6)	13(7)	1(6)
C9	27(8)	23(7)	22(7)	2(5)	-3(6)	-2(6)
C4	31(8)	20(6)	29(7)	-2(5)	0(7)	3(6)
C16	35(9)	25(7)	24(7)	-4(6)	-4(7)	1(6)
C5	38(9)	18(6)	40(9)	-1(6)	4(8)	-1(7)

Table 0.4 Bond Lengths in Å for **Frag A**.

Atom	Atom	Length/Å
Br4	C18	1.904(16)
Br3	C15	1.897(15)
Br1	C2	1.884(15)
Br2	C5	1.896(16)
F2	C12	1.375(14)
F4	C25	1.367(16)
F1	C10	1.371(18)
F3	C23	1.367(15)
N1	C1	1.340(18)
N1	C5	1.323(19)
N2	C6	1.481(18)
N3	C14	1.367(17)
N3	C18	1.329(19)
N4	C19	1.455(17)
C23	C22	1.37(2)
C23	C24	1.39(2)
C1	C6	1.534(18)
C1	C2	1.395(19)
C6	C7	1.541(18)
C20	C19	1.550(19)
C20	C21	1.503(18)
C19	C14	1.515(17)
C10	C11	1.37(2)
C10	C9	1.38(2)
C25	C24	1.387(19)
C25	C26	1.36(2)
C13	C12	1.36(2)
C13	C8	1.383(19)
C12	C11	1.38(2)
C14	C15	1.371(19)
C17	C18	1.379(19)
C17	C16	1.38(2)
C22	C21	1.391(18)
C2	C3	1.41(2)
C15	C16	1.39(2)
C3	C4	1.38(2)
C21	C26	1.410(19)
C8	C7	1.519(18)
C8	C9	1.40(2)
C4	C5	1.40(2)

Table 0.5 Bond Angles for **Frag A**.

Atom	Atom	Atom	Angle/°
C5	N1	C1	118.9(12)
C18	N3	C14	117.6(12)
F3	C23	C22	118.7(13)
F3	C23	C24	116.8(13)
C22	C23	C24	124.5(13)
N1	C1	C6	115.9(11)
N1	C1	C2	121.1(12)
C2	C1	C6	122.9(12)
N2	C6	C1	113.3(11)
N2	C6	C7	109.2(11)
C1	C6	C7	107.9(11)
C21	C20	C19	110.8(12)
N4	C19	C20	110.2(11)
N4	C19	C14	114.3(11)
C14	C19	C20	110.6(12)
F1	C10	C9	118.2(13)
C11	C10	F1	117.2(13)
C11	C10	C9	124.6(15)
F4	C25	C24	116.8(13)
C26	C25	F4	118.3(12)
C26	C25	C24	124.9(14)
C12	C13	C8	119.5(13)
F2	C12	C11	117.0(12)
C13	C12	F2	119.1(13)
C13	C12	C11	123.9(12)
N3	C14	C19	115.5(12)
N3	C14	C15	120.5(12)
C15	C14	C19	123.9(12)

Atom	Atom	Atom	Angle/°
C16	C17	C18	117.3(13)
N3	C18	Br4	114.6(10)
N3	C18	C17	125.0(15)
C17	C18	Br4	120.4(11)
C23	C22	C21	118.6(13)
C25	C24	C23	114.3(13)
C1	C2	Br1	122.3(10)
C1	C2	C3	118.6(14)
C3	C2	Br1	119.0(11)
C10	C11	C12	114.8(13)
C14	C15	Br3	121.0(10)
C14	C15	C16	120.7(13)
C16	C15	Br3	118.3(11)
C4	C3	C2	120.1(14)
C22	C21	C20	121.6(13)
C22	C21	C26	119.4(13)
C26	C21	C20	119.0(12)
C13	C8	C7	121.5(14)
C13	C8	C9	119.1(13)
C9	C8	C7	119.4(13)
C25	C26	C21	118.3(13)
C8	C7	C6	113.0(12)
C10	C9	C8	118.1(14)
C3	C4	C5	116.1(13)
C17	C16	C15	118.8(13)
N1	C5	Br2	115.3(11)
N1	C5	C4	124.9(14)
C4	C5	Br2	119.7(11)

Table 0.6 Torsion Angles in ° for **Frag A**.

Atom	Atom	Atom	Atom	Angle/°
Br3	C15	C16	C17	178.6(12)
Br1	C2	C3	C4	-179.2(11)
F2	C12	C11	C10	178.4(13)
F4	C25	C24	C23	178.6(13)
F4	C25	C26	C21	-179.2(13)
F1	C10	C11	C12	179.5(13)
F1	C10	C9	C8	-178.7(13)
F3	C23	C22	C21	-179.3(13)
F3	C23	C24	C25	-179.9(13)
N1	C1	C6	N2	-25.3(18)
N1	C1	C6	C7	95.7(14)
N1	C1	C2	Br1	-178.8(11)
N1	C1	C2	C3	-2(2)
N2	C6	C7	C8	-62.9(16)
N3	C14	C15	Br3	-176.6(10)
N3	C14	C15	C16	3(2)
N4	C19	C14	N3	-32.3(18)

Atom	Atom	Atom	Atom	Angle/°
N4	C19	C14	C15	145.8(14)
C23	C22	C21	C20	-177.4(13)
C23	C22	C21	C26	-1(2)
C1	N1	C5	Br2	-179.1(11)
C1	N1	C5	C4	2(2)
C1	C6	C7	C8	173.5(12)
C1	C2	C3	C4	4(2)
C6	C1	C2	Br1	1(2)
C6	C1	C2	C3	177.5(13)
C20	C19	C14	N3	92.8(14)
C20	C19	C14	C15	-89.1(16)
C20	C21	C26	C25	177.3(13)
C19	C20	C21	C22	82.8(16)
C19	C20	C21	C26	-94.0(15)
C19	C14	C15	Br3	5.4(19)
C19	C14	C15	C16	-175.1(14)
C13	C12	C11	C10	-1(2)
C13	C8	C7	C6	105.9(16)
C13	C8	C9	C10	-1(2)
C12	C13	C8	C7	178.0(14)
C12	C13	C8	C9	-1(2)
C14	N3	C18	Br4	-179.6(10)
C14	N3	C18	C17	-3(2)
C14	C15	C16	C17	-1(2)
C18	N3	C14	C19	177.0(13)
C18	N3	C14	C15	-1.1(19)
C18	C17	C16	C15	-3(2)
C22	C23	C24	C25	1(2)
C22	C21	C26	C25	0(2)
C24	C23	C22	C21	0(2)
C24	C25	C26	C21	0(2)
C2	C1	C6	N2	155.2(14)
C2	C1	C6	C7	-83.8(17)
C2	C3	C4	C5	-2(2)
C11	C10	C9	C8	1(2)
C3	C4	C5	Br2	-179.0(11)
C3	C4	C5	N1	-1(2)
C21	C20	C19	N4	-70.6(15)
C21	C20	C19	C14	162.0(12)
C8	C13	C12	F2	-177.9(13)
C8	C13	C12	C11	2(2)
C26	C25	C24	C23	-1(2)
C7	C8	C9	C10	-179.3(14)
C9	C10	C11	C12	0(2)
C9	C8	C7	C6	-75.5(17)
C16	C17	C18	Br4	-178.7(12)
C16	C17	C18	N3	5(3)
C5	N1	C1	C6	179.4(13)
C5	N1	C1	C2	-1(2)

Table 0.7 Hydrogen Fractional Atomic Coordinates ($\times 10^4$) and Equivalent Isotropic Displacement Parameters ($Å^2 \times 10^3$) for **Frag A**. U_{eq} is defined as 1/3 of the trace of the orthogonalised U_{ij}.

Atom	x	y	z	U_{eq}
H2A	9200(400)	5600(40)	1590(100)	32
H2B	12300(400)	5740(50)	1610(100)	32
H4A	2300(200)	5930(40)	5970(90)	35
H4B	5500(300)	6040(40)	6140(80)	35
H6	9743.24	5752.07	272.4	26
H20A	-535.47	6269.19	4894.13	28
H20B	204.56	6708.71	4814.77	28
H19	4993.19	6580.01	5509.57	26
H13	13843.05	6625.29	1537.56	31
H17	-2153.94	7022.65	8068.15	31
H22	2862.84	5802.33	4186.33	32
H24	8084.32	6204.81	2397.05	30
H11	8011.72	7390.43	614.59	29
H3	15636.04	4803.24	-921.82	33
H26	3904.33	6933.64	3887.73	28
H7A	15373.23	6078.99	805.29	33
H7B	14440.41	6052.62	-99.01	33
H9	9616.24	6406.4	-526.59	29
H4	17892.63	4509.8	170.82	32
H16	669.76	7420.49	7239.61	34

4.6 Acronyms

AIDS	acquired immunodeficiency syndrome
ART	antiretroviral therapy
ATR	attenuated total reflection
A%	area percent
BMGF	Bill and Melinda Gates Foundation
DCM	dichloromethane
DMSO	dimethyl sulfoxide
DMF	Dimethyl formamide
ESI	electrospray ionization
FDA	food and drug administration
FID	flame-ionization detector
GCMS-TIC	gas chromatography-mass spectrometry total ion chromatogram
HIV	human immunodeficiency virus
HRMS	high-resolution mass spectrometry
i-PrMgCl·LiCl	isopropyl magnesium chloride lithium chloride complex
i-PrOAc	isopropyl acetate
IR	infrared spectroscopy
LiHMDS	lithium hexamethyldisilazide (Lithium bis(trimethylsilyl)amide)
LCMS	liquid chromatography–mass spectrometry
LiTMP	Lithium 2,2,6,6-tetramethylpiperidide

M4ALL	Medicines for All Institute
MS-EI	mass spectrometry – electron ionization
NADL	N-Acetyl-D-Leucine
NMR	Nuclear Magnetic Resonance
OPT	scale-up optimization
RMC	raw material cost
SRS	synthetic route scouting
SFC	Supercritical fluid chromatography
TE	techno-economic
THF	tetrahydrofuran
TMP	2,2,6,6-tetramethylpiperidine
TMP-MgCl·LiCl	2,2,6,6-tetramethylpiperidinylmagnesium chloride lithium chloride complex solution
TMS	tetramethylsilane
UV	ultraviolet
□ max	wavenumber
qNMR	quantitative Nuclear Magnetic Resonance

5 Acknowledgements

This work was supported with funding from BMGF. M4ALL would like to express our gratitude to Dr. Trevor Laird, Dr. John Dillon, Dr. Ryan Nelson (BMGF), and Dr. Mark Krook for their helpful technical guidance throughout this project, as well as Silpa Sundaram (BMGF), Dr. Susan Hershenson (BMGF), Dr. John Walker (BMGF) and Scott Rosenblum (BMGF) for the ongoing collaboration and support of the M4ALL mission. The authors thank Dr. Saeed Ahmad and his team for their boundless effort in TE analysis. We also would like to thank Dr. B. Frank Gupton, Dr. Douglas Klumpp, Dr. G. Michael Laidlaw, Dr. Charles Shanahan, Michael Osberg, and Sarah Cox for their input on this work.

6 References

(1) Bester, S. M.; Wei, G.; Zhao, H.; Adu-Ampratwum, D.; Iqbal, N.; Courouble, V. V.; Francis, A. C.; Annamalai, A. S.; Singh, P. K.; Shkriabai, N.; Van Blerkom, P.; Morrison, J.; Poeschla, E. M.; Engelman, A. N.; Melikyan, G. B.; Griffin, P. R.; Fuchs, J. R.; Asturias, F. J.; Kvaratskhelia, M. Structural and Mechanistic Bases for a Potent HIV-1 Capsid Inhibitor. *Science* **2020**, *370* (6514), 360–364. https://doi.org/10.1126/science.abb4808.

(2) Chun, H. M.; Dirlikov, E.; Cox, M. H.; Sherlock, M. W.; Obeng-Aduasare, Y.; Sato, K.; Voetsch, A. C.; Ater, A. D.; Romano, E. R.; Tomlinson, H.; Modi, S.; Achrekar, A.; Nkengasong, J.; CDC Global HIV Working Group; CDC Global HIV Working Group; Agolory, S.; Amann, J.; Baack, B.; Behel, S.; Date, A.; Hanson, J.; Killam, W. P.; Patel, H.;

Patel, S.; Pati, R.; Porter, L.; Warner, A.; Wuhib, T.; Zeh, C.; Faria E Silva Santelli, A. C.; Guevara, G.; Morales, R. E.; Ekra, A. K.; Kitenge, F.; Bonilla, L.; Mazibuko, S.; Damena, T.; Joseph, P.; Upadhyaya, S.; Aitmagambetova, I.; Mwangi, J.; Usmanova, N.; Xaymounvong, D.; Asiimwe, M.; Alice, M.; Masamha, G. J.; Mutandi, G.; Odafe, S.; Romel, L.; Musoni, C.; Mogashoa, M.; Bolo, A.; Nabidzhonov, A.; Mgomella, G.; Lolekha, R.; Alamo-Talisuna, S.; Podolchak, N.; Nguyen, C. K.; Quaye, S.; Mwila, A.; Nyika, P. *Vital Signs* : Progress Toward Eliminating HIV as a Global Public Health Threat Through Scale-Up of Antiretroviral Therapy and Health System Strengthening Supported by the U.S. President's Emergency Plan for AIDS Relief — Worldwide, 2004–2022. *MMWR Morb. Mortal. Wkly. Rep.* **2023**, *72* (12), 317–324. https://doi.org/10.15585/mmwr.mm7212e1.

(3) Phillips, A. N.; Venter, F.; Havlir, D.; Pozniak, A.; Kuritzkes, D.; Wensing, A.; Lundgren, J. D.; De Luca, A.; Pillay, D.; Mellors, J.; Cambiano, V.; Bansi-Matharu, L.; Nakagawa, F.; Kalua, T.; Jahn, A.; Apollo, T.; Mugurungi, O.; Clayden, P.; Gupta, R. K.; Barnabas, R.; Revill, P.; Cohn, J.; Bertagnolio, S.; Calmy, A. Risks and Benefits of Dolutegravir-Based Antiretroviral Drug Regimens in Sub-Saharan Africa: A Modelling Study. *Lancet HIV* **2019**, *6* (2), e116–e127. https://doi.org/10.1016/S2352-3018(18)30317-5.

(4) Margot, N. A.; Naik, V.; VanderVeen, L.; Anoshchenko, O.; Singh, R.; Dvory-Sobol, H.; Rhee, M. S.; Callebaut, C. Resistance Analyses in Highly Treatment-Experienced People With Human Immunodeficiency Virus (HIV) Treated With the Novel Capsid HIV Inhibitor Lenacapavir. *J. Infect. Dis.* **2022**, *226* (11), 1985–1991. https://doi.org/10.1093/infdis/jiac364.

(5) Dvory-Sobol, H.; Shaik, N.; Callebaut, C.; Rhee, M. S. Lenacapavir: A First-in-Class HIV-1 Capsid Inhibitor. *Curr. Opin. HIV AIDS* **2022**, *17* (1), 15–21. https://doi.org/10.1097/COH.0000000000000713.

(6) Zhang, J.-Y.; Wang, Y.-T.; Sun, L.; Wang, S.-Q.; Chen, Z.-S. Synthesis and Clinical Application of New Drugs Approved by FDA in 2022. *Mol. Biomed.* **2023**, *4* (1), 26. https://doi.org/10.1186/s43556-023-00138-y.

(7) Zhuang, S.; Torbett, B. E. Interactions of HIV-1 Capsid with Host Factors and Their Implications for Developing Novel Therapeutics. *Viruses* **2021**, *13* (3), 417. https://doi.org/10.3390/v13030417.

(8) Margot, N.; Ram, R.; Rhee, M.; Callebaut, C. Absence of Lenacapavir (GS-6207) Phenotypic Resistance in HIV Gag Cleavage Site Mutants and in Isolates with Resistance to Existing Drug Classes. *Antimicrob. Agents Chemother.* **2021**, *65* (3), e02057-20. https://doi.org/10.1128/AAC.02057-20.

(9) Guinle, M. I. B. A New Way to Prevent HIV Delivers Dramatic Results in Trial. *NPR*. July 3, 2024. https://www.npr.org/sections/goats-and-soda/2024/07/03/g-s1-7988/hiv-prevention-drug-clinical-trial (accessed 2024-07-23).

(10) *Gilead's Twice-Yearly Lenacapavir Demonstrated 100% Efficacy and Superiority to Daily Truvada® for HIV Prevention*. https://www.gilead.com/news-and-press/press-room/press-releases/2024/6/gileads-twiceyearly-lenacapavir-demonstrated-100-efficacy-and-superiority-to-daily-truvada-for-hiv-prevention (accessed 2024-07-23).

(11) *Gilead to Highlight Landmark Progress in Research Across HIV Prevention, Treatment and Cure Programs at AIDS 2024*. https://www.gilead.com/news-and-press/press-room/press-releases/2024/7/gilead-to-highlight-landmark-progress-in-research-across-hiv-prevention-treatment-and-cure-programs-at-aids-2024 (accessed 2024-07-23).

(12) Bauer, L. E.; Gorman, E. M.; Mulato, A. S.; Rhee, M. S.; Rowe, C. W.; Sellers, S. P.; Stefanidis, D.; Tse, W. C.; Yant, S. R.; Chiu, A. Capsid Inhibitors for the Treatment of Hiv.

WO2020018459A1, January 23, 2020. https://patents.google.com/patent/WO2020018459A1/en?oq=WO%C2%A02020018459 (accessed 2021-02-17).

(13) Allan, K. M.; Batten, A. L.; Brizgys, G.; Dhar, S.; Doxsee, I. J.; Goldberg, A.; Heumann, L. V.; Huang, Z.; Kadunce, N. T.; Kazerani, S.; Lew, W.; Ngo, V. X.; O'keefe, B. M.; Rainey, T. J.; Roberts, B. J.; Shi, B.; Steinhuebel, D. P.; Tse, W. C.; Wagner, A. M.; Wang, X.; Wolckenhauer, S. A.; Wong, C. Y.; Zhang, J. R. Methods and Intermediates for Preparing a Therapeutic Compound Useful in the Treatment of Retroviridae Viral Infection. WO2019161280A1, August 22, 2019.

(14) Link, J. O.; Rhee, M. S.; Tse, W. C.; Zheng, J.; Somoza, J. R.; Rowe, W.; Begley, R.; Chiu, A.; Mulato, A.; Hansen, D.; Singer, E.; Tsai, L. K.; Bam, R. A.; Chou, C.-H.; Canales, E.; Brizgys, G.; Zhang, J. R.; Li, J.; Graupe, M.; Morganelli, P.; Liu, Q.; Wu, Q.; Halcomb, R. L.; Saito, R. D.; Schroeder, S. D.; Lazerwith, S. E.; Bondy, S.; Jin, D.; Hung, M.; Novikov, N.; Liu, X.; Villaseñor, A. G.; Cannizzaro, C. E.; Hu, E. Y.; Anderson, R. L.; Appleby, T. C.; Lu, B.; Mwangi, J.; Liclican, A.; Niedziela-Majka, A.; Papalia, G. A.; Wong, M. H.; Leavitt, S. A.; Xu, Y.; Koditek, D.; Stepan, G. J.; Yu, H.; Pagratis, N.; Clancy, S.; Ahmadyar, S.; Cai, T. Z.; Sellers, S.; Wolckenhauer, S. A.; Ling, J.; Callebaut, C.; Margot, N.; Ram, R. R.; Liu, Y.-P.; Hyland, R.; Sinclair, G. I.; Ruane, P. J.; Crofoot, G. E.; McDonald, C. K.; Brainard, D. M.; Lad, L.; Swaminathan, S.; Sundquist, W. I.; Sakowicz, R.; Chester, A. E.; Lee, W. E.; Daar, E. S.; Yant, S. R.; Cihlar, T. Clinical Targeting of HIV Capsid Protein with a Long-Acting Small Molecule. *Nature* **2020**, *584* (7822), 614–618. https://doi.org/10.1038/s41586-020-2443-1.

(15) Graupe, M.; Henry, S. J.; Link, J. O.; Rowe, C. W.; Saito, R. D.; Schroeder, S. D.; Stefanidis, D.; Tse, W. C.; Zhang, J. R. Therapeutic Compounds Useful for the Prophylactic or Therapeutic Treatment of an Hiv Virus Infection. WO2018035359A1, February 22, 2018.

(16) Du, Z.; Farand, J.; Guney, T.; Kato, D.; Link, J. O.; Mack, J. B. C.; Mun, D. M.; Watkins, W. J.; Zhang, J. R. Therapeutic Compounds for HIV Virus Infection. WO2023102529A1, June 8, 2023.

(17) Brands, K. M. J.; Davies, A. J. Crystallization-Induced Diastereomer Transformations. *Chem. Rev.* **2006**, *106* (7), 2711–2733. https://doi.org/10.1021/cr0406864.

(18) Caravez, J. C.; Hu, Y.; Oftadeh, E.; Mamo, K. T.; Lipshutz, B. H. Preparation of a Key Intermediate En Route to the Anti-HIV Drug Lenacapavir. *J. Org. Chem.* **2024**, *89* (6), 3995–4000. https://doi.org/10.1021/acs.joc.3c02855.

(19) Dach, R.; Song, J. J.; Roschangar, F.; Samstag, W.; Senanayake, C. H. The Eight Criteria Defining a Good Chemical Manufacturing Process. *Org. Process Res. Dev.* **2012**, *16* (11), 1697–1706. https://doi.org/10.1021/op300144g.

(20) Sheldon, R. A. *Chirotechnology*; Marcel Dekker Inc.: New York, 1993.

(21) Kanth, J. V. B.; Periasamy, M. Selective Reduction of Carboxylic Acids into Alcohols Using Sodium Borohydride and Iodine. *J. Org. Chem.* **1991**, *56* (20), 5964–5965. https://doi.org/10.1021/jo00020a052.

(22) Adams, R.; Weeks, L. F. Action of Oxalyl Chloride on Primary, Secondary and Tertiary Alcohols. *J. Am. Chem. Soc.* **1916**, *38* (11), 2514–2519. https://doi.org/10.1021/ja02268a028.

(23) Lewis, E. S.; Boozer, C. E. The Kinetics and Stereochemistry of the Decomposition of Secondary Alkyl Chlorosulfites1. *J. Am. Chem. Soc.* **1952**, *74* (2), 308–311. https://doi.org/10.1021/ja01122a005.

(24) Jung, M. E.; Hatfield, G. L. Preparation of Bromides from Alcohols via Treatment with Trimethylsilyl Bromide. *Tetrahedron Lett.* **1978**, *19* (46), 4483–4486. https://doi.org/10.1016/S0040-4039(01)95258-X.
(25) Diethyl (2s,3r)-2-(N-tert-Butoxycarbonyl)amino- 3-Hydroxysuccinate. *Org. Synth.* **1996**, *73*, 184. https://doi.org/10.15227/orgsyn.073.0184.
(26) Hudson, H. R. Synthesis of Optically Active Alkyl Halides. *Synthesis* **2002**, *1969*, 112–119. https://doi.org/10.1055/s-1969-34195.
(27) Shinde, A.; Sayini, R.; Singh, P.; Burns, J.; Ahmad, S.; Laidlaw, G.; Gupton, F.; Klumpp, D.; Jin, L. A New Synthesis of the Amine Fragment: An Important Intermediate to the Anti-HIV Drug Lenacapavir. ChemRxiv May 8, 2024. https://doi.org/10.26434/chemrxiv-2024-79678.
(28) Bordwell, F. G.; Branca, J. C.; Bares, J. E.; Filler, R. Enhancement of the Equilibrium Acidities of Carbon Acids by Polyfluoroaryl Substituents. *J. Org. Chem.* **1988**, *53* (4), 780–782. https://doi.org/10.1021/jo00239a016.
(29) Crossley, F. S.; Moore, M. L. Studies on the Leuckart Reaction. *J. Org. Chem.* **1944**, *09* (6), 529–536. https://doi.org/10.1021/jo01188a006.
(30) Bernacka, E.; Klepacz, A.; Zwierzak, A. Reductive BOC-Amination of Aldehydes. *Tetrahedron Lett.* **2001**, *42* (30), 5093–5094. https://doi.org/10.1016/S0040-4039(01)00895-4.
(31) Ellman, J. A. Applications of Tert-Butanesulfinamide in the Asymmetric Synthesis of Amines. *Pure Appl. Chem.* **2003**.
(32) Tan, L.; Tao, Y.; Wang, T.; Zou, F.; Zhang, S.; Kou, Q.; Niu, A.; Chen, Q.; Chu, W.; Chen, X.; Wang, H.; Yang, Y. Discovery of Novel Pyridone-Conjugated Monosulfactams as Potent and Broad-Spectrum Antibiotics for Multidrug-Resistant Gram-Negative Infections. *J. Med. Chem.* **2017**, *60* (7), 2669–2684. https://doi.org/10.1021/acs.jmedchem.6b01261.
(33) Toba, T.; Murata, K.; Nakanishi, K.; Takahashi, B.; Takemoto, N.; Akabane, M.; Nakatsuka, T.; Imajo, S.; Yamamura, T.; Miyake, S.; Annoura, H. Minimum Structure Requirement of Immunomodulatory Glycolipids for Predominant Th2 Cytokine Induction and the Discovery of Non-Linear Phytosphingosine Analogs. *Bioorg. Med. Chem. Lett.* **2007**, *17* (10), 2781–2784. https://doi.org/10.1016/j.bmcl.2007.02.081.